ABSTRACT

Title of dissertation: STRUCTURE AND DYNAMICS OF MICROTENTACLES: FROM A PHYSICAL PERSPECTIVE

Eleanor Claire-higgins Ory,
Doctor of Philosophy, 2016

Dissertation directed by: Professor Wolfgang Losert
Department of Biophysics

While modern cancer diagnostics and treatments are often interpreted through a biomolecular perspective, cancer abounds with many mechanically interesting characteristics and questions. Metastasis, the process by which a primary tumor spreads and forms a second tumor in a distant site is currently responsible for 90% of cancer fatalities [1–3]. One of the key limiting steps in metastasis is extravasation; the process by which a circulating tumor cell (CTC) moves from the bloodstream into surrounding tissue. So far, most *in vitro* studies in metastasis focus on cell migration and invasiveness with few focused on reattachment of cells to a blood vessel wall, and extravasation. One possible attachment mechanism involves tubulin-based structures called microtentacles, which have been observed to poke into crevices between cells that line blood vessels. Based on biomolecular assays, the current hypothesis is that microtentacles are formed as the result of unbalanced, mechanical interactions between microtubules and actin, allowing microtubules to push the plasma membrane beyond the cell body. The focus of my thesis is to gain

insights into the dynamics and mechanical properties of microtentacles and evaluate how microtentacles may be altered by cytoskeletal drugs.

In this thesis, I will measure changes in microtubule dynamics using cytoskeletal drugs to the actomyosin cortex and microtubules. The first study presented examines how drug treatments targeting the actomyosin cortex impact microtubule dynamics for attached cells. The results of the first study demonstrate that weakening the actomyosin cortex allows microtubule end-binding-protein-1 (EB1) to move beyond the cell body boundary. Weakening the actomyosin cortex also results in changes to the speed and straightness of microtubule growth. In the second study, an image analysis framework is presented to quantify microtentacles as well as an evaluation of the dynamics of microtubules in suspended cells. The study demonstrates a successful image analysis technique that can evaluate microtentacle phenotype for both free-floating and tethered cells as well as dynamics for tethered cells. This second study shows that while microtubule stabilizing drug treatment with Taxol increases total microtentacle phenotype, it also reduces microtentacle dynamics. On the other hand, while microtubule destabilizing drug treatment Colchicine decreases total microtentacle phenotype, Colchicine also reduces microtentacle dynamics. As a summary and outlook, I present a mechanical framework and present hypotheses for 4 different genetic modifications spanning a spectrum of different cytoskeletal states. I also show preliminary, qualitative results for 3 out of the 4 different cell lines. Critical to evaluating microtentacles within this physical framework is a direct mechanical assay; here, I show preliminary work taken at the University of Leipzig on an optical stretcher.

Given that microtentacles have demonstrated to be a sufficient prerequisite for reattachment, better understanding of what circumstances lead to microtentacles is a critical basic research question. My work applies a physical perspective to the balance between the actomyosin cortex and microtubules and demonstrates changes in microtubule dynamics. Such work contributes towards the possibility of identifying morphological and dynamics signatures of CTCs with higher metastatic potential.

STRUCTURE AND DYNAMICS OF MICROTENTACLES FROM A PHYSICAL PERSPECTIVE

by

EChO
Eleanor Claire-higgins Ory

Dissertation submitted to the Faculty of the Graduate School of the
University of Maryland, College Park in partial fulfillment
of the requirements for the degree of
Doctor of Philosophy
2016

Advisory Committee:
Wolfgang Losert, Chair/Advisor
Stuart Martin, Co-Advisor
Professor Arpita Uphadhyaya
Professor Marco Colombini
Professor Kimberly Stroka

Preface

Nature uses only the longest threads to weave her patterns, so that each small piece of her fabric reveals the organization of the entire tapestry. -Richard Feynman

Simplicity is the ultimate sophistication -Leonardo DiVinci

Dedication

Dedication: I dedicate my research in memory to the family members who have profoundly impacted my life and succumbed to their battles with cancer most especially to my late grandparents Grandma, Gigi, and Gramps.

To my busybody Grandma (Rita Higgins), who was a teacher, nurse, entrepreneur of a craft store, president of the Chicago women′s club, a mother of 9 children, and a very dedicated catholic who instilled in me a sense of civic duty and work ethic.

To Gigi (Norma Ory), a free-spirited artist who filled my childhood with all the imagination and art supplies a kid could ever wish for. She was passionate about art and education; she was the dean for many years and founded many of the outreach programs that continue 30+ years later at the Glassel School of Arts; and inspired me to always follow my heart and dreams.

To Gramps (Edwin M Ory), an MD who pioneered research in infectious diseases and internal medicine. Who never ceased to be amazed and interested in the latest technologies and their future roles in medicine and impressed upon me the impact that basic and clinical research can have on the lives of Americans.

Acknowledgments

This work would not have been possible without the help of so many people. Here are a few notable ones:

First of all, I cannot thank my parents enough for all their love and support throughout the entirety of my education and for always being there for me no matter what. I would like to thank them for listening to all my technical rants and for never giving up on trying to understand what it is I do.

I want to thank several people from my undergraduate education at Smith College. I am grateful to all my professors for encouraging me to pursue interdisciplinary projects early on. A special thanks to my philosophy mentor Nalini Bhushan for continuing to give me advice on finishing my thesis and writing techniques in the final stretch of my graduate education. I must thank all my wonderful Smithie engineering girls for putting up with my doing work even on vacations; for supplying a steady stream of hilarious youtube videos and messages, especially the cat ones, when I was most stressed out; and for persistently insisting that I can do this!

I want to thank my wonderful labmates in both the Losert and Martin lab for all their help and camaraderie: to Keyata, for her encouragement, great sense of humor, and being an all-around awesome officemate; to Michele, for teaching me so much about the phenotypes of many of the cancer cell models; to Becky, for showing me the ropes in lab and feedback with so many biological techniques; to Kristi, for teaching me and helping me with tethering techniques; to Lek, for teaching me immunohistochemistry; to Josh, for all the carpooling and help with exponential

fits; to Desu, for so much assistance with image analysis; to Chenlu and Rachel for sharing ideas, articles, resources, and an office; and to anyone I haven′t listed.

I would like to say thank you to my committee for their time and patience and making this defense possible on such a short time scale. I would like to extend a thank you to Kimberly Stroka for joining my committee this summer. I would also like to thank Marco Colombini for helping me out when I first got started on this journey at College Park and for teaching me everything I know about membranes. A sincere thanks to Arpita Uphadhaya for her patience with me on the NBT2 project, for co-advising in the beginning, and for teaching me so much about EMT, image analysis, and traction force microscopy.

I would like to express my gratitude to co-advisor Stuart Martin for all his support, guidance, and direction throughout this process. For all the times I walked into his office overwhelmed, I never managed to leave without an improved research strategy and renewed enthusiasm for science. I greatly appreciate his sharing of so much wisdom and encouragement.

Lastly, I want to give a special thanks to my advisor Wolfgang Losert for this opportunity and having the courage to pursue high-risk research projects. It has been a pleasure working with someone who has the collaborative vision to couple together the right synergy between questions, technologies, and models in this fast-growing interdisciplinary world. Every time that I hit a research roadblock, he always had a new technique to try or question to pursue.

Table of Contents

List of Figures

List of Abbreviations

α	alpha
β	beta
AMP	Adenosine monophospate
AMPK	AMP-activated protine kinase
CSC	Cancer Stem Cells
CTC	Circulating Tumor Cells
DMSO	Dimethyl sulfoxide
ECM	Extracellular Matrix
EMT	Epithelial to Mesenchymal Transition
ENT	Etinostat
EB1	End-Binding Protein-1
FITC	Fluorescein isothiocyanate
GFP	Green Fluorescent Protein
HMLE	Human mammary epithelial cells
IREAP	Institute for Research in Electronics and Applied Physics
McTN	Microtentacles
MLCK	Myosin Light Chain Kinase
MTOC	Microtubule-Organizing Center
NF-κB	Nuclear factor-kappaB
NMII	Non-Muscle Myosin-II
NIH	National Institute of Health
shRNA	Small hairpin RNA
PTEN	Phosphatase and tensin homolog
ROCK	Rho-associated protein kinase

Chapter 1: Introduction

1.1 Cancer and Physics: a Historical Perspective

Humanity has known about cancer for thousands of years. The first documentation of cancer is found in the Edwin Smith Papyrus dating back to 3,000 BC and describes breast cancer [4]. The word 'cancer' itself dates back to the ancient Greeks' father of medicine Hippocrates due to the way cancer moves about and has crab-like projections [4, 5] (See Figure 1.1A). Since antiquity overall knowledge of cancer has sophisticated greatly from a large macroscopic tissue perspective down to the biomolecular level of signaling pathways. No timeframe has seen as extensive changes and strides in the epistemology of cancer as the last 150 years. Only in the this late modern period of the 1940s did cancer treatments begin to have less surgical approaches and usher in radically new advances such as chemotherapy, novel imaging techniques, and anticancer drugs [6].

As far back as antiquity and continuing into the more contemporary age of research, cancer has been noted for its physical properties. In fact, it has been argued that the first involvement of physics in cancer also dates back to the ancient Edwin Smith Papyrus papers which describe a cauterization technique using a fire drill [7]. Cancer is universally recognized by patients to have mechanically stiff and

lump-like properties. The term 'biophysics', however, was not coined until Karl Pearson′s publication of "Grammar of Science" book in 1892 [8]. Only 5 years later in 1897, Emil Grubbe treated breast cancer with radiation for the first time [9, 10]. Eventually, many of those developments in radiation research formed the foundations of what is now called medical physics and is usually applied to fields such as radiation oncology, nuclear medicine, and radiology [11]. The field of 'biophysics' has grown to encompass a much broader scope of applications including migration, environmental sensing, mechanosensing, gene regulatory networks, protein interactions, electrophysiology, membrane channels, dynamics of self-assembly, soft matter, molecular machines, etc.

Today, cancer continues to pose many interesting questions for physicists. Possibly no cancer process is richer in biomechanically interesting problems than the metastatic cascade. Currently, most metastatic studies examine causal relations between metastasis and biomolecular dominant mechanisms such as cell signaling pathways, growth hormones, and genetics [12, 13]. Research in this inherently motile phenomenon paints a picture of a plethora of mechanically driven systems including motility, cell material properties (i.e. viscoelasticity), attachment, and mechanosensing. Clinically, changes in mechanical properties in situ are associated with higher metastatic risk; for example, increased collagen stiffness in human luminal breast tumor tissue is correlated with a poor prognosis for survival [14]. Cells with higher metastatic potential exhibit changes in mechanical phenotype both in terms of mechanosensitivity [15] and material properties [16]. Perhaps cancer research has spiraled full circle since antiquity, from tissue down to the cellular level,

as contemporary cancer research has recently discovered morphologically fingerlike structures on the cellular level sufficient for cancer reattachment in breast cancer cell lines called microtentacles (See Figure 1.1B). Microtentacles are hypothesized to form as the result of unbalanced forces between microtubules and actin resulting in the extension of the plasma membrane beyond the actin cortex. A pubmed search for cancer and cytoskeleton yields 16,037 publications; most of these studies focus on migration though. A search for circulating tumor cells and cytoskeleton, on the other hand, yields only 20 results, 10 of which examine microtentacles. Given that microtentacles dominate the cytoskeletal literature for CTCs, and understanding the mechanics of CTCs is arguably as important as understanding migration in cancer research, I propose that understanding the dynamics and mechanics of microtentacles is a critical biophysical question.

In today′s world of modern technology, the tools to probe cancer have grown far beyond ancient fire drills and gross anatomy. With the advances of transfection and fluorescent techniques, virtually any protein can be visualized; this, alongside strides in microscopy that allow high-speed imaging at super-resolutions and comprehensive computational power for analysis, open up new scientific opportunities never before explored. The goal of my thesis is better understand the mechanical interplay between the actomyosin cortex and microtubules, and how these interactions contribute to Microtentacle formation. I hypothesize that using drugs to alter the actomyosin cortex or microtubule stability will result in differences in the protrusiveness and dynamics of microtubule growth in both attached and suspended cells.

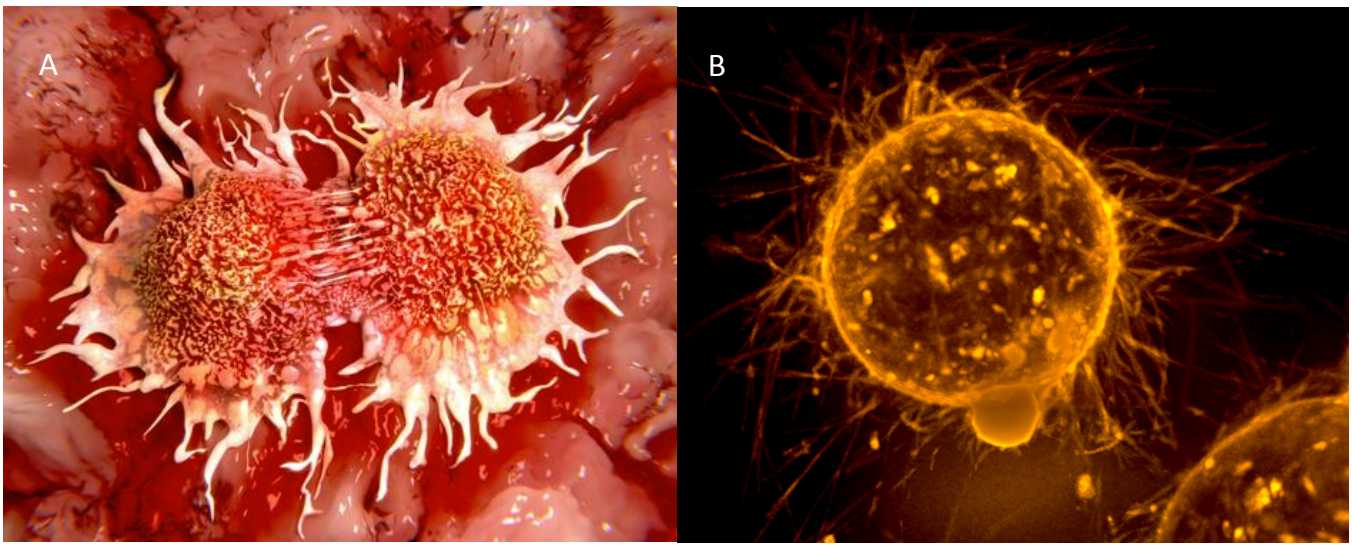

Figure 1.1: Cancer at Tissue and Cellular level. A. Tissue level illustration of Crab shaped tumor shows finger-like protrusions *Permission granted from Journal of Pioneering Medical Sciences Blogs, 2014* [17]. B. Cellular level suspended Tumor cells show long spindly protrusions called microtentacles. Early cellmask image taken by Eric Balzer.

1.2 Metastasis Causes Cancer Mortality

Cancer continues to be an epidemiologically significant disease responsible for killing approximately 590,000 people every year [18]. Also, there are currently an estimated 20 million people in the US who have been diagnosed with cancer [19]. This high number makes cancer the 2nd leading cause of death in the United States [18]. Within that cancer mortality figure, metastasis is currently responsible for 90% of all those cancer fatalities [1–3]. Despite the fact that metastasis is the major mechanism of death for the overwhelming majority of cancer, only 5% of cancer research funding goes towards studies specifically investigating metastasis for both basic and clinical research [20].

The metastatic cascade begins with a primary tumor in the host site where tumor cells are pathological cells of the host tissue (See Figure 1.2). Next, tumor cells begin to push out of the primary tumor and migrate, a process known as invasion. Following, cells squeeze out of the primary tissue and into the blood stream or lymphatic system in a process called intravasation. Once cells are circulating in the bloodstream, they are known as circulating tumor cells or CTCs. Reattachment happens when CTCs embed themselves on the endothelial cells. Finally, the pathological cells will undergo extravasation or exiting the bloodstream and invading into a distant tissue site. Once out of the bloodstream, the cancer cells colonize the second organ forming a secondary or metastatic tumor.

While primary and secondary tumors tend to have similar genetic profiles, there are often distinct differences in the genetic signatures and more mutations

in the primary than secondary tumors [21–23]. Predictably, secondary sites often respond differently to drug therapies than the primary site behaves; the result is a dearth in the efficacy of metastatic treatments [24]. In order for cancer therapies to be more effective in preventing metastasis, more research studies that focus on mechanisms specific to metastasis need to be conducted.

It is worth noting that the vast majority of cancers, in fact 90%, are carcinoma types or comprised of epithelial cells; this is probably due to the fact that epithelial cells frequently divide [25]. Interestingly, most epithelial cells die in the bloodstream by a process called anoikis; anoikis is a form of cell suicide triggered by loss of attachment to the extracellular matrix (ECM). Cells that don′t die by anoikis are often ripped apart by the high magnitude of shear forces especially in the small capillary tubes [26]. Overall, only an estimated .01% of CTCs are thought to survive the bloodstream [27]. Even within research on the metastatic cascade though, most studies focus on invasion and migration rather than the behavior of CTCs or reattachment. With so many natural obstacles between when a cancer cell enters the bloodstream until when it extravasates, this phase would seem a critical rate-limiting stage within the metastatic cascade and an ideal place to target with interventive therapies.

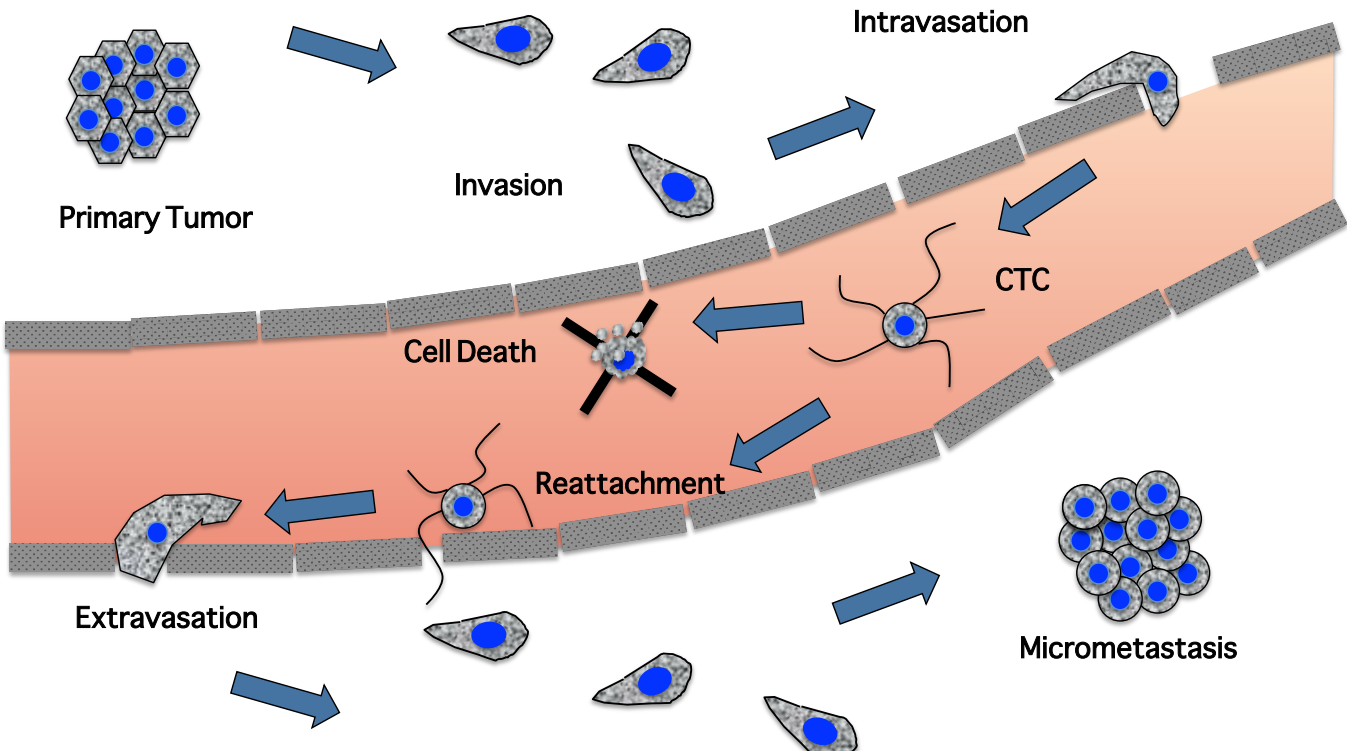

Figure 1.2: Metastatic cascade. Cancer begins as a *primary tumor*. Next, tumor cells begin to push out of the primary tumor and migrate, a process known as *Invasion*. Following, cells squeeze out of the primary tissue and into the blood stream or lymphatic system in a process called *Intravasation*. Once cells are circulating in the bloodstream, they are known as circulating tumor cells or a *CTC*. Most CTCs undergo *Cell Death* due to being ripped apart from fluidic shear forces or an epithelial apoptotic process called anoikis. *Reattachment* happens when CTCs embed themselves on the endothelial cells. Afterwards, the pathological cells will undergo *extravasation* or exiting the bloodstream and invading into a distant site in a process called *MET/Colonization*. Once out of the bloodstream, the cancer cells colonize the second organ forming a *Micrometastasis* or secondary tumor.

1.3 Tumor Cell Circulation and Reattachment During Metastasis

Currently, two of the most poorly understood steps in the metastatic cascade are reattachment and extravasation, and there exist very few therapeutics targeting these steps. The extravasation cascade as a whole, can be broken down into 3 steps: loose attachment, tight attachment, and squeezing between the very tightly connected epithelial cells lining the blood vessels called endothelial cells [28]. Thus, for the purposes of this section, reattachment will be treated as a sub-step of extravasation. For cancer specific extravasation, not a lot of basic research has honed in on the exact mechanism by which a CTC manages to reattach itself to the blood vessel walls, break through, and wedge itself in between those tightly connected endothelial cells. Here, I review and summarize some of the existing research and theories positing how CTCs manage to reattach and exit the blood stream as well as why the discovery of microtentacles is significant.

1.3.1 *Leukocyte extravasation*

Perhaps one of the most studied forms of extravasation is the extravasation of non-pathological leukocytes or white blood cells. Much of cancer extravasation research studies leukocyte extravasation in the hopes of finding similarities between the leukocyte extravasation and CTC extravasation. In healthy individuals, leuko-

cytes are responsible for dealing with inflammation and infections; to accomplish this task, leukocytes travel through the bloodstream and must extravasate through the endothelial cells to the site of injury or infection [28]. Leukocytes initiate contact with endothelial cell adhesion molecules called selectins to form a transient connection with the endothelial cells [28]. Because this adhesion is weak, the bloodstream continues to push and ultimately causes the leukocyte to 'roll'. It is proposed that this rolling behavior may be how CTCs also reattach [29]. It is also possible that leukocytes act directly in cancer extravasation by forming a linker between tumor cells and endothelial cells as shown in a study with neutrophil granuloctyes between MDA-MB-468 and pulmonary epithelial cells [30]. More direct evidence of CTC rolling behavior is demonstrated in one study by flowing MCF-7s across surfaces functionalized with E-selectin [31]. Unlike leukocytes where L-selectin is established as responsible for binding to the endothelial cells′ E-selectins, on the MCF-7 cells, CD24 was implicated as the ligand responsible for rolling [31]. However, there maybe be a considerable gap between E-selectin coated surfaces versus endothelial E-selectin expression. Clinically, tumors with high levels of activated leukocytes are associated with a more aggressive disease [27]. Furthermore, a rolling mechanism of CTCs has not been observed in in vivo studies [26].

1.3.2 *Platelet and CTC interactions*

Interactions between platelet and CTCs interactions are also thought to play a critical role in extravasation. It has been demonstrated that activation of platelets

increases metastatic potential [26, 32]. Platelets may play a role helping CTCs survive the bloodstream by attaching and preventing cell death mediated by natural killer cell lymphocytes [27, 33]. There is also evidence that platelets protect CTCs from shear forces directly [33]. Additionally, platelets may be involved in leukocyte assisted reattachment. Evidence suggests that in places where there are high shear forces that would make a rolling mechanism unlikely, platelets are involved in assisting leukocytes [28]. In addition to helping CTCs survive the blood stream, studies show that platelets can activate EMT pathways in circulating tumor cells [23]. Furthermore, genetically modifying the platelet pathway or depleting platelets reduces metastasis [23, 26, 33]. Clinically, an increase in platelet count is associated with poor patient prognosis [23]. Also, for melanoma cancer, platelet behavior increases metastasis in the lung [33].

1.3.3 *Vascular permeability*

Another important factor that may contribute to CTCs′ ability to exit the bloodstream is vascular permeability. Endothelial cells use connections called Tight junctions and Adherens junctions to control paracellular transport [34]. Indeed, the endothelial junctions are so tight that it prevents transit of macromolecules larger than 3 nm [34]. It has been shown that damaging the endothelial cells in mice can increase metastasis [34]. Furthermore, studies show examples of cancer cells with higher metastatic potential excreting factors known to disrupt endothelial cell-to-cell junctions [23, 34]. On the other hand, only 20% of leukocytes use transcellular mi-

gration. Also it is unclear that an increase in vascular permeability is even necessary for leukocytes to migrate through endothelial cells. [34].

1.3.4 *Capillary Entrapment*

Perhaps the simplest mechanism of reattachment proposed in the literature, suggests that CTCs simply get trapped in narrow capillary tubes before extravasating [29]. This mechanism makes sense for places with narrow capillary tubes like the lungs. Considering that lungs are the most frequent site of metastasis for breast cancer [2, 24], this is conceivably an important factor for some metastases but not all.

1.3.5 *Microtentacles*

While the above research shows many potential signaling pathways, none of this research suggests a particular cell morphology identifying which CTCs are most likely to metastasize. Additionally, research shows that under the shear forces of the bloodstream, integrin mediated binding of tumor cells with endothelial cell selectins is insufficient and suggests that the actomysin cortex or microtubule involvement may be necessary [35]. It has been demonstrated that more malignant cancer cells are more resistant to fluid shear forces [36]. More recently, morphological protrusions called microtentacles (McTNs) have been discovered. Previous studies demonstrate McTN protrusions poking in between endothelial cells indicating that a McTN-mediated reattachment would most likely would assist CTCs between a loose and

tight attachment phases [37, 38].

1.4 Microtentacles Promote Tumor Cell Reattachment

One particularly interesting mechanism on how circulating tumor cells reattach posits that tubulin-based structures called microtentacles or McTNs increase the retention of circulating tumor cells in the capillaries of distant tissues (Figure 1.3). Based on reviewing the McTN literature, the presence of McTNs appears to be a sufficient condition for *in vitro* attachment [38–46]. Evidence also supports that McTN-positive cells attach to endothelial cells [37, 38] (See Figure 1.4). Injection of cells with McTNs into mice show that they get trapped and retained in the lungs [47].

Previous research has implicated detyrosinated α-tubulin for the unique McTN structure [38, 48]. Detyrosinated α-tubulin is also called glu-tubulin due to the loss of the c-terminal tyrosine resulting in the exposure of the glutamic acid residue. Immunofluorescence of suspended cells stained for α-tubulin demonstrate that the protrusions are made up primarily of microtubules [41]. Furthermore, Electron Microscopy results show McTNs comprised of several microtubules [49]. On a clinical level this is relevant because an increase in the levels of glu-tubulin is an indicator of poor prognosis [50]. Cell culture experiments demonstrate that glu-tubulin turnover has a much longer persistence time on the scale of hours compared to α-tubulin which only has a persistence on the scale of minutes [38,51]. Thus glu-tubulin is potentially an important indicator of the possibility of McTN formation. Furthermore, it has

been demonstrated that McTNs are not the result of actin-based invadapodia [47].

From a biochemical and signaling perspective, pathways that stabilize tubulin also stabilize McTNs. For example, vimentin is an intermediate filament that colocalizes and aligns along microtubules which may help stabilize the tubulin struts. [42]. Removing or inhibiting vimentin reduced McTNs and reattachment [42]. In a less direct technique, entinostat (ENT), a histone deacetylase inhibitor demonstrated vimentin disassembly, weakening microtubules and causing a decrease in McTN phenotype [45]. On a clinical level, vimentin has been identified as a marker for breast cancer cells more likely to metastasize [42]. Anti-inflammatory agents Parthenolide and costunolide destabilize tubulin, decrease detyrosinated tubulin, and reduce McTNs [40]. Lastly, kinesin motor proteins are thought to cross-link vimentin and glu-tubulin; inhibiting kinesin motors with tetracaine also inhibited McTN formation [44]. Basically, McTNs can be increased by stabilizing microtubules and decreased by depolymerizing microtubules.

In addition to microtubule manipulations, it appears that McTN formation can also be modulated by manipulating the actin cortex. Unlike actin-based invadapodia, McTNs are predominantly composed of microtubules, and do not require actin support. Studies that remove actin polymerization by using Latrunculin-A still have McTNs, [42, 44, 52]. Inhibiting actin cortex contractility indirectly via Rho-associated kinase (ROCK) inhibitor Y27632 increases McTNs, while using Rho Activator II decreases McTNs by making the actin cortex more contractile [39]. Another study used genetic modifications of c-Src to make the actomyosin cortex more contractile or by making c-Src less active and weakening the actomyosin cortex [47]

The more contractile actomyosin cortex from overactive c-Src had less McTNs, and weaker actomyosin cortex from inactive c-Src had more McTNs [47]. Additionally, inhibiting AMP-activated protein kinase AMPK, activates actin severing protein cofilin, weakening the actomyosin cortex causing an increase in McTNs and reattachment [43]. Yet another example used shRNA to downregulate obscurins, decrease RhoA phosphorylation, ultimately decrease actomyosin contractility through the myosin light chain causing an increase in McTNs [46].

Cells thought to have higher metastatic potential also have more McTNs. For example, breast cancer cell lines scored positive for McTNs also positively correlated with Cancer Stem Cell (CSC) markers [53]. Cells undergoing EMT have long been of interest in metastatic research due to their association with invasion, and EMT cells have a similar phenotype to CSCs [54]. Cells induced for EMT phenotype by overexpressing transcripton factors twist and snail also increase McTNs [37]. Loss of well-known tumor suppressor gene PTEN is also with associated high metastatic potential and induces EMT [55–58]. Research shows that knocking down PTEN in mammary epithelial cells induces McTNs [41].

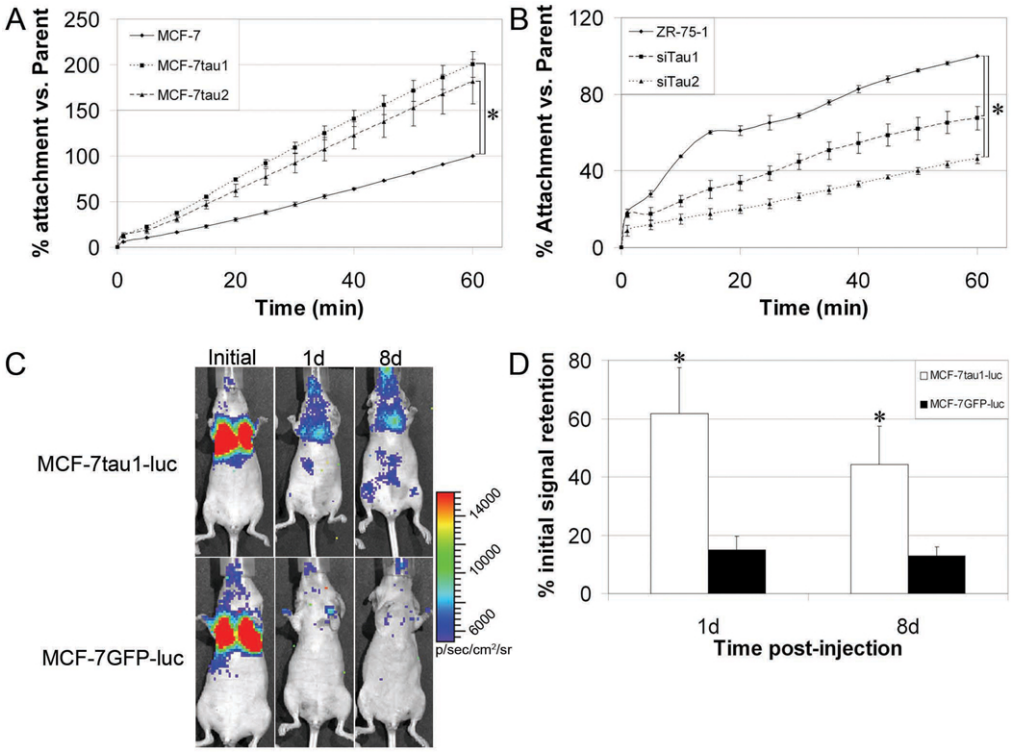

Figure 1.3: Initial cell attachment is dependent on McTN formation as affected by tau. (a) Over 1 h, MCF7 cells stably overexpressing GFP-tau (MCF-7tau1 and MCF-7tau2) attach more efficiently (200 and 180%, respectively) compared with MCF-7 controls. Data (n=4) represent the mean percentage of attachment±s.d. *P<0.01. (b) Over 1 h, siTau1 and siTau2 attach less efficiently (67 and 46%, respectively) compared with ZR-75-1 controls. Data (n=3) are represented as the mean percentage of attachment±s.d.*P<0.01. (c) Glowscale of luciferase-expressing cells injected into the tail vein of nude mice show equal initial signal retention in regions of interest (ROI) emcompassing the lungs. Over a period of 8 days post-injection, MCF-7tau1-luc cells are more retained than control MCF-7GFP-luc cells. (d). On average over all injections, 61.8 and 44.4% of MCF-7tau1-luc cells (n=6) were retained in lung capillaries 1 day and 8 days post-injection. In comparison, 15.9 and 12.9% of control MCF-7GFP-luc cells (n=5) were retained at the same time points. This difference was significantly different for both 1 day (*P<0.02) and 8 days (**P<0.05) post-injection by a non-parametric t-test. *Figure reproduced with permission from Nature Publishing Group* [59].

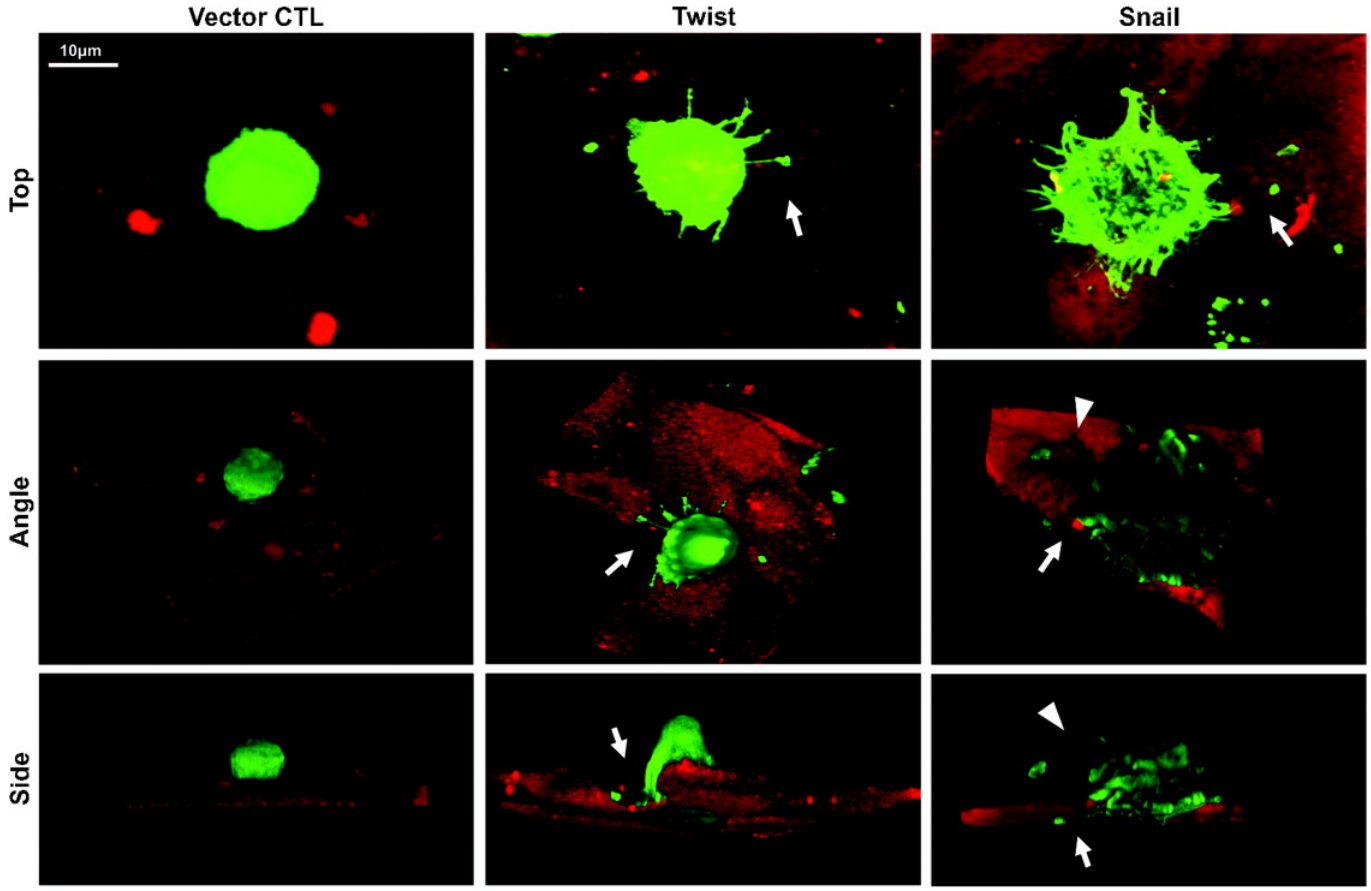

Figure 1.4: Microtentacles facilitate HMLE-endothelial attachment. Confocal imaging of GFP-Membrane transfected HMLE cells suspended for 20 min over a confluent layer of mCherry-labeled HBME. Top, angle, and side views of HMLE cells at the early stages of attachment show HMLE-GFP vector control cells rounded without observable microtentacles. HMLE-Twist displays a microtentacle anchoring to the top of the HBME (white arrow). HMLE-Snail exhibits microtentacles extending under (white arrow) or bending toward (white arrowheads) the HBME layer. *Figure reproduced with permission from American Association for Cancer Research* [40].

1.5 Microtentacles from a Biophysical Perspective

McTNs are a particularly interesting phenomenon, not just for their potential role in metastasis, but also as a physical phenomena that most likely stems from mechanical interactions within the cytoskeleton. Based on the biochemical alterations outlined in previous studies reviewed above, it has been proposed that McTNs are the result of unbalanced forces between the actin cortex and microtubules following a tensegrity model [38]. The mechanical tensegrity model consists of stiff struts that act as continuous compression members while cables connected to these struts are in continuous tension and maintain the shape [60] (Figure 1.5A). Applied to a biological cell, actin filaments act as the tension members, microtubules as compression members, and apply these forces to anchor proteins (i.e. integrin) where the cell adheres to the ECM [60] (Figure 1.5A). Thus, the tensegrity model is really only applicable to attached cells and not fully applicable to CTCs. Furthermore, the tensegrity model does not account for dynamically growing and shrinking microtubules, constantly changing actin cortex, nor the viscoelastic properties of the cell [61]. Here, I discuss some the relevant cytoskeletal literature and present possible scenarios for how the tubulin and the actomyosin network interact mechanically. I propose that ultimately, even though there are many possible scenarios, a simplified assumption that microtentacles form as the result of unbalanced forces remains valid.

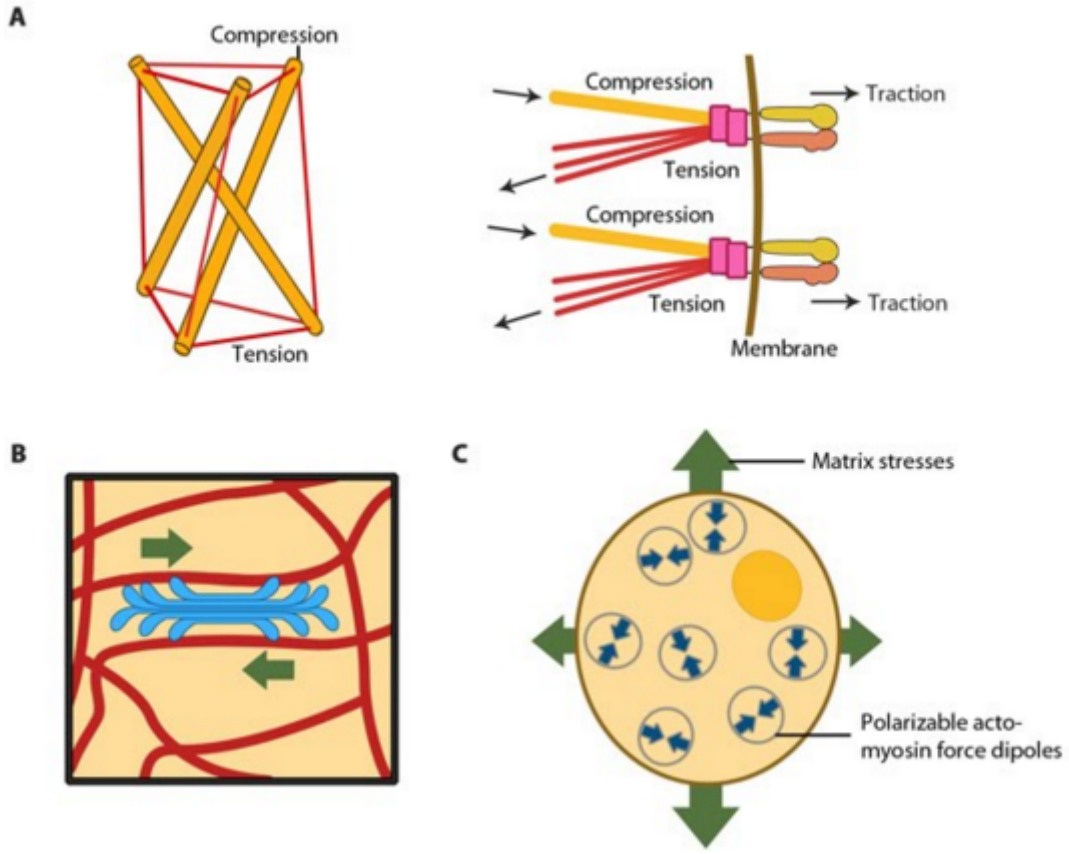

Figure 1.5: Models for force-induced modulation of cytoskeletal stiffness. (A) Tensegrity model: Top left- A simplified version with compression struts and tensed cables exemplifying that stress levels regulate cytoskeletal rigidity. Top right- In the cellular context, microtubules (gold rod) apply compression on cell-matrix adhesions (represented by actin linking modules in pink and integrin dimers) while the actin filaments (red) experience the cellular tension and hence stiffen accordingly. (B) Semiflexible chain model is represented by the flexible actin cables (red) that locally rigidify at points of stress application i.e. myosin (blue bundle) contraction. (C) Dipole polarization model: Formation of contractile actomyosin dipoles is symbolically represented by the arrow pairs. According to this model, they freely orient in response to applied stress as experienced at a particular point. Adapted from Stamenovic D. Ingber DE. Tensegrity-guided self assembly: from molecules to living cells. Soft Matter 2009; 5:1137-45. [DOI: 10.1039/B903916N] and [20816234]. *Used by permission from MBInfo: www.mechanobio.info; Mechanobiology Institute, National University of Singapore.* [62]

1.5.1 *Tubulin*

Detyrosinated tubulin or glu-tubulin forms the basis of the microtubules comprising McTNs [37]. The outer diameter of a microtubule filament is 25 nm; tubulin varies in strength and stability, and the contributions of tubulin detyrosination to stabilized McTNs is unclear. In *in vitro*, for example glu-tubulin and α-tubulin have similar polymerization rates [63]. In *in vivo* experiments, though, there is evidence to suggest that detyrosinated tubulin depolymerizes more slowly [64]. However, glu-tubulin alone does not increase *in vivo* microtubule stability [65]. Also, the cell can quickly adjust detyrosination; for example, if glu-tubulin is microinjected into the cell, it is quickly tyrosinated [66]. More likely, glu-tubulin gets its stability from binding to intermediate filaments (IFs) like vimentin. It has been shown that vimentin colocalizes to glu-tubulin as well as binds to glu-tubulin with 3 times the affinity as α-tubulin [67,68]. Tau stabilizes microtubules by bundling them together and can work competitively with taxol [69, 70]. It is also noteworthy that kinesin, another tubulin crosslinker, prefers to bind to glu-tubulin [68]. Mechanically, buckling experiments support the idea that microtubules bear significant compressive cellular load [61, 71].

1.5.2 *Actomyosin Cortex and Model*

The actomyosin cortex is a contractile meshwork near the cell membrane that ranges in thickness from 50nm - 1 μm [72] (Figure 1.6). The actomyosin cortex is a meshwork of actin filaments near the plasma membrane; mesh size can vary from

20 nm [73] to as large as 200 nm [74]. The actomyosin cortex is a dynamic system where actin filaments are being continuously polymerized and breaking. Additionally important, the actomyosin cortex is contractile where myosin walks along the actin filaments and pulls the fibers towards each other (See Figure 1.5B and 1.6). On a cellular level, one can think of the net effect of these moving actin filaments as creating localized anisotropic contraction dipoles (See Figure 1.5C) and as having a net pulling force toward the center of the cell (See Figure 1.6).

Thus, there is an actomyosin cortex that pulls inward and generates tension, and compressive load-bearing microtubules pushing outward [15, 75, 76]. In a normal cell, the microtubule pushes against the actin meshwork, the actomyosin cortex contracts along the membrane causing the membrane to pull inward, and no McTNs form (See Figure 1.7). For McTN formation, I propose 3 possible ways in which microtubules can penetrate the actomyosin cortex: loose network, deforming network, and a breaking network. In a loose actomyosin network, variations in meshwork size are sufficient perhaps for a 25 nm microtubule to push through a 200nm hole and beyond the actin cortex for cases of larger mesh size (See Figure 1.8) 200 nm [74]. Furthermore, in at least one immunofluorescent study with blebbistatin treated cells, microtubule protrusion extension beyond the cell body boundary shows minimal or sparse colocalization with F-actin [77]. Another possibility, is that the actomyosin network exerts a weaker force, but gets stretched or deforms along the microtubule (See Figure 1.9). Experiments showing colocalization of actin and McTNs might suggest this mode [41]. At least one immunofluorescent study in attached cells shows a thick, consistent layer of actin alongside microtubule protrusions [78]. Lastly, it

is possible that the actomyosin cortex would simply fail, either due to the strength of the microtubules, brittleness of the actin cortex, or signaling that locally depolymerizes the actin filaments (See Figure 1.10). In at least one immunofluorescent study of bacterial toxin on mammalian cells, microtubules protrude beyond the cell body boundary and there are very distinct gaps of the actomyosin cortex where the protrusions stick out suggesting breaks in the actomyosin cortex [79]. Another study supporting this model shows that the actomyosin cortex breaks under tension from a aspirating micropipette and creates a 'window′ in the actomyosin cortex [80]. Regardless of how the microtubules interact with the actomyosin cortex directly, this process can be simplified to the idea that the cortex acts as a mechanical barrier (See Figure 1.11).

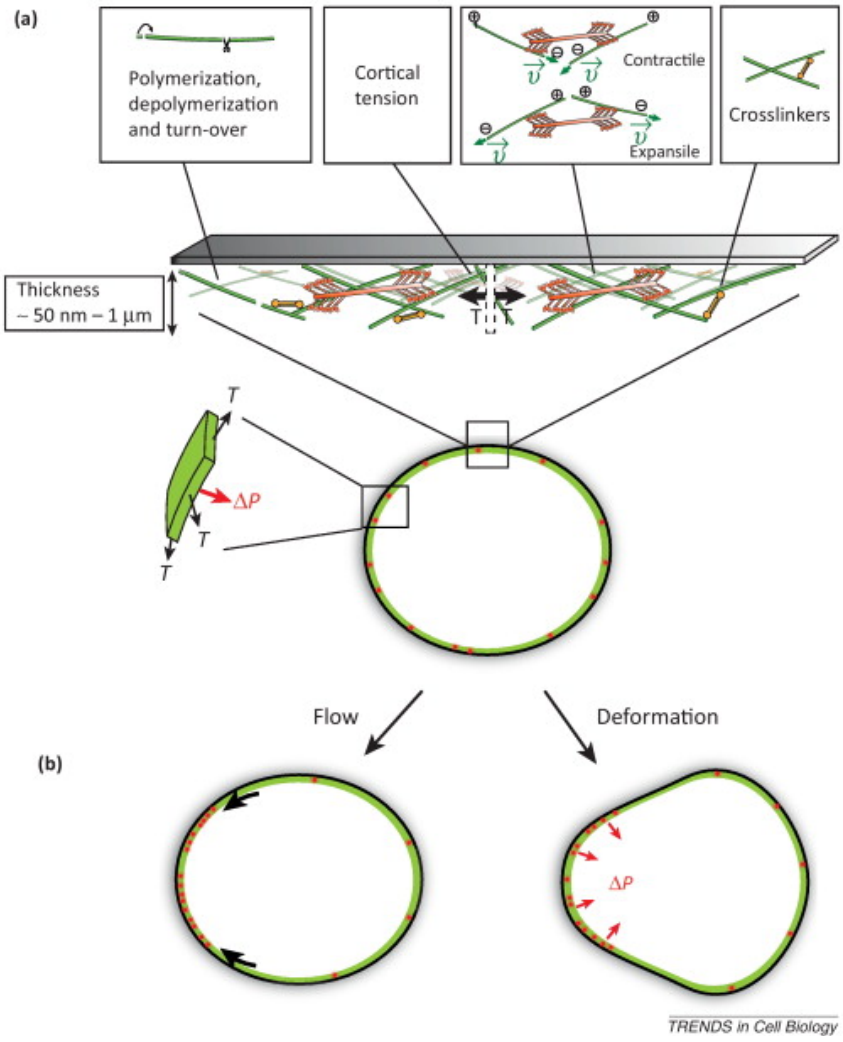

Figure 1.6: Cortex tension and cell shape. (a) Actin filaments assemble into a thin network connected to the cell membrane and undergoing continuous turnover. Myosin motors exert forces in the network, giving rise to a cortical tension, T. Motors are assembled into mini-filaments, which connect pairs of actin filaments and slide them with respect to each other. This can result in contractile or expansile stresses, depending on the position of the motors on the actin filaments (top right). Why contractile stresses dominate, giving rise to a positive tension in the network, is not fully understood. Crosslinks in the network could contribute to the generation of tension; crosslink turnover is a major determinant of cortex viscoelasticity. (b) Because of the cell curvature, cortical tension gives rise to a hydrostatic pressure in the cytoplasm. Gradients of motor-generated contractility within the cortex can drive tangential flows of cortex in the plane of the membrane (left), whereas normal forces can drive cell deformations with net displacement of the cytoplasm (right). *Figure reproduced with permission from Elsevier* [72]

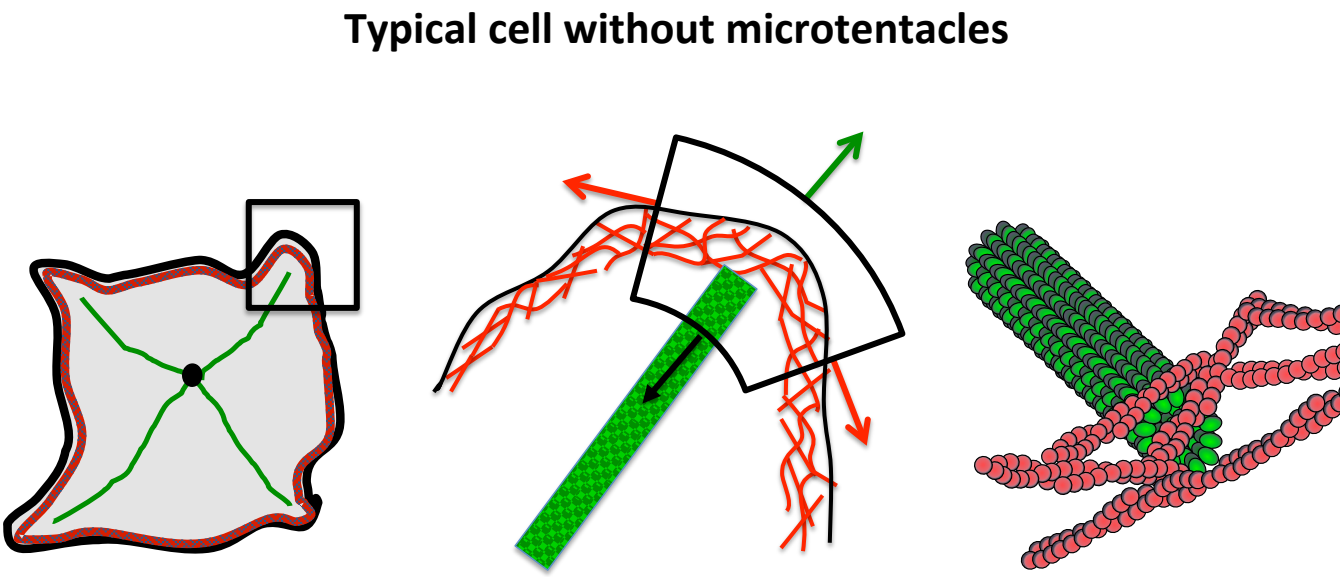

Figure 1.7: In a normal cell, forces between microtubules and actin cortex are balanced. Red arrows represent pull of actin cortex toward center of cell; green arrow, microtubule pushing outward; black arrow, membrane pulling back against microtubule (red-actomyosin cortex, green-microtubules, black membrane).

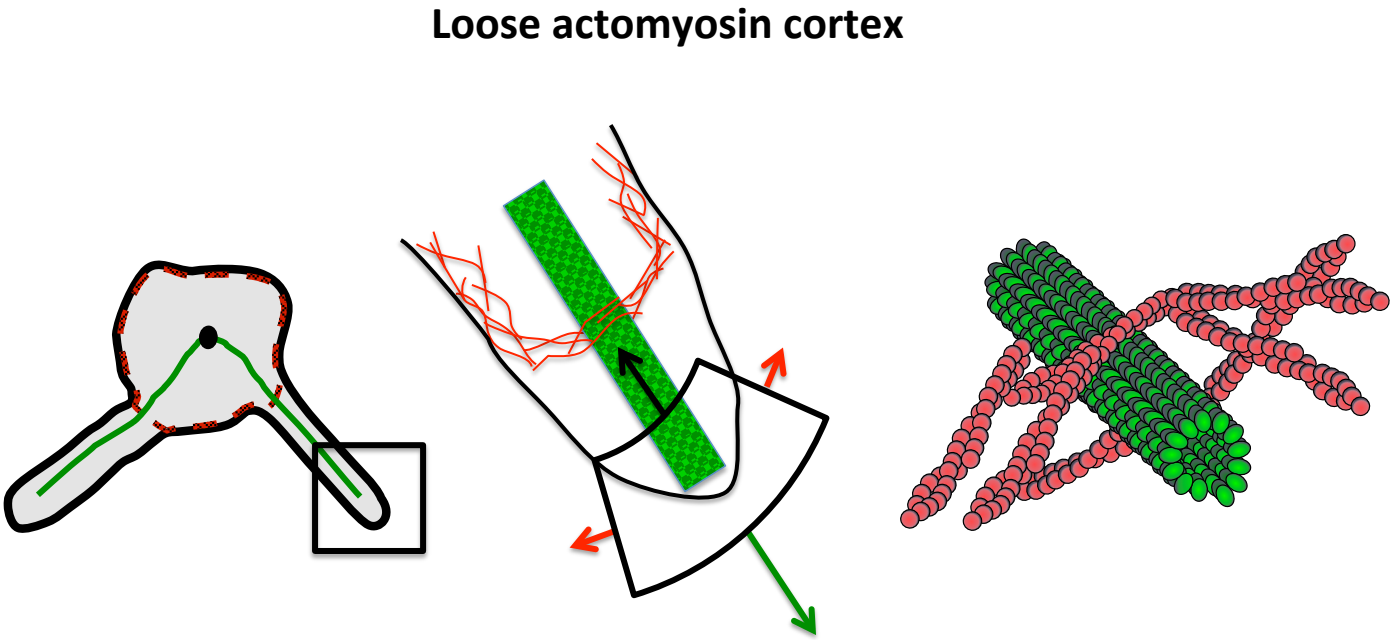

Figure 1.8: One hypothesis is that Microtentacles form when the actomyosin cortex is loose, pushing through the meshwork. Red arrows represent pull of actin cortex toward center of cell; green arrow, microtubule pushing outward; black arrow, membrane pulling back against microtubule (red-actomyosin cortex, green-microtubules, black membrane).

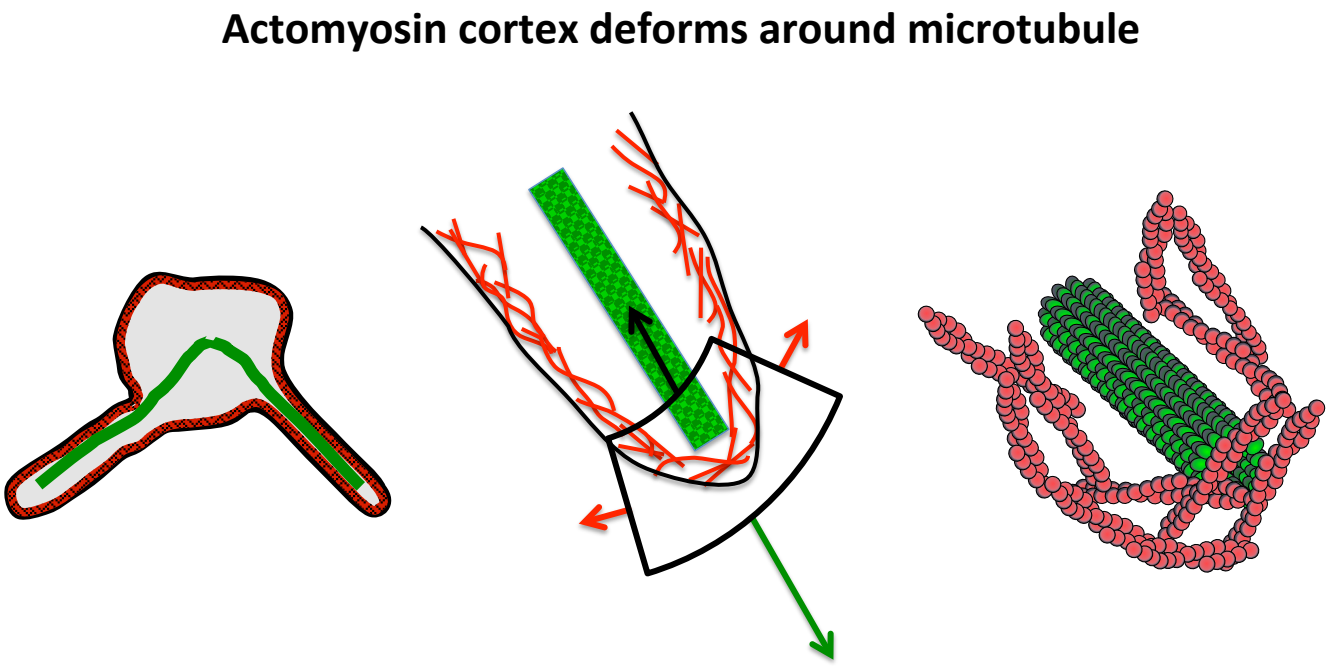

Figure 1.9: One hypothesis is that Microtentacles form when Actomyosin cortex deforms and stretches around the microtubule. Red arrows represent pull of actin cortex toward center of cell; green arrow, microtubule pushing outward; black arrow, membrane pulling back against microtubule (red-actomyosin cortex, green-microtubules, black membrane).

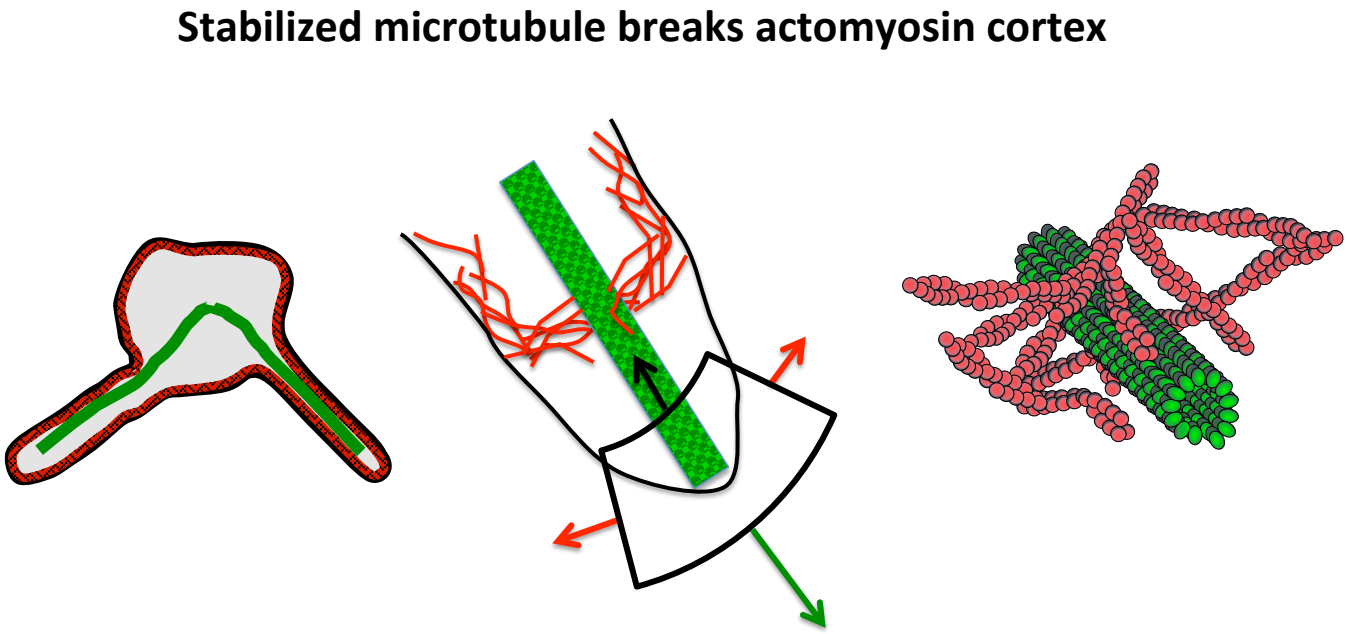

Figure 1.10: One hypothesis is that Microtentacles form when Actomyosin cortex breaks and the microtubule is allowed to move through. Red arrows represent pull of actin cortex toward center of cell; green arrow, microtubule pushing outward; black arrow, membrane pulling back against microtubule (red-actomyosin cortex, green-microtubules, black membrane).

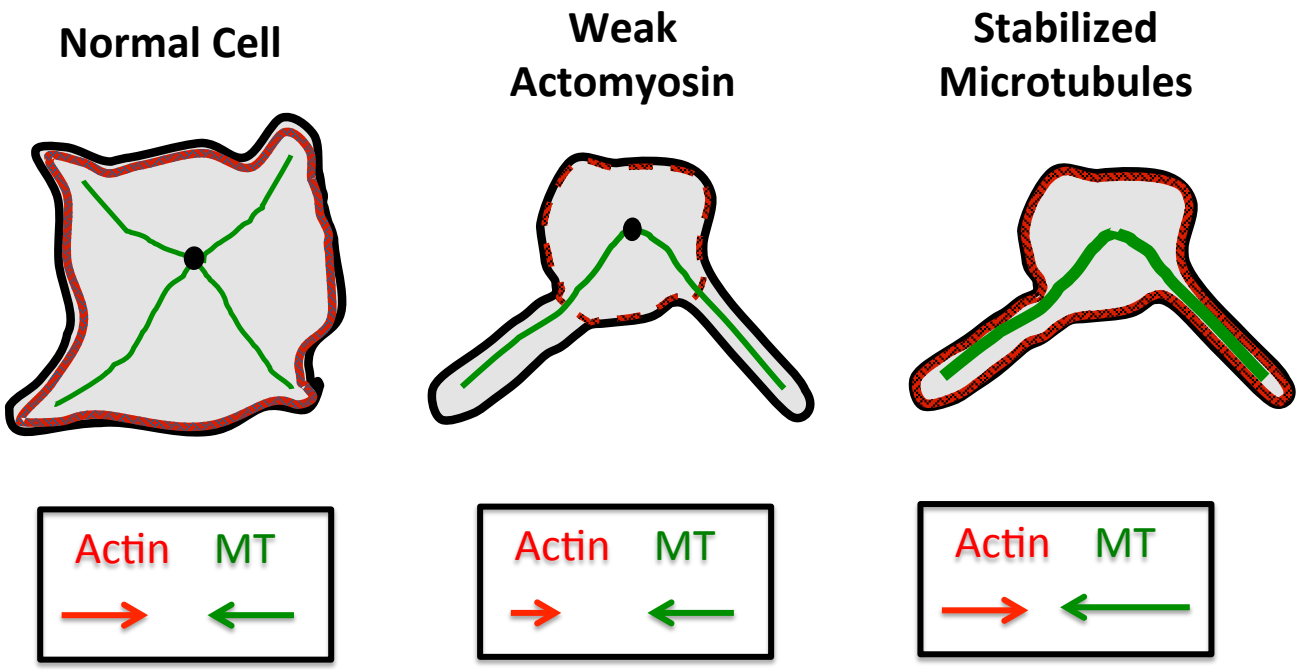

Figure 1.11: Microtentacles for when Actomyosin cortex is weak or tubulin is stabilized where actomyosin cortex is in tension and microtubules are in compression.

1.5.3 *Differences in adherent cells and suspended cells*

The models outlined above are intended primarily for suspended cells, however it is worth discussing some of the differences in mechanics between suspended and attached cells. The tensegrity model is also mostly intended for attached cells but makes the claim that cytoskeletal prestress exists for suspended cells [61]. Additionally, the tensegrity model cites a study where increasing contact density to ECM or substrate attachment causes an increase in cell stiffness [81] and argues that the tensegrity model predicts cell softening for cells in suspension [61]. This is in direct conflict with the studies in the literature that compare attached and fully detached cells where measurements by both AFM and optical stretching show that detached cells increase in stiffness [82, 83]. Also in contrast with the tensegrity model are the prevailing migration models where protrusions are actin based, form due to actin polymerization, and push rather than pull the edge of the cell [84–86]. In the migration literature, the pushing of actin polymerization causes a decrease in local membrane tension allowing the cell to move forward [86]. In one of the more contemporary mechanotransduction models, integrin acts as a clutch and stiffer ECM substrates are able to provide a stronger reaction force and increase the push of the plasma membrane outward (See Figure 1.12) [85].

In general, McTNs are not normally observed in attached cells, which is most likely due to integrin anchoring unlike free-floating cells. While not outlined in my model above, based on the migration′s actin polymerization model, I would suspect that outward push of polymerization would lessen the net inward contractility.

This is consistent with some of the more recent schematics of actin protrusions, where without adhesions, the net retrograde flow of actin would be higher than the polymerizing flow [87]. As a result, there would be less opportunity for the plasma membrane to deform around the microtubules.

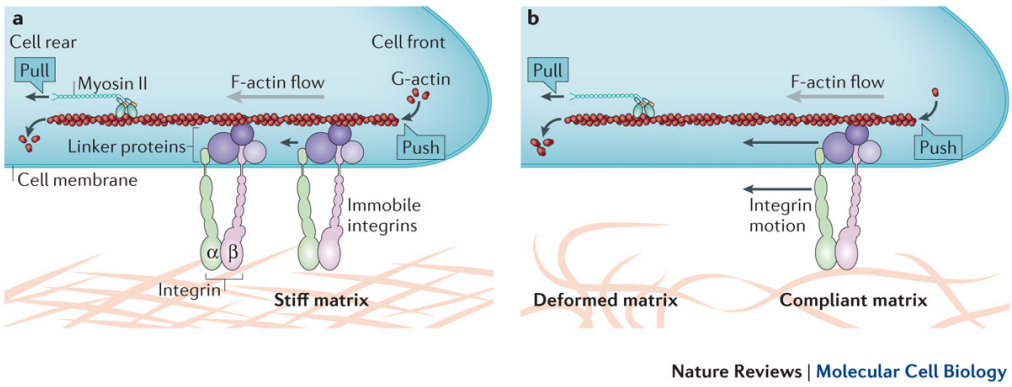

Figure 1.12: Force-mediated regulation of integrin adhesions. Schematic of the 'focal adhesion clutch′ on stiff (a) versus soft (b) extracellular matrix (ECM). In all cases, integrins are coupled to F-actin via linker proteins (for example, talin and vinculin). The linker proteins move backwards (as indicated by the small arrows) as F-actin also moves backwards, under pushing forces from actin polymerization and/or pulling forces from myosin II activity. This mechanism transfers force from actin to integrins, which pull on the ECM. A stiff ECM (a) resists this force so that the bound integrins remain immobile. A compliant matrix (b) deforms under this force (as indicated by the compressed ECM labelled as deformed matrix) so that the bound integrins can also move backwards. Their movement reduces the net loading rate on all the force-bearing elements, which results in altered cellular responses. *Reprinted by permission from Macmillan Publishers Ltd: Nature Reviews Molecular Cell Biology, copyright 2014* [85]

1.6 Goals and Hypothesis

I show in my thesis that changes to the actomyosin network, change behavior in microtubules in a manner consistent with the cortex acting as a barrier. I hypothesize that by either weakening the actomyosin cortex or stabilizing microtubules, there will be an increase in the distance of microtubule protrusions beyond the cell body boundary in both attached and suspended cells, but also to a possibly lesser extent in attached cells. I aim to develop quantitative assays to analyze the dynamics of microtubule growth and morphology in both attached and suspended cells in order to work towards determining distinct morphological signatures for different types of interactions between the actomyosin cortex and microtubules.

I demonstrate these goals, first, by showing how drug treatments targeting the actomyosin cortex impact microtubule dynamics for attached cells. Second, I demonstrate how targeting the microtubules directly in suspended cells and causes morphological changes to microtentacles. Throughout this process, I synthesize image analysis tools optimized for microtubule growth in attached cells and cell outlines in suspended cells. Additionally, I determine relevant metrics for morphology and dynamics

Chapter 2: Microtubule growth dynamics of breast tumor cells is altered by changes in actin network structure and contractility

This chapter was adapted from Ory, E.C-h., et al, "Microtubule growth dynamics of breast tumor cells is altered by changes in actin network structure and contractility", submitted to Physical Biology, 2016. Ory proposed drug treatments Blebbistatin and Latrunculin-A and Immunofluorescent experiments. Immunofluorescent experiments were conducted by Martin. EB1 experiments and imaging were conducted by both Martin and Ory. All analyses were implemented by Ory.

2.1 Summary (Abstract)

The periphery of epithelial cells is shaped by the balance of cytoskeletal physical forces generated by two dynamic force generating systems - growing microtubule ends push against the boundary from the cell center, and the actin cortex contracts the attached plasma membrane. Here we investigate how changes to the structure and dynamics of the actin cortex alter the dynamics of microtubules. Using human MCF-7 breast tumor cells expressing GFP-tagged microtubule end-binding-protein-1 (EB1) and co-expressing cytoplasmic mCherry, we analyze the trajectories of growing microtubule ends, and follow their position relative to the cell body boundary. Actin depolymerization with Latrunculin-A reduces the growth speed of microtubule ends, and increases the fraction of microtubule ends that protrude beyond the cell body boundary, forming localized tubulin rich protrusions. Reduc-

ing contractility of the actin cytoskeleton upstream of myosin II via the Rho-kinase inhibitor Y-27632 also enhances localized microtubule rich protrusions, but does not slow down microtubule growth. Direct inhibition of myosin II with Blebbistatin reduces microtubule growth speed and bends trajectories, but does not enhance localized protrusions. These results demonstrate that microtubule dynamics depend on both actin network structure and dynamics.

2.2 Introduction

The delicate balance between the physical forces of microtubule growth and actin network contraction that determines the shape of non-migratory cells is often disrupted in diseases, in particular when epithelial cells transform into carcinomas [38, 88]. Since more than 90% of human solid tumors arise as carcinomas from epithelial cells [89], understanding this balance of microtubule growth and actin network contractions in the context of epithelial cytoskeletal architecture has broad potential implications.

Microtubule polymerization initiates from the centrosome, also known as the microtubule-organizing center (MTOC), which is found in the center of eukaryotic cells (See Figure 2.1). Extension of microtubules toward the cell surface is counteracted in several ways by the cortex of actin filaments that lies beneath, and is linked to the plasma membrane [90, 91]. The mesh size of the actin cortex ranges from 20 to 250 nm [72], potentially providing a physical barrier for microtubule bundles, since individual microtubules are 25nm in diameter. Furthermore, the end-binding

protein-1 (EB1), which is attached to the growing ends of microtubules, can also bind to the actin cortex through association with the adenomatous polyposis protein (APC) [91, 92]. Thus microtubule ends couple to the actin cortex in multiple ways, thus allowing for a balance of forces between pushing and contractility [38, 90]. Unlike tensegrity networks with their balance of stationary tensile and load bearing elements, the actin cortex is dynamic with actin polymerization and depolymerization, and contraction mainly due to non-muscle myosin-II (NMII). The actin cytoskeleton can also stabilize microtubules and allow them to bear larger compressive forces within cells than is possible with purified microtubules in vitro [93]. Mechanotransduction in epithelial cells is known to be regulated by this balance between microtubules and actin filaments, and alterations of cytoskeletal structure and dynamics in epithelial tumor cells disrupt this balance [94, 95]. One important manifestation of this altered balance is microtentacles (McTNs), discovered by one of us as localized microtubule based protrusions that are found to protrude out from the otherwise spherical body of circulating tumor cells [38, 42, 96].

Given the role of actin filaments in cell division and motility, actin has also become a target for the development of cancer therapies [97, 98]. Inhibition of actin assembly and contractility are effective at reducing the growth and invasion of tumor cells [99–101]. However, there is growing evidence that targeting the actin cytoskeleton has consequences for other aspects of cancer progression. Toxins that alter either microtubules or actin can disrupt the ability of epithelial cells to respond to mechanical stimuli [102]. Compounds or genetic alterations that stabilize microtubules [59, 96] or reduce actin integrity [47, 96] promote McTN formation

and increase the retention of circulating tumor cells in the lung capillaries of living mice [47, 59]. Recently, it has also become clear that reducing actin contractility can actually increase stem cell characteristics in epithelial tumor cells [103–105], resulting in greater tumor-initiating capability.

Drugs altering the contractility of the actin cytoskeleton have recently demonstrated efficacy in enhancing the ability of patient-derived tumor cells to grow *in vitro*. Very recent studies show that even relatively short-term treatment with compounds which reduce actin contractility by targeting ROCK (Y-27632) or myosin-II (Blebbistatin) [106] can directly induce stem cell characteristics in epithelial tumor cells [103] that promote long-term growth of patient-isolated cancer cells [104, 105] and tumor formation in mice [103]. These results suggest that altering the mechanical tension of epithelial tumor cells can regulate their ability to proliferate in vitro and in vivo.

To improve our understanding of how altering actin integrity and contractility affects the cytoskeletal balance with microtubules, we use time-lapse confocal microscopy to track the movement of of the microtubule end binding protein EB1 in the epithelial breast cancer cell line MCF-7. Since EB1 is tightly coupled to the growing microtubule plus end [91, 107, 108], we infer microtubule growth from the motion of EB1. The schematic shown in Figure 2.1 shows the three manipulations of the actin cortex we use to investigate how actin integrity and contractility alters microtubule growth dynamics. Normally, the actin cortex enhances membrane tension [90] and resists growing microtubules from extending beyond the cell membrane [91]. Complete disruption of actin polymerization with Latrunculin-A should

make it easier for microtubules to grow beyond the cell body boundary. Targeting the Rho-kinase (ROCK) with the small molecule, Y-27632, inhibits activation of myosin-II and thereby reduces contractility of actin filaments within the cortex [109]. Likewise, Blebbistatin binds directly to myosin-II and disrupts actomyosin contractility [90, 106]. We selected Y-27632 and Blebbistatin also since both were shown to increase tumor stem cell characteristics [103–105] and aid proliferation of patient derived tumor cells in vitro.

2.3 Results

2.3.1 *Actin cytoskeleton integrity and contractility affects the structure of the microtubule network*

The microtubule network exhibits qualitative changes upon perturbations of the actin network integrity and contractility using three different drugs: Latrunculin-A [96], Blebbistatin [41, 106], and Y-27632 [52]. Network morphology and co-localization of actin and microtubules were analyzed in fixed cells stained for DNA with Hoechst 33342, F-actin with Alexa594-phalloidin, and α-tubulin monoclonal antibody (DM1A). The three drugs did not significantly alter nuclear structure, but observations of at least 25 cells per condition revealed qualitative changes in the microtubule network. Figure 2.2 shows representative cells for control and the three treatments.

The morphology of the MCF-7 cells under control conditions was consistent

with the relatively flat shapes associated with cultured epithelial breast tumor cells [96]. The membrane edges appeared tightly anchored to the surface and the cytoskeletal fibers were distributed throughout the cytoplasm. Polymerized actin was enhanced in diffuse spots within the cytoplasm and near the nucleus, as well as membrane ruffles at the cell periphery. Microtubule filaments were visible as a network throughout the cytoplasm with some accumulation of α-tubulin filaments near the nucleus.

In cells treated with 5μM of the actin depolymerizing compound, Latrunculin-A [96], only minimal residual polymerized F-actin was observed with phalloidin staining, as expected. Filaments of α-tubulin were distributed throughout the cell body, as in control, but exhibited straight protrusions that do not contain F-actin and extend beyond the cell body boundary. For cells treated with 25μM Blebbistatin [41], F-actin clumped both within the cytoplasm and near the cell body boundary. α-tubulin in these cells was denser near the nucleus. Small, straight local protrusions containing both actin and α-tubulin were visible outside the cell body boundary. Finally, in cells treated with 10μM of Y-27632 [52] the overall morphology of the cells had fewer localized protrusions, but also had several regions with actin membrane 'ruffles' along the cell periphery, consistent with reports that Y-27632 can result in Rac activation which is associated with laemellipodial membrane ruffles [110].

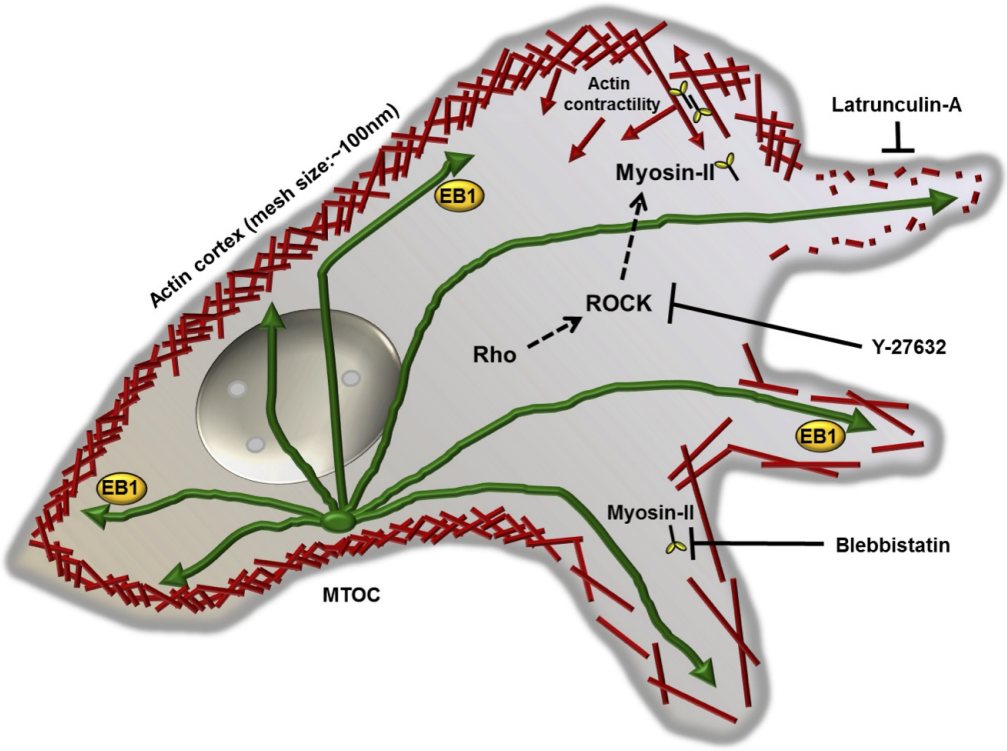

Figure 2.1: Counterbalanced forces of microtubule expansion and actin cortex contraction. In a normal, adherent epithelial cell, there is a cortex of cross-linked actin filaments beneath the plasma membrane that is under contraction mediated by the non-muscle myosin-II motor protein (red arrows). Microtubules are nucleated at the microtubule-organizing center (MTOC) and grow outward from the cell center toward the plasma membrane (green arrows). Microtubule end-binding protein-1 (EB1) binds preferentially to the growing GTP-capped microtubule plus end and forms comets projecting from the cell center. Microtubules reaching the network of cortical actin filaments, which have an estimated mesh size of 100nm. Interaction of EB1 with cortical proteins, such as APC, also mediate capture of microtubules. Latrunculin-A depolymerizes actin, reducing the barrier to microtubule expansion. Phosphorylation of myosin-II by the Rho-kinase (ROCK) increases contractility, but can be inhibited by the small molecule ROCK inhibitor, Y-27632. Similarly, Blebbistatin binds directly to myosin-II and reduces contractility.

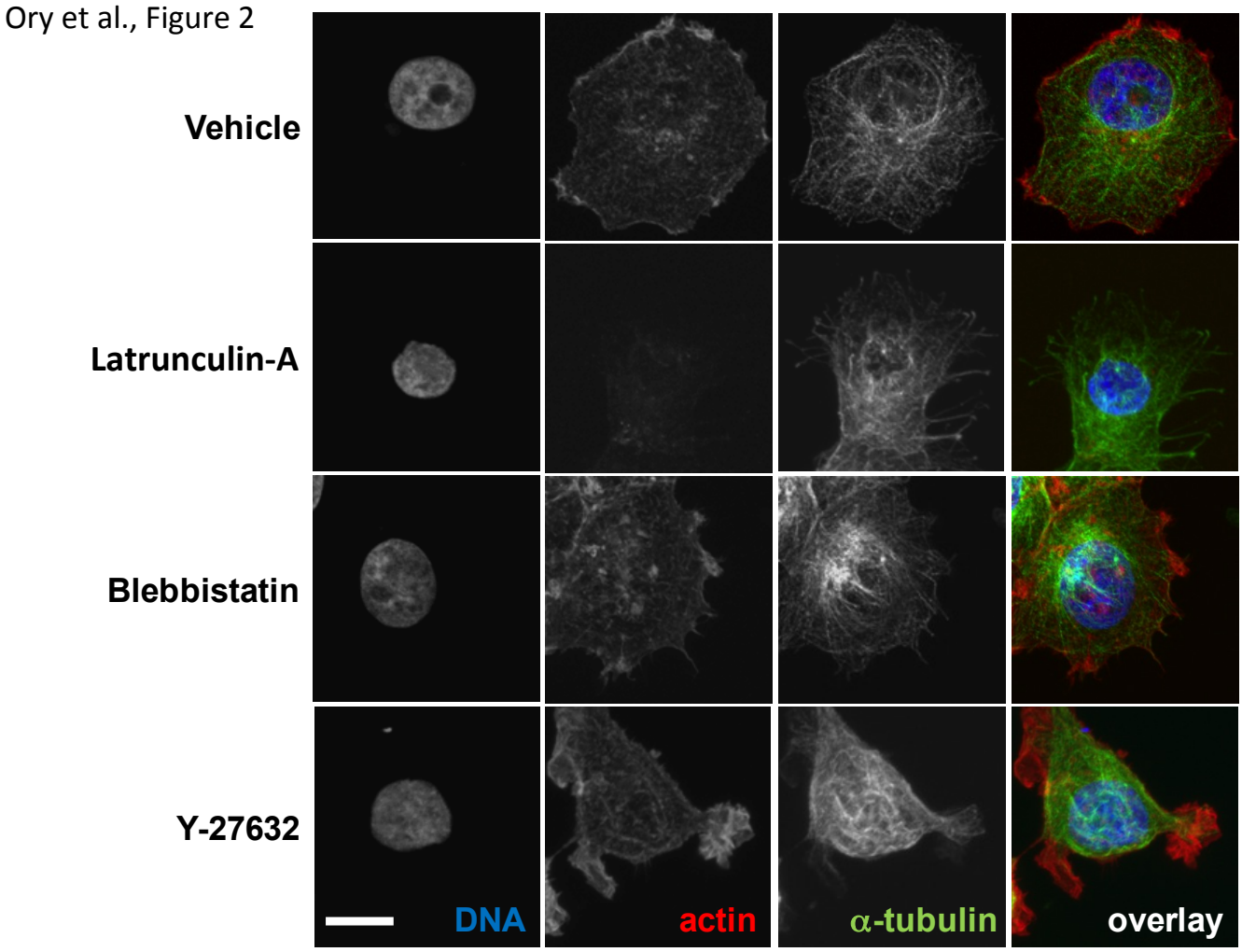

Figure 2.2: Actin disruption promotes microtubule extension beyond the cell-body boundary. Human MCF-7 breast cancer cells were treated with vehicle control (0.5% DMSO), 5μM Latrunculin-A, 25μM Blebbistatin or 10μM of Y-27632 for 30 minutes, fixed with formaldehyde and fluorescently stained for actin localization (red), microtubules (green) or DNA (blue). Confocal microscopy images are shown for each channel and condition, along with an overlay of all channels (right column)(scalebar = 10μm).

2.3.2 *Quantifying microtubule growth dynamics via live cell imaging*

In order to track microtubule tip growth, images of GFP-labeled EB1 proteins were collected via fluorescence time-lapse microscopy [107, 108]. Taking one image every 2 seconds allowed us to follow the growing trajectories of the labeled microtubule plus ends. In control movies, EB1 clusters appeared uniformly distributed across the inside of the cell (Figure 2.3-top). A maximum intensity time projection written in Matlab of images across all 50 time points illustrated the microtubule tip trajectories throughout the cell (Figure 2.3-bottom).

Blebbistatin treatment caused EB1 tips to move more slowly (Figure 2.3-top). Trajectories were fainter and shorter than for other drug treatments or control (Figure 2.3-bottom), but quantitative tracking (Figure 2.4) was still possible for an average of more than 93% of EB1 tips with an automated cluster-finding and tracking algorithm. The snapshots of Latrunculin-A treated cells showed little background fluorescence, and EB1 clusters were scattered throughout the cytoplasm inside the cell as well as outside the cell body boundary (Figure 2.3-top). The time-lapse projection images revealed long, straight trajectories, many extending beyond the cell body boundary (Figure 2.3-bottom). Microtubule tip trajectories did not encircle the nucleus, even though significant α-tubulin was seen in the immunofluorescence, indicating that the α-tubulin around the nucleus may be more stable than microtubules in other regions of the cell (Figure 2.3-bottom). In cells treated with

Y-27632 [52], microtubule tips were scattered throughout the cytoplasm and near the boundary, but scarce near the nucleus (Figure 2.3-top). The trajectories were straight, and again scarce near the nuclei (Figure 2.3-bottom).

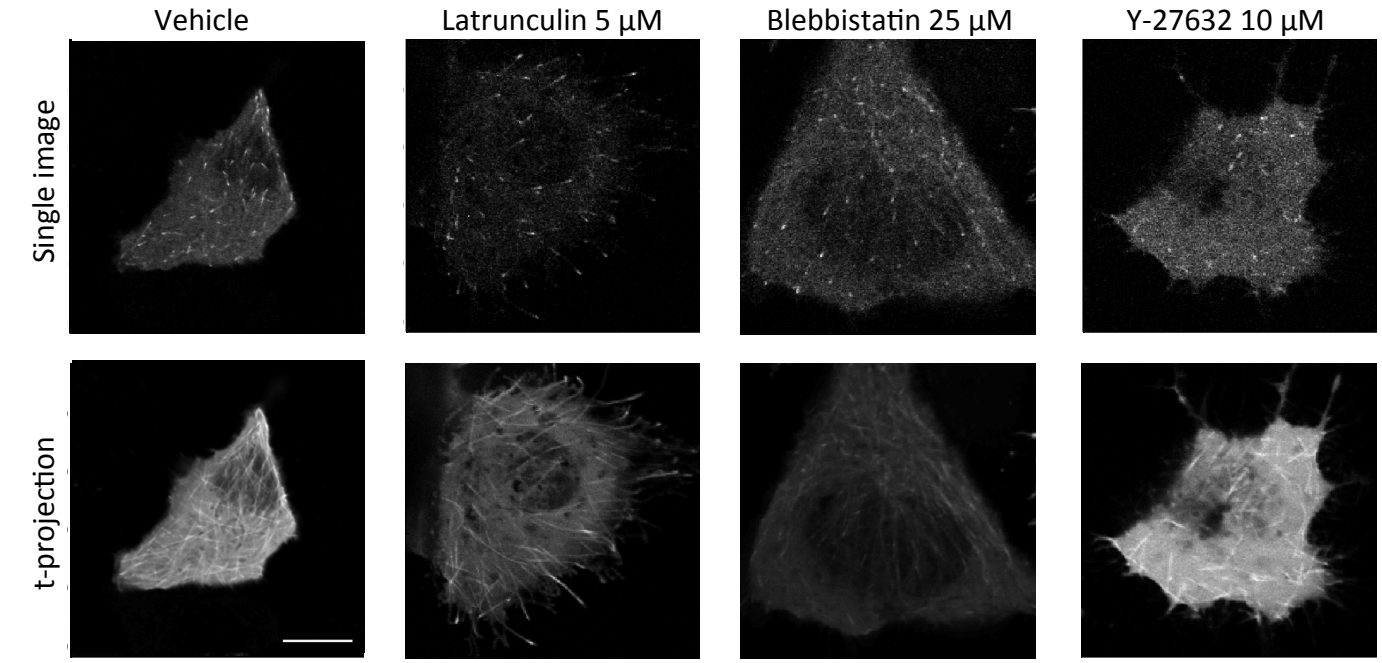

Figure 2.3: Live-cell confocal microscopy of EB1-GFP allows imaging of microtubules dynamics. (Top) Single image frame of EB1-GFP transfected cells for all 4 conditions. (Bottom) Mean image across all 50 frames (scalebar = 10μm).

Ory et al., Figure 4

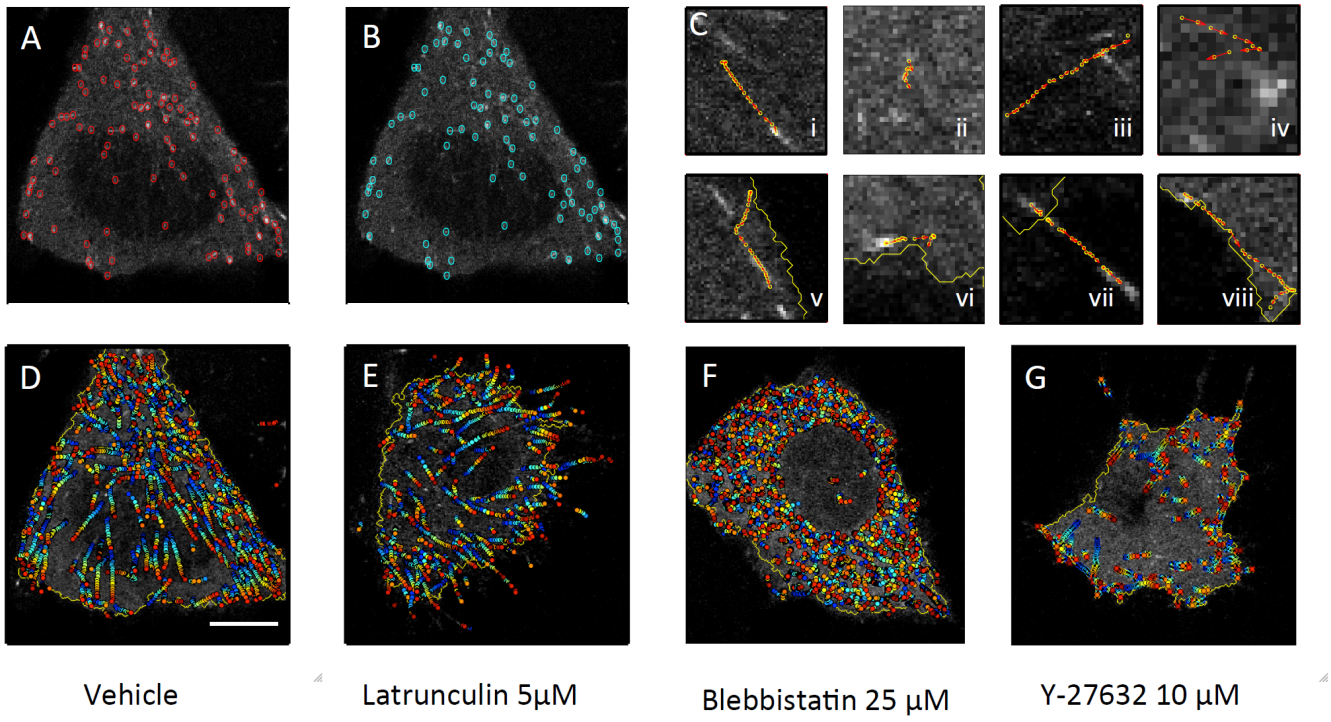

Figure 2.4: Tracking algorithm identifies dynamic EB1-GFP tips and trajectories. A) Example of EB1 tips found. B) Example of tips tracked. C) Individual trajectories: i. Normal trajectory in cell bulk. ii. Trajectory in cell bulk treated with 25μM blebbistatin. iii. Trajectory in cell bulk treated with 5μM latrunculin. iv. Trajectory in cell bulk treated with Y27632. v. Normal trajectory near cell edge. vi. Trajectory in near cell edge treated with 25μM blebbistatin. vii. Trajectory near cell edge treated with 5μM latrunculin. viii. Trajectory near cell edge treated with Y27632. D) Trajectory overlays for normal cells where blue represents earlier time frames and red represents later time frames (scalebar = 10μm). E) Trajectory overlays for cell treated with 25μM blebbistatin where blue represents earlier time frames and red represents later time frames. F) Trajectory overlays for cell treated with 5μM Latrunculin-A where blue represents earlier time frames and red represents later time frames. G) Trajectory overlays for cell treated with Y-27632 (10μM) where blue represents earlier time frames and red represents later time frames.

2.3.3 *Particle tracking microtubule end dynamics*

The tip finding algorithm successfully picked out microtubule tips from images (Figure 2.4A). We analyzed image sequences if the tip tracking algorithm tracked at least 85% of visible tips for a minimum of 4 frames (Figure 2.4B), and at least 85% of tips moved more than 1 pixel. For control and drug treated cells, typical trajectories are shown both in the cell bulk and near the cell body boundary (Figure 2.4C). For all 4 conditions, an overlay of all trajectories are shown in Figures 2.4D-G. As expected, trajectories are generally in concordance with time-projected images shown in Fig. 2.3, indicating that the microtubule tip finding and tracking algorithm output was reasonable. The trajectories are color-coded to reveal the overall outward motion of microtubules - blue indicated the starting-point of each trajectory and red the endpoint (Figure 2.4D-G).

Control cells displayed microtubule growth throughout the cytoplasm, with very few microtubule tip trajectories extending beyond the cell body boundary (Figure 2.4D). Likewise, Blebbistatin treated cells had short trajectories of microtubule tips throughout the cytoplasm, consistent with the time-projected images (Figure 2.4E). For cells treated with Blebbistatin, the tracking algorithm found few EB1 trajectories beyond the cell body boundary even though the fixed images show localized tubulin containing protrusions extending beyond the cell body boundary. The lack of actively growing microtubule tips in these Blebbistatin-induced protrusions sug-

gests that the microtubules extending the cytoplasmic edge were more stable in this case.

In Latrunculin-A treated cells, the distribution of microtubule tips was similar in fixed cells (Figure 2.2) and in live cell imaging (Figure 2.4F), indicating that localized tubulin containing protrusions in this case did not contain significantly more stable microtubules than other regions. Similar to Blebbistatin treated cells, Y-27632 treated cells had short-lived tubulin growth near the edge of the cell body boundary (Figure 2.4G). Beyond the cell body boundary, Y-27632 treated cells exhibited localized α-tubulin protrusions. Though we found fewer protrusions compared to blebbistatin treatment in both fixed imaging (Figure 2.2), we found more protrusions than in blebbistatin treatment for live cell imaging (Figure 2.4G). This suggests that in Blebbistatin-treated cells, localized tubulin containing protrusions were stable, while Y-27632 and Latrunculin-A lead to more dynamic protrusions with active microtubule growth.

2.3.4 *Localizing microtubule tip relative to the cell body boundaries*

Next, location of microtubule tips in relation to the cell body boundary was measured. Analysis for control (0.1% DMSO) was comprised of 2 experiments from 19 independent cells at 950 frames (50 frames each) or 48,497 tip distance measurements. The average distance of microtubule tips from the cell body boundary measured 1.7 $\pm$0.2 μm from the cell body boundary(Figure 2.5C). Similar analy-

sis of Latrunculin-A treated cells (2 experiments, 18 cells, 900 frames, 45,148 tips) showed that the average distance of microtubule tips from the cell body boundary decreased significantly to only 0. 16±0.2 μm compared to control (anova p<.0001 and ks-test p=1.0178e-6). Blebbistatin treated cells (2 experiments, 16 cells, 800 frames, 41,161 tips) had microtubule tip locations at an average distance comparable to controls at 1.5±0.2 μm with no significant difference (anova p=.9397 and ks-test p=.0528). Cells treated with Y-27632 (2 experiments, 19 cells, 950 frames, 44,821 tips) also exhibited a significantly smaller microtubule tip distance from the boundary at 0.8±0.3 μm compared to control (anova p=.0263 and ks-test p=.0181). Additionally, microtubule tip distance from the boundary for Latrunculin-A treated cells was significantly less than Blebbistatin treated cells (anova p=.0004 and ks-test p=6.4616e-6).

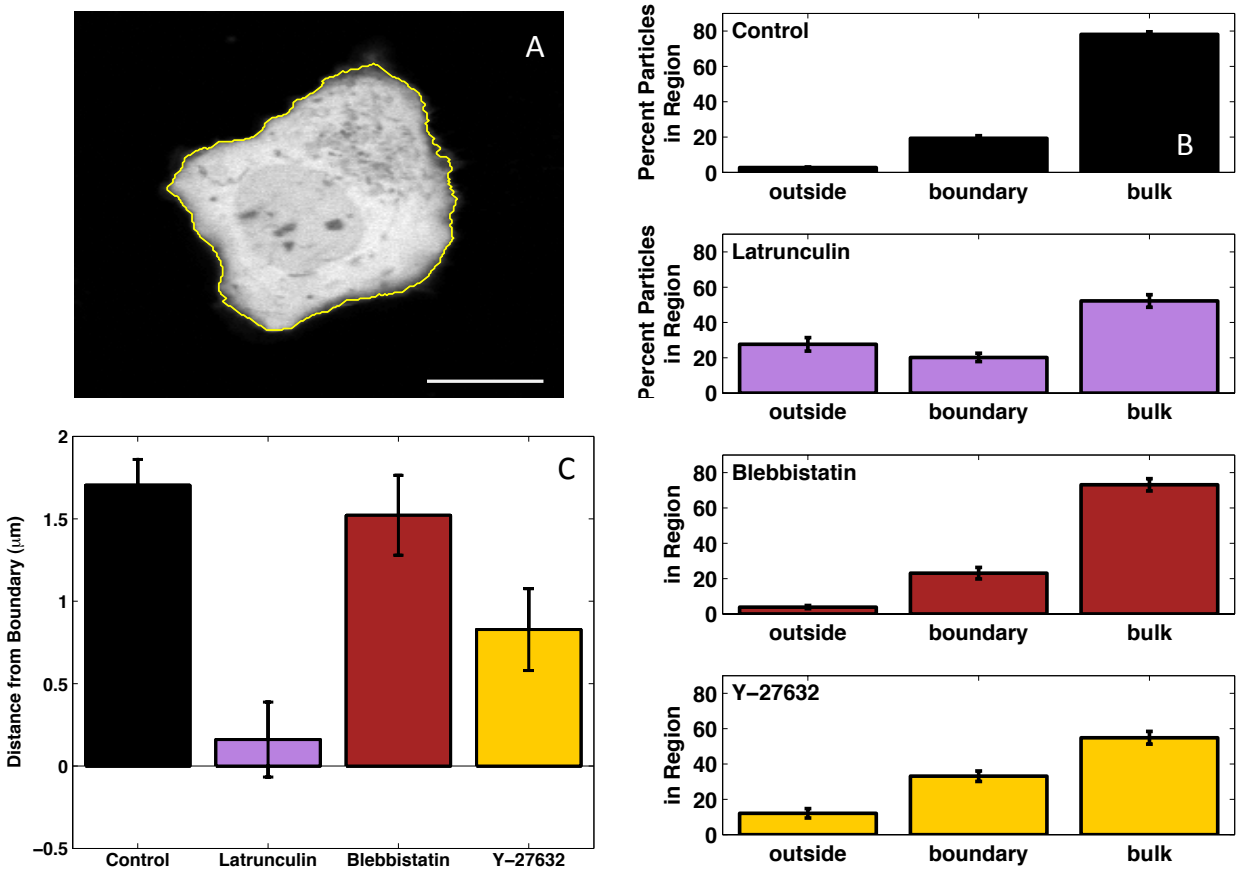

Figure 2.5: Analysis of localization and distribution of dynamic microtubule ends. A) Cell body boundary from mean mCherry image taken across 50 frames (left). B) Mean distance from the boundary for all 4 conditions (bottom left). Control treated cells (.1% DMSO) show an average distance from cell body boundary of measured 1.7 $\pm$0.2 μm. Cells treated with 5μM Latrunculin-A show an average distance of 0. 16$\pm$0.2 μm which is a significant decrease when compared to control (anova p<.0001 and ks-test p=1.0178e-6). Cells treated with 25μM Blebbistatin have an average distance of 1.5 $\pm$0.2 μm comparable to controls with no significant difference (anova p=.9397 and ks-test p=.0528). Cells treated with 10μM Y-27632 have an average tip distance of 0.8$\pm$0.3 μm which is significantly smaller than control (anova p=.0263 and ks-test p=.0181). Additionally, microtubule tip distance from the boundary for latrunculin treated cells was significantly less than blebbistatin treated cells (anova p=.0004 and ks-test p=6.4616e-6). C) Percentage of particles outside the boundary (left), near the cell body boundary (within 10% of mCherry-defined cell body boundary) and in the cell bulk (right).

2.3.5 *Measuring the fraction of microtubule tips that are part of localized protrusions*

Next we quantified the fraction of growing microtubule tips located near the cell body boundary, tips that were part of localized protrusions, and tips that were in the cell′s interior (Figure 2.5C). Tips near the boundary were defined as those within 10% of the cell′s cytoplasmic area that is closest to the boundary. For control treated cells the percentages of tips in the regions outside the cell body boundary, near the cell body boundary, and in the cytoplasmic bulk were 3±2%, 19±2%, and 78±2% where percentages for all 3 regions were significantly different (anova $p<.0001$). For Latrunculin-A treated cells the percentages of tips in the regions outside the cell body boundary, near the cell body boundary, and in the cytoplasmic bulk were 28±2%, 20±2%, and 52±2%. For cells treated with Latrunculin-A outside the cell body boundary, the distribution had a skew of 12; thus, an additional ks-test was conducted on all comparisons including the population of Latrunculin-A treated EB1 tips outside the cell body boundary to check for significance. For Latrunculin-A treated cells outside the cell body boundary, there was no significant difference when compared to EB1 tips near the cell body boundary (anova $p=.2663$ and ks-test $p=.4255$). For Latrunculin-A treated cells, there were significantly fewer EB1 tips outside the cell body boundary and near the boundary compared to inside the cell body bulk with anova computed p-values less than .0001 for both (ks-test p=2.9003e-

07 and p=3.8098e-08 respectively). For Blebbistatin treated cells the percentages of tips in the regions outside the cell body boundary, near the cell body boundary, and in the cytoplasmic bulk were 4±2%, 23±2%, and 73±2% where percentages for all 3 regions were significantly different (anova p<.0001). For Y-27632 treated cells the percentages of tips in the regions outside the cell body boundary, near the cell body boundary, and in the cytoplasmic bulk were 12±2%, 33±2%, and 55±2% where percentages for all 3 regions were significantly different (anova p<.0001).

For the region outside the cell body boundary, Latrunculin-A had a significantly higher percentage of EB1 tips compared to all other regions control, Blebbistatin, and Y-27632 (anova p<.0001 for all 3 and ks-test p=2.6693e-09, 1.3309e-08, and 1.6487e-04 respectively). Additionally, while Y-27632 treated cells had significantly less EB1 tips outside the cell body boundary, there were significantly more EB1 tips outside the cell body boundary compared to control treated cells (anova p=.0334 ks-test p=4.6625e-04). In the region closest to the boundary, only Y27632 had significantly more EB1 tip localization compared to control, Latrunculin-A, and Blebbistatin (anova p=0.0011, 0.0031, 0.0391 respectively). Both the control and Blebbistatin had over 70% of the EB1 tips in the cytoplasmic bulk and significantly more EB1 tips in the bulk region compared to Latrunculin-A (anova p<.0001 for both) and Y27632 (anova p<.0001 and 0.0008 respectively).

2.3.6 *Measuring microtubule tip speed*

In addition to quantifying EB1 tip localization, speeds of EB1 tips were measured to see whether actomyosin cortex integrity changed the speed of the EB1 tips for different drug treatments. For speed and dynamics experiments, videos without mcherry staining were used. Analysis for control was comprised of 5 experiments from 24 independent cells and a total of 4,979 individual EB1 tip trajectories measured over time. The average speed of microtubule tips in untreated cells was 0.075±0.002μm/s (Figure 2.6A). When broken down by regions outside, boundary, and bulk, the average speeds were 0.057±0.003μm/s, 0.065±0.003μm/s, and 0.084±0.003μm/s respectively. For cells treated with 5μM Latrunculin-A there was a total 3 experiments, 22 cells and 3,703 trajectories where the average speed was 0.065±0.004μm/s; when broken down by regions outside, boundary and bulk: 0.048±0.003μm/s, 0.058±0.004μm/s, and 0.071±0.005μm/s respectively. For cells treated with 25μM Blebbistatin there was a total of 5 experiments, 18 cells, and 4,240 trajectories moving an average speed of 0.053±0.002μm/s; when the trajectories were broken down into their regions of outside, boundary and bulk, the speeds were 0.037±0.003μm/s, 0.046±0.002μm/s, and 0.056±0.003μm/s respectively. For cells treated with 10μM Y-27632, there was a total of 3 experiments, 25 cells, and 5,117 trajectories moving an average speed of 0.077±0.003μm/s; when the trajectories were broken down into their regions of outside, boundary and bulk, the speeds were 0.059±0.004μm/s, 0.062±0.002μm/s, and 0.088±0.003μm/s respectively. For cells treated with 25μM Blebbistatin, the average speed of EB1 tips moved sig-

nificantly slower than Control, 5μM Latrunculin-A, and 10μM Y-27632 ($p<.0001$, $p=0.0228$, and $p<.0001$ respectively). Additionally, cells treated with Latrunculin-A had an average EB1 tip speed moving significantly slower than trajectories in cells treated with Y-27632 ($p=.0130$).

Within each cell treatment, the speed of trajectories was compared between all 3 regions: outside the cell body boundary, near the cell body boundary, and inside the cytoplasmic bulk. For the control and all drug treatments: Latrunculin, Blebbistatin, and Y-27632 EB1 trajectories outside the cell body boundary moved significantly slower than trajectories inside the cytoplasmic bulk ($p<.0001$, $p=.0002$, $p=.0001$, and $p<.0001$ respectively). It is evident from this change in speed that the membrane can exert a force that counteracts microtubule growth, even without intact actin or actomyosin contraction. For the control and all drug treatments: Latrunculin, Blebbistatin, and Y-27632 boundary region trajectories moved significantly slower than bulk region trajectories($p<0.0001$, $p=0.0475$, $p=0.0394$, and $p<.0001$ respectively), but no significant difference in speed between trajectories near the boundary and those outside the cell body boundary. However the differences in speed between the EB1 trajectories in the bulk region of the cell verses boundary region of the cell were more pronounced in control conditions and Y-27632 compared to Latrunculin-A treated cells and Blebbistatin treated cells suggesting that when contractility of the actomyosin cortex is compromised, there is less barrier to slow down the speed of microtubule growth.

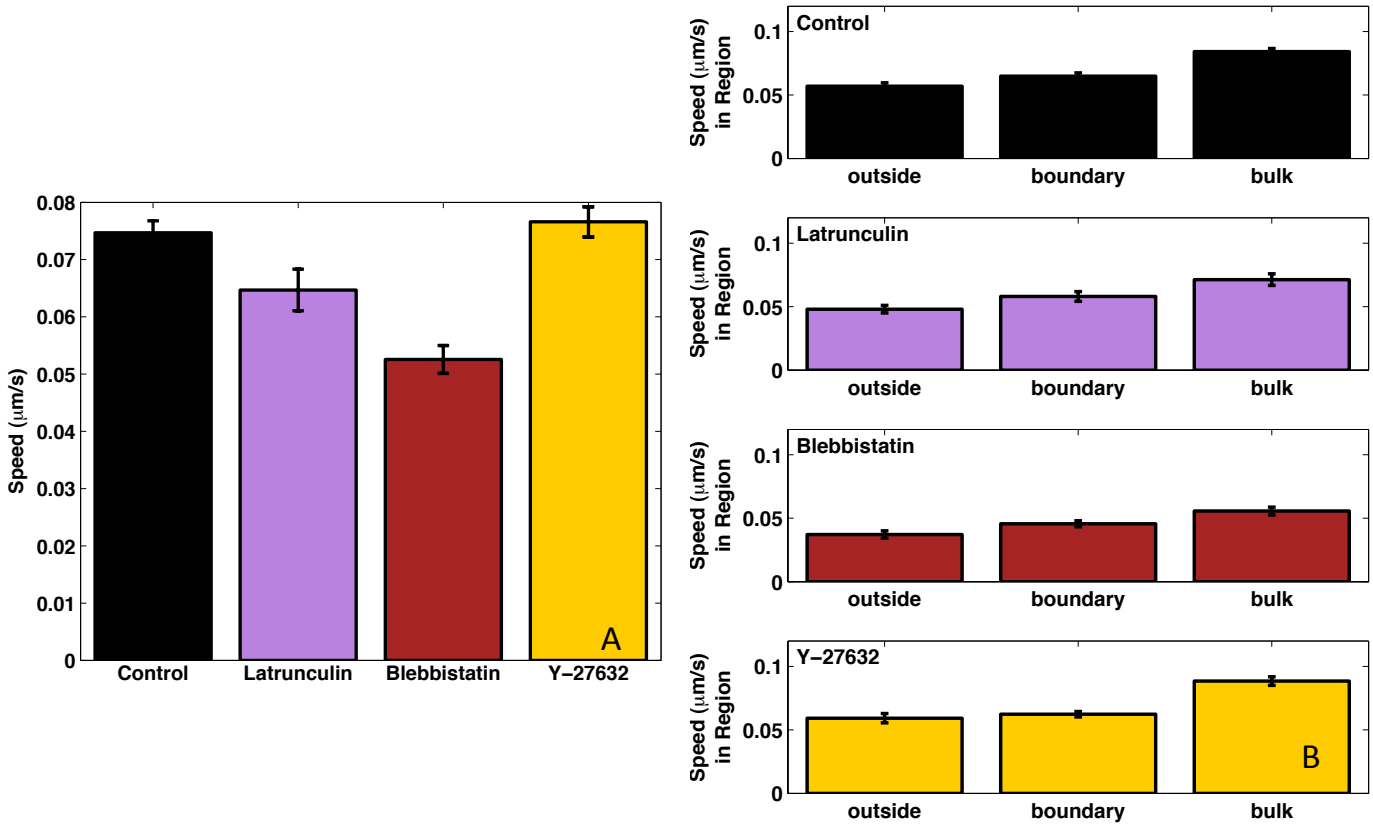

Figure 2.6: Average speed (μm/s) for all 4 conditions: control (black) at 0.075±0.002μm/s, 5μM Latrunculin-A (purple), at 0.065±0.004μm/s, 25μM Blebbistatin (red) at 0.053±0.002μm/s, and 10μM Y-27632 (yellow) at 0.077±0.003μm/s. B. Break down of speed for all 4 conditions broken into 3 regions from left to right: outside the cell body boundary, near the cell body boundary (the 10% of points inside the cell body closest to the boundary) and within the cell bulk (remaining area inside the cell body): speeds for control (black) were 0.057±0.003μm/s, 0.065±0.003μm/s, and 0.084±0.003μm/s respectively; speeds for 5μM Latrunculin-A (purple), were 0.048±0.003μm/s, 0.058±0.004μm/s, and 0.071±0.005μm/s respectively; speeds for 25μM Blebbistatin (red) were 0.037±0.003μm/s, 0.046±0.002μm/s, and 0.056±0.003μm/s respectively; and speeds for 10μM Y-27632 (yellow) were 0.059±0.004μm/s, 0.062±0.002μm/s, and 0.088±0.003μm/s respectively. Error bars represent SEM.

2.3.7 *Measuring microtubule tip trajectory straightness*

To determine the straightness of trajectories of growing microtubules, the orientation autocorrelation function was measured separately for each microtubule tip trajectory. We measured both the change in direction of motion over time, which yielded a characteristic turning time for growing tips, and the distribution of the temporal orientation autocorrelation as a function of position, which yielded a characteristic lengthscale over which trajectories bent. We analyzed all trajectories in 24 control cells, 22 cells treated with Latrunculin-A, 18 cells treated with Blebbistatin, and 25 cells treated with Y-27632. The orientation correlations, averaged over all trajectories for each condition (50 frames per cell) are shown as a function of time delay (Figure 2.7) and as a function of cumulative distance (Figure 2.8) . We found that microtubules in cells treated with Y-27632 maintained their direction similar to control cells. In contrast, microtubules in Blebbistatin and Latrunculin-A treated cells changed direction more quickly, and over shorter distances than control cells. Note that Blebbistatin and Latrunculin-A treated cells also had microtubule tips that move notably slower (Figure 2.6). An exponential fit of the time delay autocorrelation function yielded a characteristic time and distance over which microtubule tips change direction, as shown in Table 2.9. The higher τ and lower κ decay constants in Control and Y-27632 indicate less change in direction and curving over time and space.

Ory et al., Figure 6

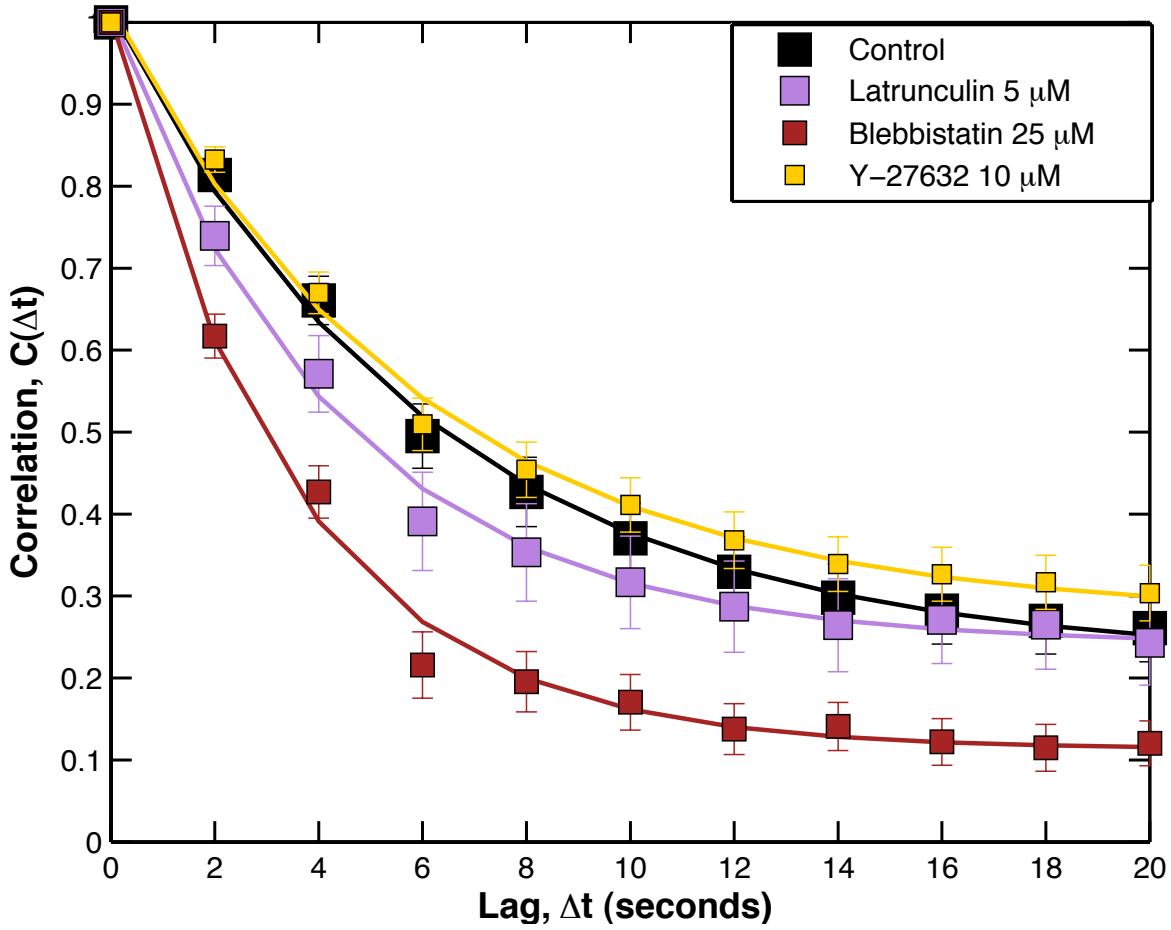

Figure 2.7: Orientation Autocorrelation as a function of time for control (black squares), Blebbistatin (red squares), Latrunculin-A (purple squares), and Y-27632 (yellow squares).

Ory et al., Figure 7

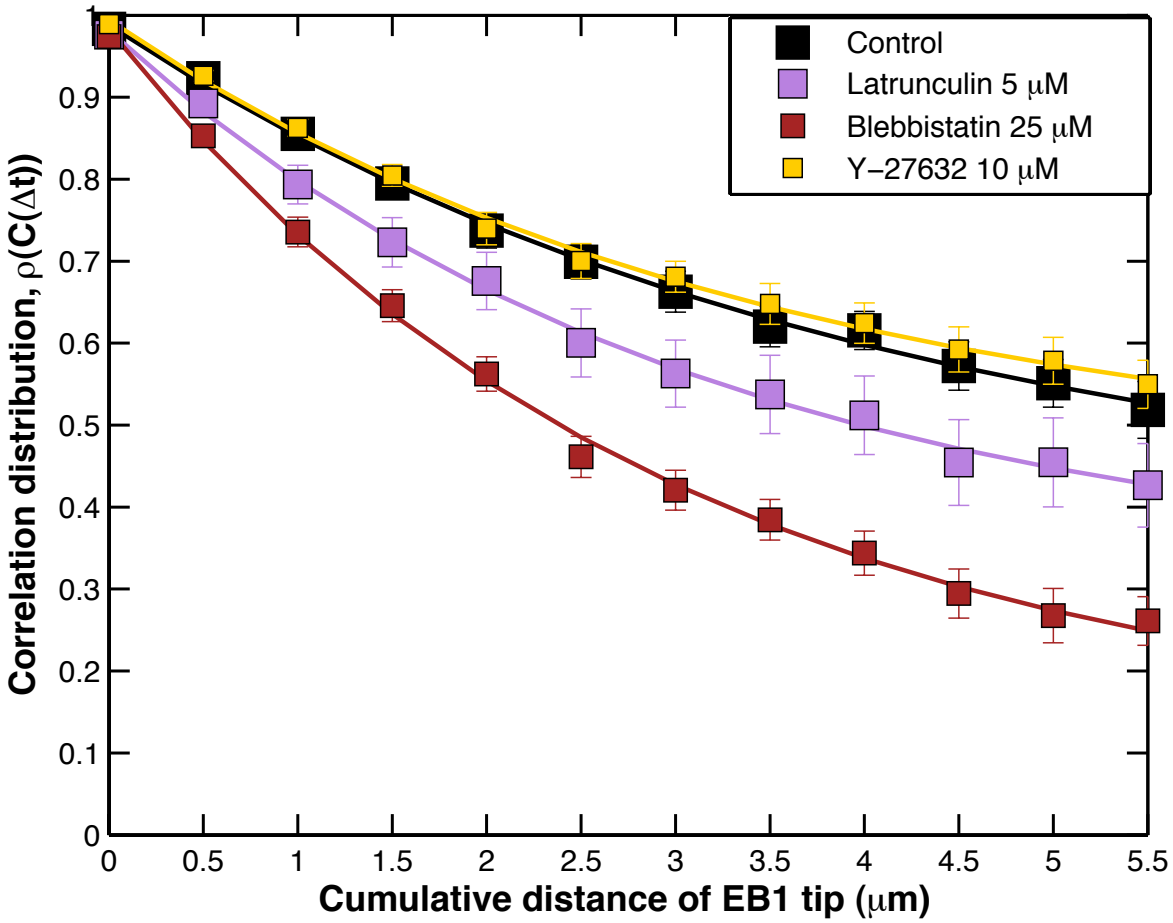

Figure 2.8: Distribution of Temporal orientation Autocorrelation as a function of cumulative distance for control (black squares), Blebbistatin (red squares), Latrunculin-A (purple squares), and Y-27632 (yellow squares).

Ory et al., Table 1

Orientation Autocorrelation as a function of time

$$Ae^{-t/\tau} + B$$

	A	B	τ (s)
Vehicle	0.78	0.24	3.09
LA	0.77	0.24	1.71
Blebbistatin	0.89	0.11	2.14
Y-27632	0.74	0.28	2.92

Spatial Distribution of Temporal Orientation Autocorrelation

$$Ae^{-\kappa x} + B$$

	A	B	1/κ (μm)
Vehicle	0.61	0.38	0.25
LA	0.67	0.31	0.32
Blebbistatin	0.87	0.12	0.34
Y-27632	0.55	0.44	0.29

Figure 2.9: Orientation autocorrelation coefficients as a function of time (top) and spatial distribution of temporal orientation autocorrelation (bottom) for control, Latrunculin-A, Blebbistatin, and Y-27632.

2.4 Discussion

Previous research suggests that microtentacles form in suspended cells when the actomyosin cortex is compromised supporting a model where microtentacle formation is the result of unbalanced forces between the actomyosin cortex and microtubules [39, 43, 46]. Here we present results that show, changes in microtubule growth for attached cells as the result of changes in the actomyosin cortex. We focused on the drugs listed above that target the actin cytoskeleton yet induce changes in cell behavior that are strongly microtubule dependent (e.g. proliferation). The drugs are small molecule inhibitors of the actin cytoskeleton, both perturbing its integrity (Latrunculin-A) and contractility (Blebbistatin, Y-27632) [106]. Latrunculin-A binds directly to β-actin monomers, sequestering them and preventing their assembly into F-actin filaments [111, 112]. Blebbistatin and Y-27632 do not alter actin polymerization, but reduce actomyosin contractility through independent mechanisms. Blebbistatin binds to non-muscle myosin-II (NMII) and slows down the release of phosphate that primes myosin-II for reattachment to actin filaments [106]. As a result, NMII is blocked in an intermediate state with low actin affinity, effectively releasing the actin-myosin cross-bridges that promote contractility [106]. The small molecule drug Y-27632 suppresses Rho-associated kinase (ROCK) which in turn stimulates actomyosin contractility. Y-27632 competes with ATP in the ROCK active site, reducing the kinase activity of ROCK and therefore

reducing NMII-induced actomyosin contractility [90]. Additionally, Y-27632′s inhibition of ROCK results in the activation of cofilin an actin severing protein [101]. Therefore, while each of the three compounds target actin function, Latrunculin-A broadly disrupts actin polymerization, Blebbistatin targets actomyosin contractility, and Y-27632 targets both the actin filaments and actomyosin contractility.

Our analysis of microtubule structure and dynamics for the controls and three drugs is carried out on MCF-7 breast tumor cells expressing the fluorescently tagged microtubule end-binding-protein-1 (EB1) [107, 108]. Differences in localization and amounts of all microtubules (Figure 2.2) and the actively growing microtubules measured via EB1 are used to infer microtubule stability. We find that microtubules overall are more stable under Latrunculin A treatment, with few growing tips overall, and a low concentration of tips near the cell body bulk region. Our results further show that most active microtubule tips with EB1 are concentrated a few microns from the cell body boundary (Figure 2.5A,C). Control cells showed less than 10% of microtubule tips beyond the cell body boundary (Figure 2.5B), while Latrunculin-A and Y-27632 increase localized protrusions, indicating that both the structural integrity and the dynamics of the cortex prevent localized protrusions of microtubules through the actin cortex. Since microtubules will buckle and break when encountering a barrier [113], the relative softening of the actin cortex by Blebbistatin and Y-27632 could produce a more flexible actin cortex that improves cortical capture of growing microtubules, rather than breakage.

EB1 trajectories treated with Latrunculin-A move significantly slower than control cells or cells treated with Y-27632. This suggest that the membrane ten-

sion beyond the cell body boundary is the largest inhibitor of speed and is further supported by the fact that EB1 trajectory speeds are slower outside the cell body boundary across all conditions where Latrunculin-A has significantly more EB1 tips beyond the cell body boundary than all other conditions. Interestingly, Blebbistatin moves significantly more slowly than any other conditions despite not having more EB1 tips beyond the cell body boundary. It is worth considering that while other results provide evidence supporting the notion of growing microtubules contained by a contractile actomyosin cortex, all the above experiments were conducted on attached cells. One of the key, widely accepted models for attached cells posits that actin-based protrusions form from actin polymerization pushing the plasma membrane outward [114, 115]. Also, studies show that Blebbistatin weakens the protrusive force of lamellipodia [116]. Furthermore, the speed of actin in the lamellipodia is around speed 25nm/s and 2nm/s for retrograde flow [117]. The speed of the EB1 tips in control cells was around $0.075 \pm 0.002 \mu$m/s and blebbistatin, $0.053 \pm 0.002 \mu$m/s or a speed difference of about 22 nm/s and comparable to actin in the lamellipodia.

Straightness of microtubule tip trajectories is decreased by either actin depolymerization (Latrunculin-A) or the inhibition of actomyosin contractility with Blebbistatin (Figure 2.7) In support of this model, previous studies have shown that the cytoplasm provides a barrier to microtubule persistence length, compared to in vitro microtubule growth [118]. Depolymerization of actin with Latrunculin-A also decreased the straightness of the EB1 trajectories overall, but trajectories were deflected in localized protrusions outside the cell body boundary.

Cells sense their mechanical microenvironment and the presence of wounds

through both actin contraction and microtubule extension [15, 38, 119]. Persistent pulling of actomyosin contraction on both cell-matrix and cell-cell adhesion points serve as signals for appropriate cell attachment [120]. Imbalances between actin cortical contraction and microtubule extension from the cell center can also influence metastatic potential through the formation of microtentacles on the surface of free-floating tumor cells [38]. Reducing actin contractility with Blebbistatin enhances microtentacles that promote tumor cell reattachment and aggregation [41]. Further supporting a role for cytoskeletal balancing, microtentacles are induced by either inhibition of actin polymerization with Latrunculin-A or hyperstabilization of microtubules with Paclitaxel [59, 96]. The importance of this microtubule-actin force balancing is also demonstrated by several studies in the past year that have shown that compounds which reduce actomyosin contractility, including Blebbistatin and Y-27632, are capable of allowing long-term in vitro culture growth of patient-derived tumor cell from many cancers [104, 105] using a new method termed 'conditional reprogramming′, because cells treated with cytoskeletal inhibitors divert from their differentiation program and become capable of growing efficiently and for many generations [104, 105]. These results suggest that some stem cell characteristics may be regulated by mechanical changes in the cytoskeleton. In support of this model, both Blebbistatin and Y-27632 induce stem cell characteristics in primary colon cancer cells, including spheroid formation, CD44v expression and increased tumorgenicity in mice [103]. If the balance of microtubule expansion against actin contraction is partly responsible for these effects, it would be predicted that microtubule stabilization would also be influenced by cell detachment and produce increased stem cell

characteristics. In fact, both increased microtubule stabilization upon cell detachment [48] and the induction of stem cell characteristics by the common microtubule stabilizing compound, Paclitaxel, have already been observed [121].

Currently, many clinical chemotherapeutic drugs target the cytoskeleton such as Vinblastine, Paclitaxel, and Demecolcine. Cytoskeletal compounds which promote actin disruption or microtubule stabilization could inadvertently induce surviving cancer cells to elevate microtentacles in circulating tumor cells, or localized protrusions in attached cells, and increase stem cell characteristics. Overall our results show that it will be important to more clearly understand how proposed cancer drugs alter the balance between microtubule extension and actin cortical contraction. We conclude that it will be important to understand this balance for a broad range of cancer treatments.

2.5 Materials and Methods

2.5.1 *Breast cancer cells and culture conditions*

Human MCF-7 breast cancer cells, which retain many epithelial characteristics [122, 123], were used to model the effects of actin disruption on cytoskeletal balancing in epithelial carcinoma cells. MCF-7 cells were cultured in DMEM containing 10%FBS and 1%Pen/Strep [59]. At 80% confluency, cells were detached by trypsinization and replated onto dishes with glass coverslip bottoms to enable imaging with confocal microscopy [59].

Drug reagents were obtained from Sigma Aldrich and concentrations were based on previous studies: 5μM Latrunculin-A [37, 44], 25μM Blebbistatin [41, 52], 10μM Y-27632 [39, 46]. Cell viability for the above concentrations were determined by previous work in the Martin Lab employing a variety of different assays at 24-hour time points. To determine whether drug treatment kills the cells by necrosis, an XTT or CellTiter assay is frequently employed [37, 39, 44, 46, 53]. The XTT assay works by staining for metabolically active cells. To determine whether the drug treatments might induce apoptosis, a western blot of PARP cleavage is often conducted [37, 46].

An additional functional assay to consider when determining whether drug treatments may cause cytotoxicity is a washout test. For a wash-out test, media with drug treatment is removed and several subsequent exchanges of clean media and removal are administered to remove drug exposure from the cells. Next, the cells would be reimaged and the same analyses executed as control and treatment. Finally, wash-out results are compared to control results to ensure that the drug treatments had no additional adverse effects.

Drug reagents were obtained from Sigma Aldrich and concentrations were based on previous studies: 5μM Latrunculin-A [37, 44], 25μM Blebbistatin [41, 52], 10μM Y-27632 [39, 46]. Cell viability for the above concentrations were determined by previous work in the Martin Lab employing a variety of different assays at 24-hour time points. To determine whether drug treatment kills the cells by necrosis, an XTT or CellTiter assay is frequently employed [37, 39, 44, 46, 53]. The XTT assay works by staining for metabolically active cells. To determine whether the

drug treatments might induce apoptosis, a western blot of PARP cleavage is often conducted [37, 46].

2.5.2 *Indirect Immunofluorescence*

MCF-7 cells grown on glass coverslips were treated with vehicle (DMSO 0.1%) or the indicated drug for 30 minutes, Blebbistatin (25μM), Latrunculin-A (5μM) or Y-27632 (10μM). Cells were then fixed (3.7% formaldehyde/PBS, 15 minutes), permeabilized (0.25% Triton X-100/PBS, 10 min), and blocked for 1h [PBS/5% bovine serum albumin (BSA)/0.5% NP40]. Immunostaining was performed for one hour at 4 °C with monoclonal α-tubulin DM1A (1:1000, Sigma) and Alexa488-conjugated secondary antibody (1:1000, Invitrogen), along with Hoechst 33342 (1:5000, Sigma) to label DNA and Alexa594-Phalloidin (1:200, Molecular Probes) to visualize polymerized actin. Images were acquired on an Olympus FV1000 laser scanning confocal microscope (Olympus, Center Valley, PA).

2.5.3 *Transfection and confocal microscopy*

To observe the growth of microtubules, cells were transfected using Exgen-500 (Fermentas) with full-length APC-associated end-binding protein-1 (EB1) that was fused at its C-terminus to green fluorescent protein (EB1-GFP) [108]. To compare cells with relatively similar levels of EB1 expression, cells were imaged at a short time point (16 hours post-transfection) and cells with comparably low levels of particulate EB1-GFP fluorescence were used for analysis. Cells with bright and

diffuse cytoplasmic EB1-GFP were excluded from the analysis, since this level of expression presumably saturates the microtubule binding sites for EB1. Cells were imaged on an Olympus FV-1000 point scanning confocal microscope, and live images were taken every 2 seconds in 50 sets of 256x256 image frames, using a 60x oil immersion objective. GFP fluorescent signal was collected using excitation from a 488nm laser line (10% power) and FITC emission filter set (Olympus, 41001). For boundary analysis datasets only, cells were co-transfected with mCherry to serve as a non-targeted cytoplasmic marker. Time-lapse videos were collected from at least 19 cells for each of the 4 different treatment conditions in 2 independent experiments: Vehicle control (0.1% DMSO), Latrunculin-A (5μM), Blebbistatin (25μM), and Y-27632 (10μM).

2.5.4 *Image analysis, particle tracking and computation*

EB1 localizes into clusters bound to the tips of growing microtubules. Trajectories of the EB1 clusters were computed using established particle tracking methods [124]. To remove noise, a bandpass filter was applied to the images with a lower threshold at 1 pixel and higher bandpass threshold at 4 pixels. The position of each cluster was determined with subpixel accuracy via peak fitting of the bright region. To measure the dynamics of the microtubules in an image sequence, the locations of clusters in successive images are linked as belonging to the same microtubule using established maximum likelihood principles for particle tracking [124]. To reduce noise from centroid computation, a moving average over three frames was applied

to the trajectory of each EB1 cluster, truncating the first and last location of each cluster. Furthermore, only clusters that moved a minimum displacement of 1 pixel were included in velocity vector computations. The average speed was calculated by taking the mean of all speeds between two frames.

In order to find the cell body boundary, we modified image analysis methods developed previously [125]. Since the cells do not move significantly, aside from localized protrusions, the boundary was measured from the mean image of 50 frames in the cytoplasmic (mCherry) channel. This yields a cell body boundary that ignores short lived cellular extensions (microtentacles, filopodia, etc.), i.e. such extensions are considered "outside" the cell body boundary for our further analysis. In our analysis we did not include image sequences that were very noisy, where less than 85% of identified particles were successfully tracked; or less than 85% of the trajectories showed notable displacements of $\geq$1 pixel. For further analysis, we defined the distance from the boundary to be positive inside the cell body (cytoplasmic) boundary, and negative outside the boundary of the main cell body, e.g. in McTNs. Microtubule tip locations were characterized as outside the cell body, in the cell interior, or near the boundary. The cell body boundary region is defined as the 10% of the cell area closest to the boundary from the inside.

2.5.5 *Statistics*

For all statistical analysis, code was written in MATLAB. In order to determine whether a the data had a normal distributions, measurements of skew and kurtosis

were conducted. Data was accepted as normal if the skew had a value ±2 and the kurtosis was between 0 and 6. For comparing multiple conditions, anova tests measure p-values. In the event that the data did not meet the criteria for a normal distribution, an additional Kolmogorov-Smirnov (ks-test) was conducted in parallel.

2.6 Acknowledgements

This research supported by R01-CA154624 from the National Cancer Institute and an Era of Hope Scholar award from the Department of Defense (BC100675). WL was supported by NIH grant R01GM085574. We thank Lynne Cassimeris and Michelle Piehl for generously providing the EB1-GFP expression vector.

Chapter 3: Extracting Microtentacle Dynamics in Non-adherent Cells

This chapter was adapted from Ory, E.C-h., et al, "Extracting Microtentacle Dynamics in Non-adherent Cells", In preparation for Oncotarget, 2016. Experiments were proposed and conducted by Ory. Tethering slides were prepared by Chakrabarti. First iteration of anisotropic filtering code was written by Chen. All other code and analysis was conducted by Ory.

3.1 Abstract

The study of circulating tumor cells (CTCs) is one of the fastest growing fields of cancer research and holds exciting potential for less invasive clinical research and diagnostics. Using recently developed tethering techniques, we present a novel image analysis framework for extracting the outlines of microtentacles (McTNs). From full cell outlines, we were able to measure total number of microtentacles, distance of McTN tips from cell body, as well as develop 2 total McTN phenotype metrics. Having a robust, automated analysis of microtentacle phenotype allowed us to measure dynamic morphological fluctuations by computing the autocorrelations coefficients. We demonstrate that while microtubule stabilizing drug treatment taxol increases total microtentacle phenotype, it reduces microtentacle dynamics. This work has potential implications for developing techniques to quickly measure drug response to small patient samples of CTCs.

3.2 Introduction

The study of circulating tumor cells is a rapidly growing field of research and diagnostics [126]. Considering that 90% of cancer fatalities are the result of metastasis [1], tumors surviving in the circulation is a rate-limiting step in the metastatic cascade and presents a valuable opportunity for understanding patient prognosis and preventing dissemination. Already, research has demonstrated that CTCs can be detected early during cancer disease progression [126, 127]; furthermore, a higher CTC count is correlated with a poorer prognosis [126]. Better understanding of CTC characteristics and reattachment mechanisms represent an underutilized approach for improving patient diagnostics and drug therapies.

Historically, the incredibly low concentration of CTCs, which are as rare as 1 CTC in 100 million to 1 billion blood cells, has posed a technological hurdle to further research and better understanding of the role of CTCs in metastasis [128], Recently, an abundance of emerging technologies has improved the efficacy and efficiency of capturing and segregating CTCs [126]. For example, Vortex Bioscience′s technology now has a capture efficiency of 83% and processes up to 800 μL of blood per minute [129]. The Celsee Diagnostics′s capture method has a sensitivity of 94% and specificity of close to 100%. In these studies, between one and 2,457 CTCs were captured in 2 mL of blood. [128]. Cellsieve has a capture efficiency of 98% for chemically-fixed cells and 85% for live, unfixed cells [130]. It is now feasible to capture 10 CTCs or more from a typical patient blood sample size.

Though CTCs can now be extracted from the bloodstream, further charac-

terization of the cells is very limited, in particular, characterization of the cells in their native environment of suspension. Currently, the most frequent downstream analysis only enumerates total number of CTCs or presence of particular biomarkers using immunostaining [126]. Most image analysis techniques for suspended cells have focused on detecting and measuring immunofluorescence levels for a particular biomarker. Due to the dynamic and motile nature of non-attached cells, few studies have focused on time-lapsed single cell imaging.

Little is known about which circulating tumor cells succeed in surviving the blood stream and ultimately forming metastases [131]. However, one likely morphological phenotype of cell reattachment that was found in numerous metastatic breast tumor cell lines is the presence of microtentacles, McTNs [42, 59]. McTNs are tubulin-based protrusions found in detached cells; McTN positive cells reattach to endothelial cells, get trapped in the capillaries of the lungs, and are a potential indicator for evaluating reattachment potential [38, 42]. A higher microtentacle number is found in more invasive breast cancer cell lines [42]. Furthermore, molecular mechanisms that support McTNs are associated with increased metastasis and poor patient prognosis [38, 132].

Standard image analysis techniques cannot reliably capture the faint, thin McTN structures since most standard fluidic systems for CTCs allow cells to float out the field of view quickly, thus limiting data to snapshots of CTCs as they passed by the imaging area. Thus, most prior work on McTNs relied on a blinded observer to manually score the presence or absence of McTNs..

Here we use a novel cell tethering technique, recently developed and validated

by the Martin group that allows us to hold a cell in place within the field of view of the microscope over long time periods, and thus enable extended time-lapse imaging of McTN behavior [133]. To analyze these much larger datasets we adapted image analysis approaches to quantify microtentacle number, microtentacle tip distance, and their dynamics.

3.3 Results

As the study of circulating tumor cells progresses, there is a growing need for techniques to analyze such unattached cells. We have previously shown that tethering suspended cells is an effective technique for studying non-adherent tumor cells [133]. The tethering technique attaches a small part of the cell's membrane to a surface while allowing the cell to retain its non-adherent characteristics. Here, we added metrics to previous techniques further validating the benefits of cell tethering quantitatively as well as demonstrating the geometric dynamics in response to tubulin targeting drugs for tethered cells.

3.3.1 *Anisotropic Filter allows us to capture outline of microtentacles*

To test the ability of our image analysis to detect microtentacles, we used MDA-436 cells, a mesenchymal triple-negative cell line with a high metastatic potential known to form microtentacles. In order to compare free-floating cells with tethered cells, microfluidics chambers were prepared with 2 different surface treat-

ments. For free-floating cells, microfluidic chambers were coated with pluronic F-127, a generally cytophobic coating to prevent cell attachment. For tethered cells, microfluidic chambers were coated with a cytophobic polyelectrolyte multilayers (PEMs) followed by a lipophilic coating of DOTAP to engage the lipid membrane while maintaining free-floating cell behaviors (Figure 3.1 A) [133].

Combining several existing image analysis techniques, we devised a framework optimized for finding both the McTNs and cell body. There currently exist image analysis techniques that are optimized for attached globular shapes as well as techniques for stress fibers [134, 135]. Thus, we combined the most apposite pieces of previously developed image analysis techniques, tailored, and adapted them to finding full cell outlines that included McTNs. The most critical step for better extraction of the faint, hairlike structures of McTNs was convolving the images with a rotating anisotropic filter, taking the output of the rotating anisotropic filter, and repeating the rotating anisotropic filtering for several iterations prior to thresholding (Figure 3.1 B). Using our image analysis protocol, we were able for the first time extract pertinent attributes of suspended cells including full cell outline, cell body outline, and McTN tips (Figure 3.1C).

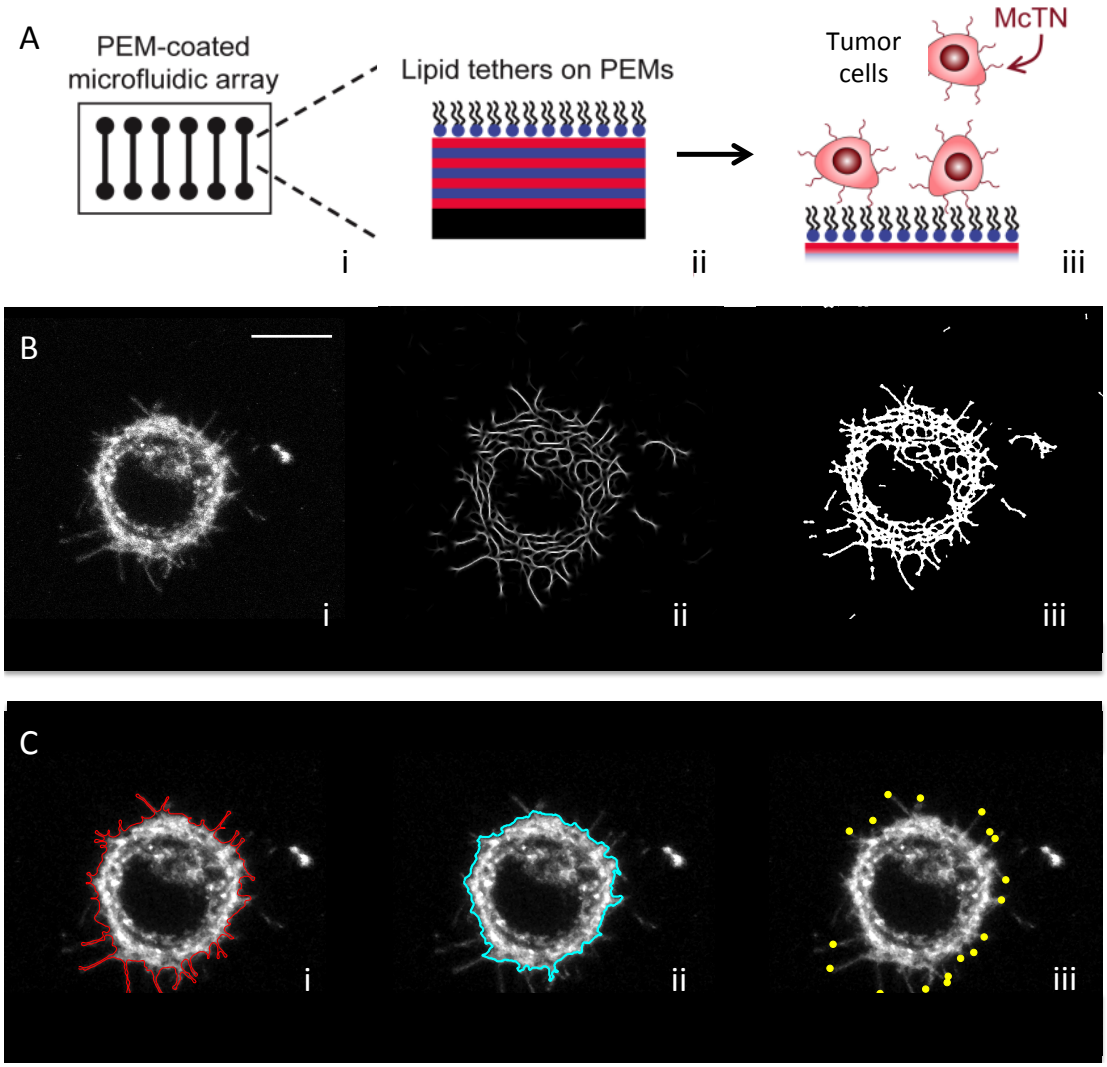

Figure 3.1: A. Lipid tethering and Image Analysis Techniques allows us to obtain morphological attributes quantitatively. A. Lipid Tethering Schematic picturing Ibidi microfluidics chamber wells (i) coated with alternating coats of lipophilic and cytophobic polyelectrolyte multilayer (PEMs) (ii) allows circulating tumor cells to attach to lipid tethers (iii). B. Image analysis methods for full cell outline enhance microtentacle visualization by taking the maximum intensity profile of 5 stack z-projection for a particular time point (i) and undergoing several iterations of anisotropic filtering (ii) before thresholding the results into a binary image (iii). C. Attributes derived from image analysis consists of outline of the full cell including microtentacles (i), outline of the cell body′s boundaries excluding microtentacles (ii) and tips of microtentacles (iii) derived from maximum local curvature of skeletonization of full cell outline (scalebar = 10μm).

3.3.2 *Tethering prevents cells from drifting and improves visualization of microtentacles*

Previous research demonstrated that tethered cells stay attached to the surface after several washes better than free-floating cells [133]. In this study, image analysis techniques allowed us to visualize drift of individual suspended and free-floating cells qualitatively by looking at the maximum intensity over time, overlays of cell body boundary as a function of time, and overlays of the centroid of the cell body boundary as a function of time (Figure 3.2A). Computing total distance traveled by cell body centroid, we demonstrated quantitatively that free-floating cells have significantly more lateral drifting than tethered cells (Figure 3.2B) where t-test p-value was 9.02e-15 and ks-test p-value was 5.5276e-09.

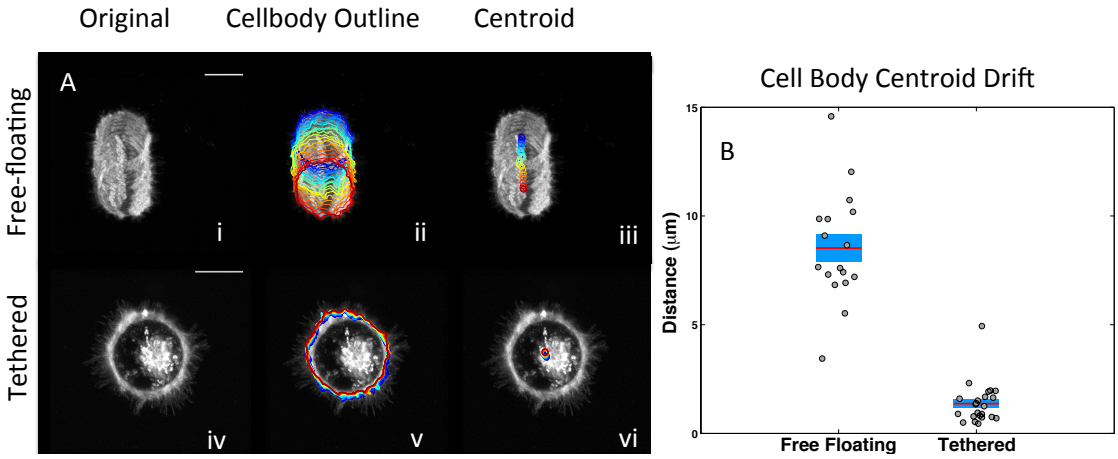

Figure 3.2: Measurements of lateral cell drifting compare free floating cells to tethered cells. A. Time projection profile of maximum intensity z-stacks for Free-floating cells (top) and Tethered Cells (bottom). Overlays of cell body outline (ii) from initial (blue) to final (red) time points for Free-floating cells (top) and Tethered Cells (bottom). Centroid of cell body (iii) from initial (blue) to final (red) time points for Free-floating cells (top) and Tethered Cells (bottom). B. Average total distance traveled by centroid of cell body for free-floating cells is greater than tethered cells. Horizontal bar represents average across cells; shaded area, SEM; and individual dots, mean per cell (scalebar = 10μm).

Using binary cell body image results from image analysis, the average cell body area over time across all cells and cell body area variance per cell across time was computed. Results showed that cell body area of free-floating cells was slightly smaller than tethered cells but not significantly with a t-test p-value of .14 (Figure 3.3B). Because all z-stacks were centered at the largest part of the cell, the slightly larger cell body area for tethered cells may indicate that free-floating cells were also drifting vertically to smaller cross-sectional cell areas in the z-plane (Figure 3.3A). Furthermore, free-floating cells had a significantly higher variance (ks-test p=.0496) in the cell body area which further substantiated that the cells were moving slightly out of plane along the z-axis (Figure 3.3C).

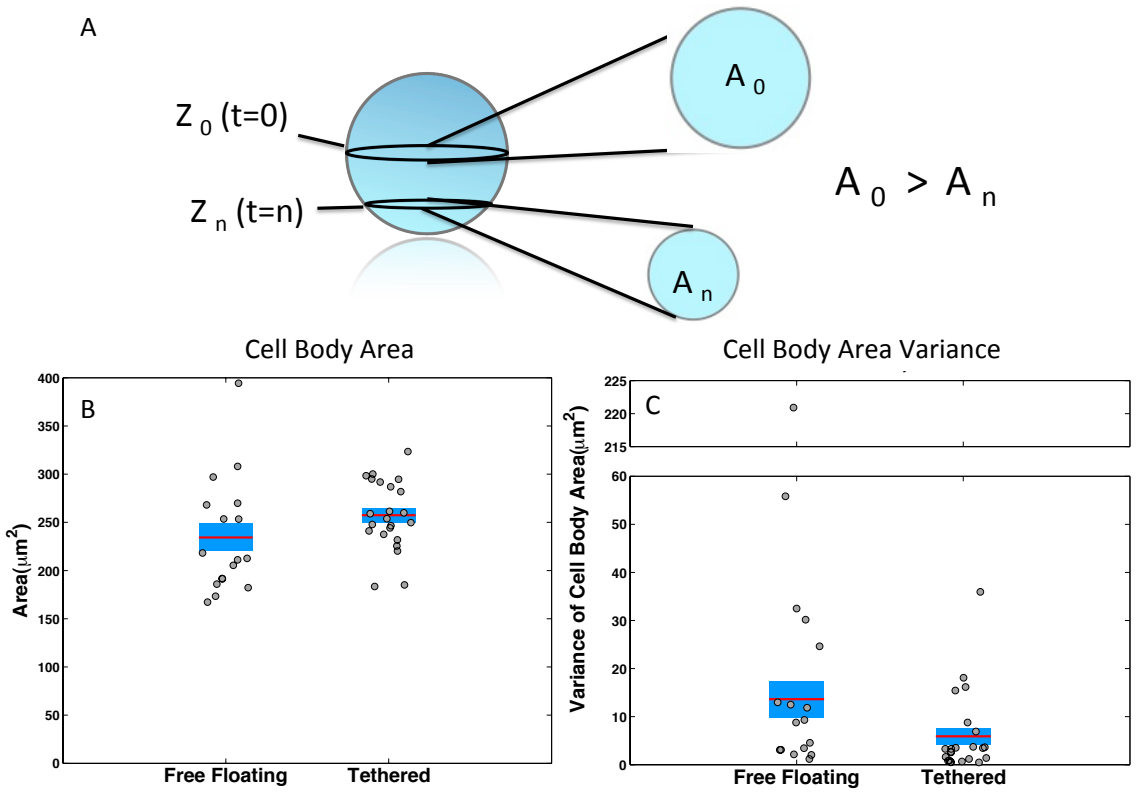

Figure 3.3: Measurements of cell body attributes for Free-floating and tethered cells. A. Schematic of cell's cross-sectional Area at different z-planes. Cross-sectional area is largest, when the slice crosses the center. B. Average cell body cross-sectional area of free-floating and tethered cells has no significant difference p=.14. C. Variance of cell body area over time for free-floating and tethered cells ks-test p=.0496. Horizontal bar represents average across cells; shaded area, SEM; and individual dots, mean per cell

We extended our image analysis technique to capture quantitative McTN metrics for both tethered and free-floating cells. From our image analysis code, we estimated McTN length by measuring the distance of the McTN tip from the nearest cell body boundary point. We found that tethered cells have a larger distance of McTN tip from cell body boundary than free-floating cells with a t-test p-value .02 (Figure 3.4A). Another way we measured total McTN phenotype was by taking the ratio between the full cell perimeter and the cell body perimeter; this allowed us to compare McTN perimeter, while normalizing by cell size. Tethered cells exhibited a higher ratio of full cell perimeter to cell body perimeter than free-floating cells (t-test p= 8.9944e-06) suggesting that tethering allows one to better capture McTNs than the free-floating technique (Figure 3.4B). For the interpretation of this analysis we assume that the average McTN length and number should be the same for tethered as for free-floating cells. While this is consistent with prior published work, prior studies did not have the accuracy of our quantitative analysis. Thus we plan to carry out manual analysis on the images to support this assumption more carefully.

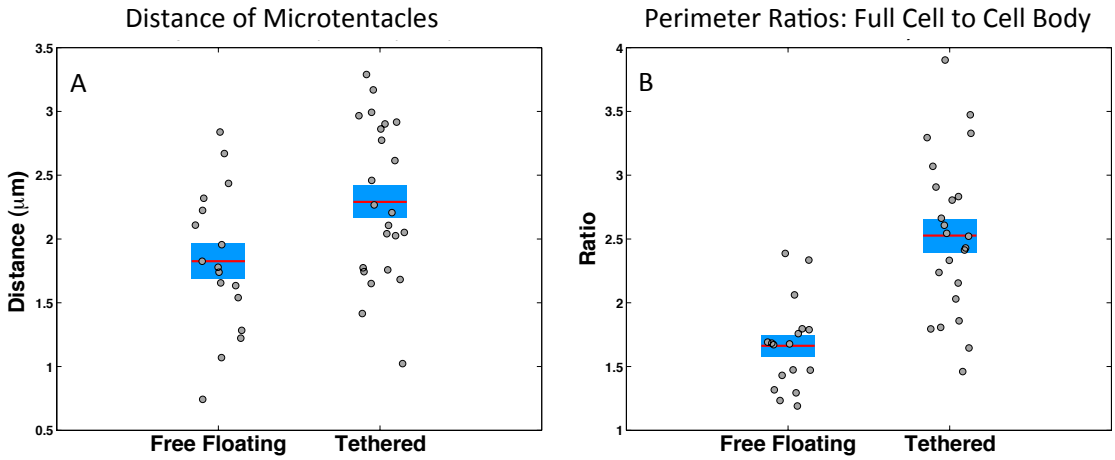

Figure 3.4: Statistics of Free floating verses Tethered Cells metrics suggest that tethered cells allow better visualization of microtentacles. A. Average distance of microtentacle tips from cell body boundary for free-floating and suspended cells (p=0.02). B. Average ratio of Perimeter of the full cell outline to cell body outline for free-floating and suspended cells (t-test p= 8.9944e-06). Horizontal bar represents average across cells; shaded area, SEM; and individual dots, mean per cell.

3.3.3 *Image Analysis captures microtentacles qualitatively and quantitatively of drug treatments*

Once we determined that we were able to visualize and effectively quantify more McTNs with the combination of cell tethering and image analysis, we used tethered cells for systematic studies of McTN length and count. For our first analysis, we selected drugs taxol and colchicine which have previously demonstrated the ability to enhance or diminish microtentacles by respectively stabilizing or destabilizing the microtubules that support McTNs. On tethered surfaces, we calculated the attributes of cell body boundary, full cell outline, and microtentacle tips for cells treated with the vehicle or 0.1% DMSO, 1 μg/mL taxol, and 125 μM colchicine (Figure 3.5).

Deriving metrics from our image analysis attributes, we were able to quantify statistically-significant differences for cells treated with vehicle, 1 μg/mL taxol, and 125 μM colchicine. Colchicine treated cells had significantly fewer McTNs than the vehicle with an anova p-value of 0.0026 (Figure 3.6A). However, there was no significant difference in the number of McTNs between vehicle and taxol treated cells (Figure 3.6A). Looking beyond McTN number per cell, the distance of the McTN tips from the cell body boundary was significantly higher in taxol-treated cells compared to vehicle-treated cells with an anova p-value of 0.0026 (Figure 3.6B). In addition to the significant decrease in McTN number with colchicine, McTN tip distance was

also significantly lower (anova p =0.0001)in colchicine treated cells than in vehicle treated cells (Figure 3.6B). A cell may be perceived as having a stronger McTN phenotype either by increasing the number of McTNs or by increasing the length of McTNs. One way that we measured the aggregate McTN phenotype, was to multiply the number of McTNs by the average distance of McTN tips from the cell body boundary per frame per cell; in essence, the cumulative McTN tip distance within a frame. Taxol-treated cells had a significantly higher (anova p= 0.0151) cumulative tip distance compared to vehicle (Figure 3.6C). Colchicine treated cells, on the other hand, had a significantly lower (anova p=0.0018) cumulative tip distance compared to control (Figure 3.6C). An additional metric we utilized to measure overall McTN phenotype was to take the ratio between the full cell outline and cell body outline; this method has the advantage of including the entire length and curve of McTNs unlike the cumulative tip distance metric, but was still normalized to the size of the cell body. For the ratio of outlines metric (Figure 3.6D), we found that taxol treated cells had a possibly higher ratio than vehicle (t-test p=0.0325 anova p=0.1318) while colchicine had a lower ratio than vehicle (t-test p= 5.4288e-04 anova p<.0001). Cumulative tip distance and ratio, were more robust than number or distance metrics independently as demonstrated by the statistical separation (Figure 3.6C and D).

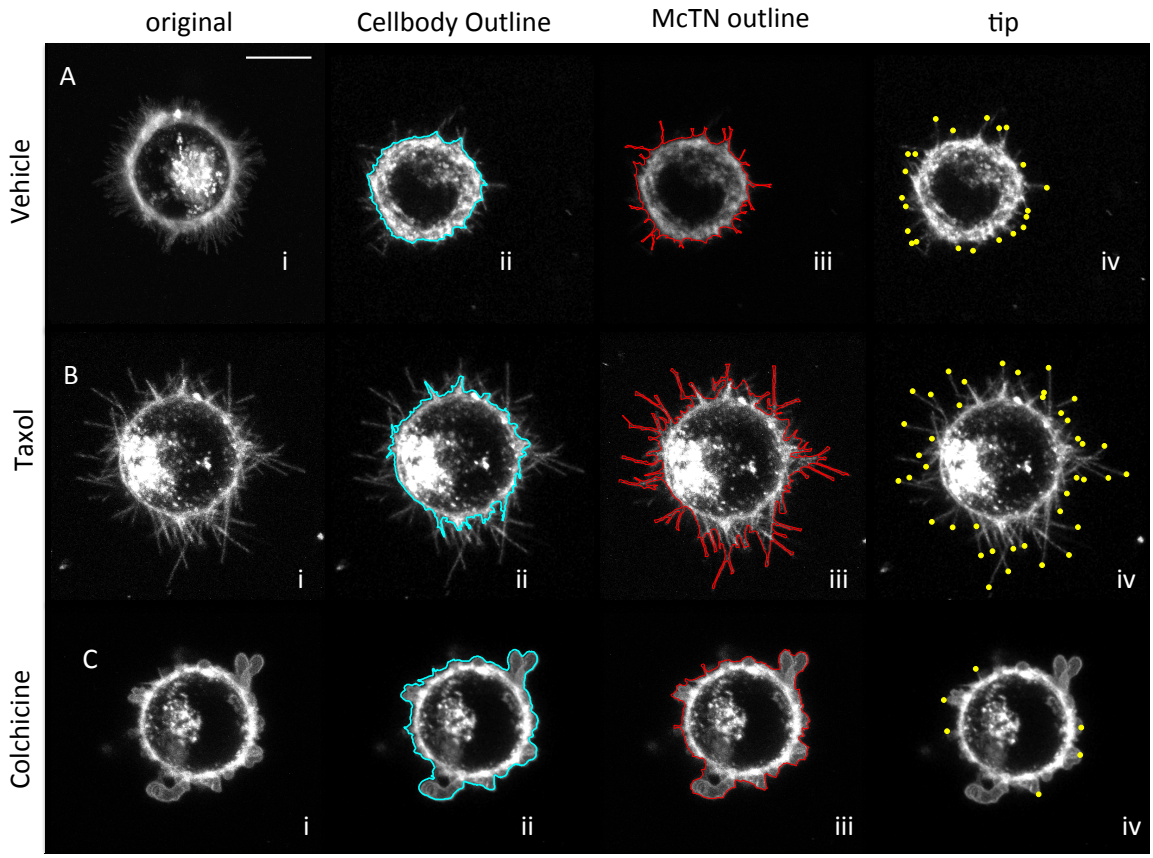

Figure 3.5: Drug Panel shows all the Image analysis attributes for all 3 drug treatments. A. Max projection of z-stack for MDA-436 cells treated with vehicle (i) is analyzed to find cell body boundary (ii), outline of full cell, (iii) and tips of microtentacles (iv). B. Max projection of z-stack for MDA-436 cells treated with 1 μg/mL taxol (i) analyzed for cell body boundary (ii), outline of full cell, (iii) and tips of microtentacles (iv) shows increase in microtentacles. C. Max projection of z-stack for MDA-436 cells treated with 125 μM colchicine (i) analyzed for cell body boundary (ii), outline of full cell, (iii) and tips of microtentacles (iv) shows a decrease in microtentacles (scalebar = 10μm).

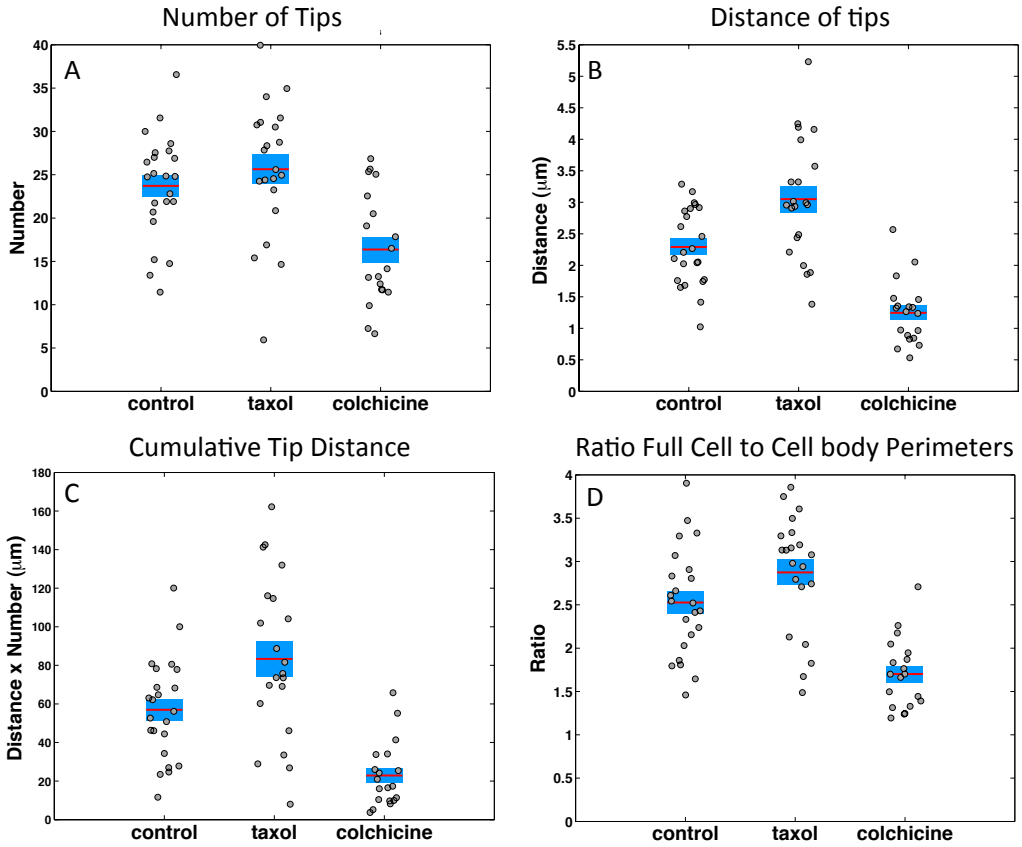

Figure 3.6: Measurements of microtentacle attributes for different drug treatments. A. Average number of microtentacle tips for cells treated with vehicle, 1 μg/mL taxol, and 125 μM colchicine. B. Average Distance of microtentacle tips from cell body boundary for cells treated with vehicle, 1 μg/mL taxol, and 125 μM colchicine. C. Average cumulative tip distance, calculated by multiplying total number of microtentacle tips by the average distance of microtentacle tip from cell body per frame, is shown for cells treated with vehicle, 1 μg/mL taxol, and 125 μM colchicine. D. Ratio of perimeters for full cell outline to cell body boundary is shown for cells treated with vehicle, 1 μg/mL taxol, and 125 μM colchicine. Horizontal bar represents average across cells; shaded area, SEM; and individual dots, mean per cell.

3.3.4 *Dynamic analysis of morphology measures stability of drug treatments*

Having a technique to identify our attributes, allowed us to measure dynamic fluctuations in response to drug treatment. Plotting cumulative distance traces as a function of time for each individual cell, we observed that some cells have more fluctuations in the cumulative tip distance than other cells (Figure 3.7A). The mean cumulative distance for each drug treatment as a function of time, however, was relatively stable suggesting a normal distribution (Figure 3.7A). In order to measure the fluctuations, the autocorrelation coefficient of cumulative tip distance was computed for different time intervals apart: 10 seconds, 20 seconds and 30 seconds. The data showed that up to 30 seconds apart, cells treated with taxol and colchicine had less fluctuations than the vehicle for cumulatie tip distance (Figure 3.7B). Consistent with the autocorrelation coefficient of cumulative tip distance, the autocorrelation coefficient of the ratio of full cell outline to cell body outline showed less fluctuations in cells treated with Colchicine compared to control as far as 30 seconds apart. For Taxol treated cells, the autocorrelation coefficient showed less fluctuations than control as far as 10 seconds apart.

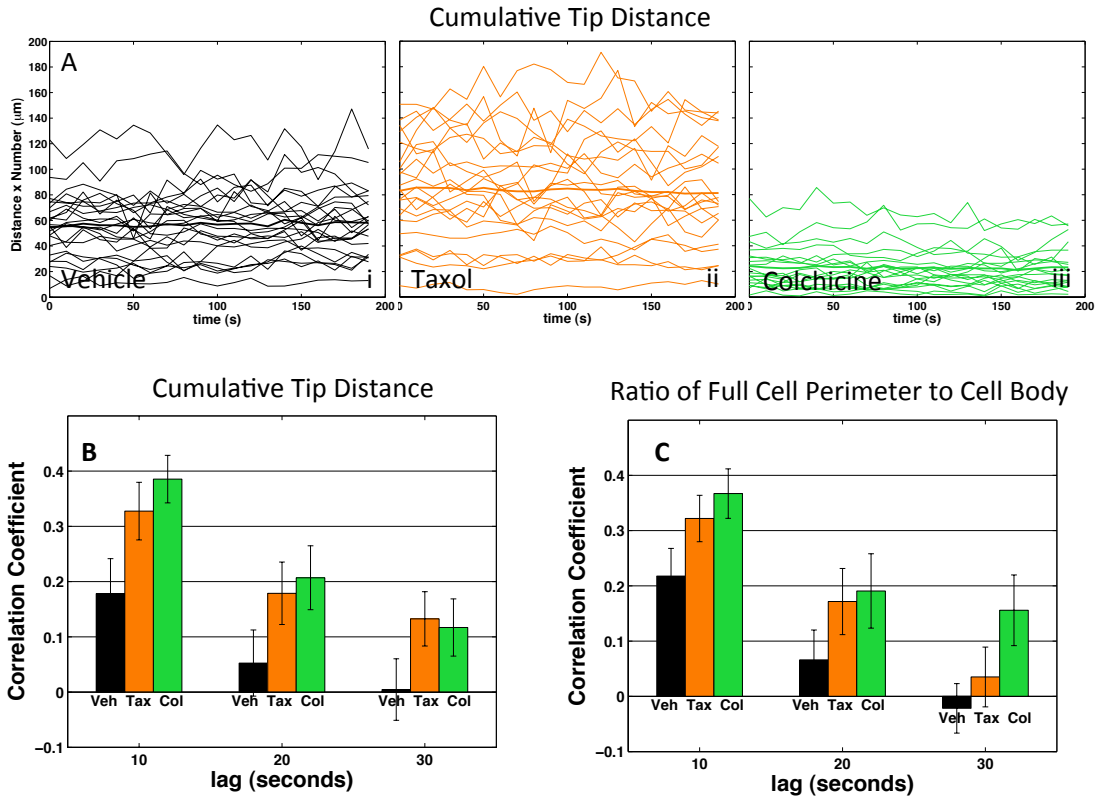

Figure 3.7: Dynamic behavior is assessed by analyzing cumulative tip distance and the ratio of full cell perimeter to cell body perimeter. A. Time traces or cumulative tip distance for individual cells cells treated with vehicle (i), 1 μg/mL taxol (ii), and 125 μM colchicine(iii). Bold time trace is average cumulative tip distance over all individual cells. B. Fluctuations of cumulative distance is shown by computing the autocorrelation coefficient at time lags 0 to 30 seconds for cells treated with vehicle, 1 μg/mL taxol, and 125 μM colchicine. C. Fluctuations of Ratio between full cell outline and cell body boundary is shown by computing the autocorrelation coefficient at time lags 0 to 30 seconds for cells treated with vehicle, 1 μg/mL taxol, and 125 μM colchicine.

3.4 Discussion

Even with the recent advances made in CTC isolation, the small quantity of cells isolated may be as little as 1-10 CTC/mL of blood [129]; this presents major limitations on which downstream analysis techniques are feasible. Desirable analysis techniques like flow cytometry can require as many as 10,000 cells for statistically relevant results. Furthermore, CTC-derived patient xenografts (CDX) have had a very low success rate [136]. Currently, the only FDA approved technique for analyzing CTCs is CELLSEARCH. Unfortunately, CELLSEARCH can only enumerate cells and requires fixation; thus, limiting parallel and downstream analyses. Our technique demonstrates the ability to yield statistically significant results with as few as 19 cells without killing the cells, potentially enabling downstream or parallel cancer assays.

Current techniques for McTN analysis require double-blinded studies where the researcher tediously counts the McTNs by hand. Such techniques are time-consuming and potentially lack uniformity. For the first time, we are able to evaluate McTN number automatically and systematically. We introduce multiple quantitative measurements of cell phenotype such as distance of McTN tip from cell body and number of McTNs. Previous research based on qualitative assessment of positive or negative McTN phenotype concluded that taxol appeared to increase mostly the length of McTNs and a combination of latrunculin and taxol appeared to increase

the number of McTNs [59,96]. In this study we were able verify quantitatively that taxol increases the McTN behavior by specifically increasing the length of existing McTNs rather than number of McTNs in general. Such distinctions may pave the way towards determining whether an increase in the number of McTNs or the length in McTNs is more likely to increase CTC reattachment.

The most promising techniques for determining targeted, personalized therapies include using patient derived xenografts (PDX) and circulating tumor DNA or ctDNA [136]. However, in patients where the primary tumor is too small, PDX is not always an option. PDX has a highly variable success rate ranging from 23-75% depending on tumor types; for breast cancer specifically, 23% [137,138]. Thus, the PDX model has a high risk of losing precious patient samples and not gaining any information. Additionally, the PDX model can take up to 6 months to establish and 2 years for a complete drug study. ctDNA, on the other hand gathers tumor DNA from the bloodstream and has the advantage of being noninvasive. While ctDNA analysis can predict drug resistance in some patients, the prediction is purely correlative. The tethering and image analysis technique allows us to quickly and directly test drug response.

For the first time ever, we were able to estimate morphological stability by measuring the autocorrelation coefficients of metrics for total McTN phenotype. The lower fluctuations in drug treatments of our autocorrelation results suggest that morphological stability is consistent with biochemical stability. Previous research shows that cells from EMT-induced cell lines have more McTNs, higher reattachment rates and embed themselves into endothelial cell layers. [37]. Cell lines rich in

McTNs due to tau-induced microtubule stabilization trap more efficiently in the lung capillaries of living mice [59]. Neither McTN dynamics of metastatic cells lines has been analyzed yet, nor whether cells treated with McTN stabilizing drugs are more likely to get stuck in the capillaries. While cells with more McTNs have higher reattachment, less dynamic McTNs may suggest cells are less able to extravasate through endothelial cells and out of the bloodstream. Future work should explore whether drug induced McTN cells that form less dynamic McTNs are more likely to get trapped in the capillaries of distant tissues in vivo, as well as whether the McTNs are more or less dynamic in different breast cancer subtypes or different stages of metastatic progression.

The ability to automatically and quantitatively compare circulating tumor phenotypes has potential applications in improving basic understanding of the role of McTNs mechanism and reattachment, studying patient CTCs, and perhaps selecting appropriate drug therapies for patients. Measuring McTNs is a fast assay that may give insight to cancer progression and drug response without the complications of culturing cells like PDX′s which can take up to 2 years for a drug study.

3.5 Materials and Methods

3.5.1 *Cell Culture*

Human MDA-MB-436 cells derived from a metastatic pleural adenocarcinoma were obtained from the American Type Culture Collection were used for all experi-

ments. Human MDA-MB-436 cells were selected as a cell model for metastatic potential and presence of microtentacles [96]. MDA-436 cells were cultured in DMEM media containing 10% Fetal Bovine Serum and 1% penicillin/streptomycin. Cells were detached from cell culture plates at a minimum of 80% confluency using trypsin.

For drug treatments, all reagents were obtained from Sigma Aldrich and concentrations were based on previous studies. For microtubule stabilization, 1.2 μM Taxol was administered, and previous studies determined cell viability using XTT, CellTiter 96, and PARP assays [40, 46, 52, 133]. For microtubule destabilization, 125 μM Colchicine was administered, and previous studies determined cell viability using CellTiter 96 and PARP assays [40, 52].

3.5.2 *Free Floating Cells*

For the experiments involved in suspended free floating cells, ibidi microfluidics chambers were coated with 1% pluronic F-127 solution for 30 minutes. Cells were treated with a 1:10,000 dilution of CellMask-Orange (Life Technologies) membrane stain in order to visualize microtentacles. Next, cells were treated with the vehicle or a drug treatment of 1 μg/mL taxol or 125 μM colchicine. A 150 μL sample of treated cells was added to each ibidi channel at a concentration of 30,000 cells per channel. Cells were incubated at 37C to allow absorption of Orange mask and drug treatment for 30 minutes prior to imaging.

3.5.3 *Tethered Cells*

For tethered cell experiments, cytophobic polyelectrolyte multilayers (PEMs) deposited on microfluidic substrates were used to prevent tumor cell adhesion, and the addition of lipid moieties to tether tumor cells to these surfaces through interactions with the tumor cell membranes (Figure 3.1A). Cells received the same treatment of Cell-Mask Orange and drugs as free floating cells.

3.5.4 *Confocal Microscopy*

All imaging was conducted on an Olympus FV-1000 confocal at a 60x magnification. For videos of suspended cells, a set of five 0.5 μm/slice z-stacks were imaged every 6.5 seconds for a total time series of 20 z-stacks. For tethered cells, z-stack slices were 1 μm thick and stacks were imaged every 10 seconds. In all cases, the middle z-slice was calibrated along the z-axis to where the cell appeared largest.

3.5.5 *Image Analysis*

For each time point, a max intensity image of each z-stack was computed, all further processing was derived from max intensity images (Figure 3.8). Outlines for the cell-body and full-cell were computed separately. Cell-body outlines were identified by using image analysis methods published previously [134].

In order to get clear outlines of the microtentacle features, we modified and

combined previously published image analysis techniques optimized for cell shape along with techniques optimized for stress fibers by using a rotating anisotropic filter [134,135]. Consequently, analysis for full cell outlines processed and optimized parameters for 3 distinct cellular regions separately: microtentacles, bright cell-body border and globular base of protrusion region, and the cell center. The full cell outline was derived from a binary image comprised of the 3 distinct analyses. (Figure 3.9).

Due to the fact that tentacle features were significantly dimmer than the cell body and filamentous rather than globular, the first analysis was optimized specifically for the McTNs. First, a 2 x 2 median filter was applied to the maximum z-projection per time-point in order to give a very fine-featured, localized smoothing optimized for approximately half the width of microtentacles (Figure 3.10A). Following, the output underwent and initial rough convolution with a rotating anisotropic filter that will be described in more detail below (Figure3.10B). After the initial iteration of rotating anisotropic filtering was applied, contrast adjustment algorithms in matlab were optimized to make the protrusions rather than cytoplasm uniformly white (Figure 3.10C). Additionally, to specifically extract the microtentacle features, the output underwent another iteration of rotating anisotropic filtering; multiple iterations of the rotating anisotropic filtering were repeated using the combined output of the previous series of filtering.(Figure 3.10D) [135]. The 60 anisotropic filters consisted of convolving a Laplacian with a 60 Gaussian kernels at different angles (Figure 3.11). The contrast adjusted image (Figure 3.10C) is convolved with anisotropic filters at 60 different angles (Figure 3.12). Each individual anisotropic

filter emphasizes alignment along a different angle (Figure 3.13). Next, the max projection of all 60 anisotropic filter results was computed and another pass of contrast adjustments (Figure 3.13). The image underwent several iterations of rotating anisotropic filtering followed by compiling them. Finally, the resulting anisotropic results was linearly multiplied with the initial rotating anisotropic results before the contrast was adjusted again and then thresholded (Figure 3.10E and F) Because the rotating anisotropic filter selects preferentially for line-like features occasionally truncating, rather than intersecting with the cell body or potentially incorrectly biasing cell-body curvature near the base of the protrusion, a second analysis optimized for features including and near the cell body boundary was conducted independently. For this second region, the initial image underwent a matched filtering technique originally designed for retinal segmentation (Figure 3.9B) [139]; this technique showed preference for the base of the protrusions. The retinal segmentation technique was image multiplied with the initial anisotropic filtering results prior to being inputed into the previously establish local, global curvature technique [134]. Lastly, to prevent the analysis optimized for tentacles from creating an annular outline, a rough estimate of the cell center was computed by using the matlab built in function of imfilter to blur the image, thresholding, and then using matlabÕs bmorph to remove any spuring and erode shape to prevent it to contributing to cell outline information (Figure 3.9C). Cell center analysis did not require any contrast optimization. Once all 3 analyses were complete, results were added together for a composite binary image (Figure 3.9D) and cleaned of debris (Figure 3.9E). Finally, the composite binary image was inputted into an active contour algorithm as an

initial estimate (Figure 3.9S2F).

Once the outline of the full cells perimeter was computed, the tips were computed by skeletonizing the binary microtentacle image. From the images′ skeletons, tips were selected by locating the coordinates of maximum local curvature.

Attributes derived from image analysis consist of microtentacle inclusive outline of the full cell, outlines of the cell body exclusively, centroid of cell body, and the tips of the microtentacles. From these attributes, measurements of microtentacle behavior were derived including, area of the cell body, variance in the cell body area, total distance traveled by the centroid of the cell body boundary, ratio of the perimeter of the full cell perimeter to the cell body perimeter, distance of microtentacle tips from cell body perimeter, number of microtentacle tips. Additionally, cumulative tip distance was measured by multiplying the number of microtentacles by the average distance of microtentacle tips from the cell body boundary per frame per cell. All attributes and metrics were computed in matlab.

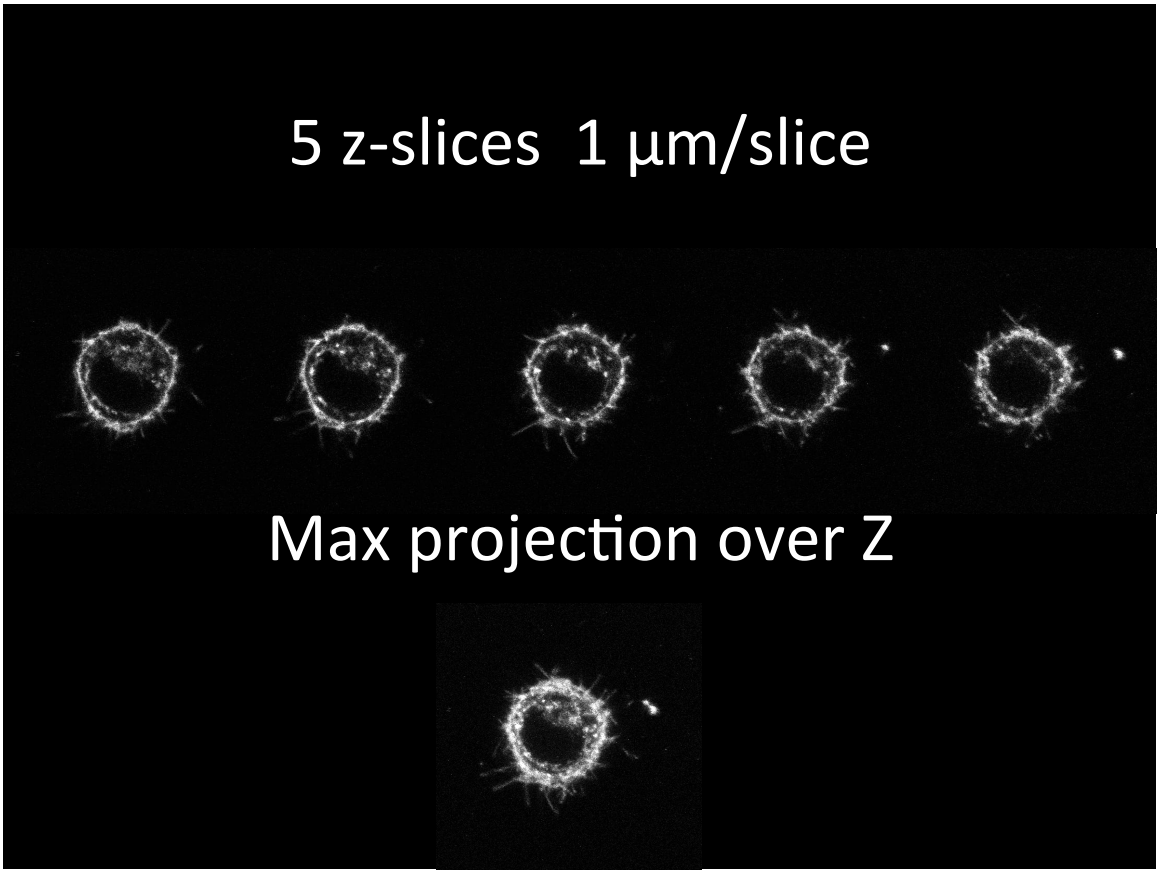

Figure 3.8: Max Intensity of z-projections. For the 5 z-slices at each time point (top), a max intensity image of each z-stack was computed (bottom).

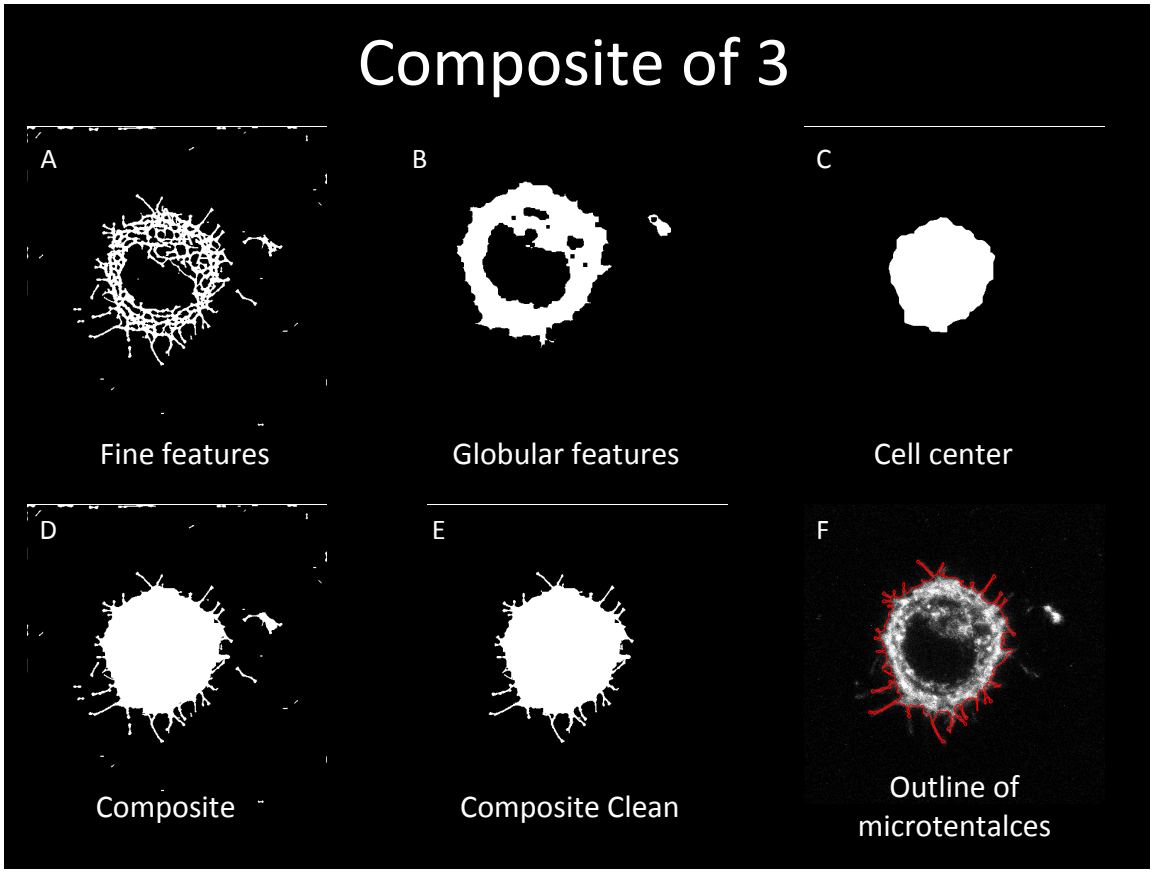

Figure 3.9: Full cell outline is the composite of analyses optimized for 3 distinct cellular regions. A. Binary image results for algorithms optimizing for fine featured tentacles. B. Binary image results for algorithms optimizing for globular features. C. Binary image results for computing a rough cell center. D. Binary image composite of 3 binary results from different cell regions. E. Binary image composite cleaned of debris. F. Outline overlay of final results on initial image includes microtentacles.

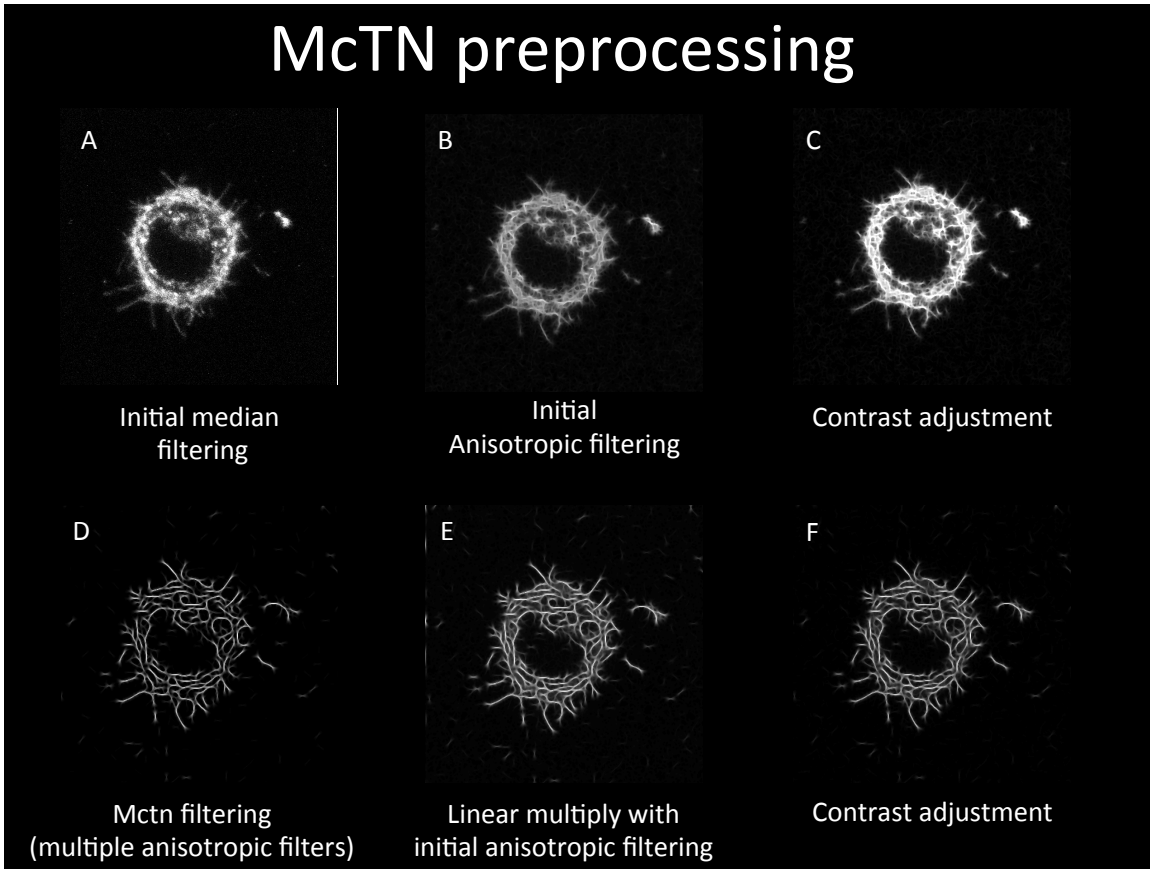

Figure 3.10: Results of processing steps optimizing for fine featured tentacles. A. Median filter was applied to the maximum z-projection results B. Results from first convolution with a rotating anisotropic filter routine called 'pixelalign' C. Contrast adjustment results optimizing contrast for fine featured tentacles D. Results from multiple iterations of a rotating anisotropic filter. E. Results from linear multiplication between intial and final rotating anisotropic filter results. F. Final contrast adjustment results prior to thresholding.

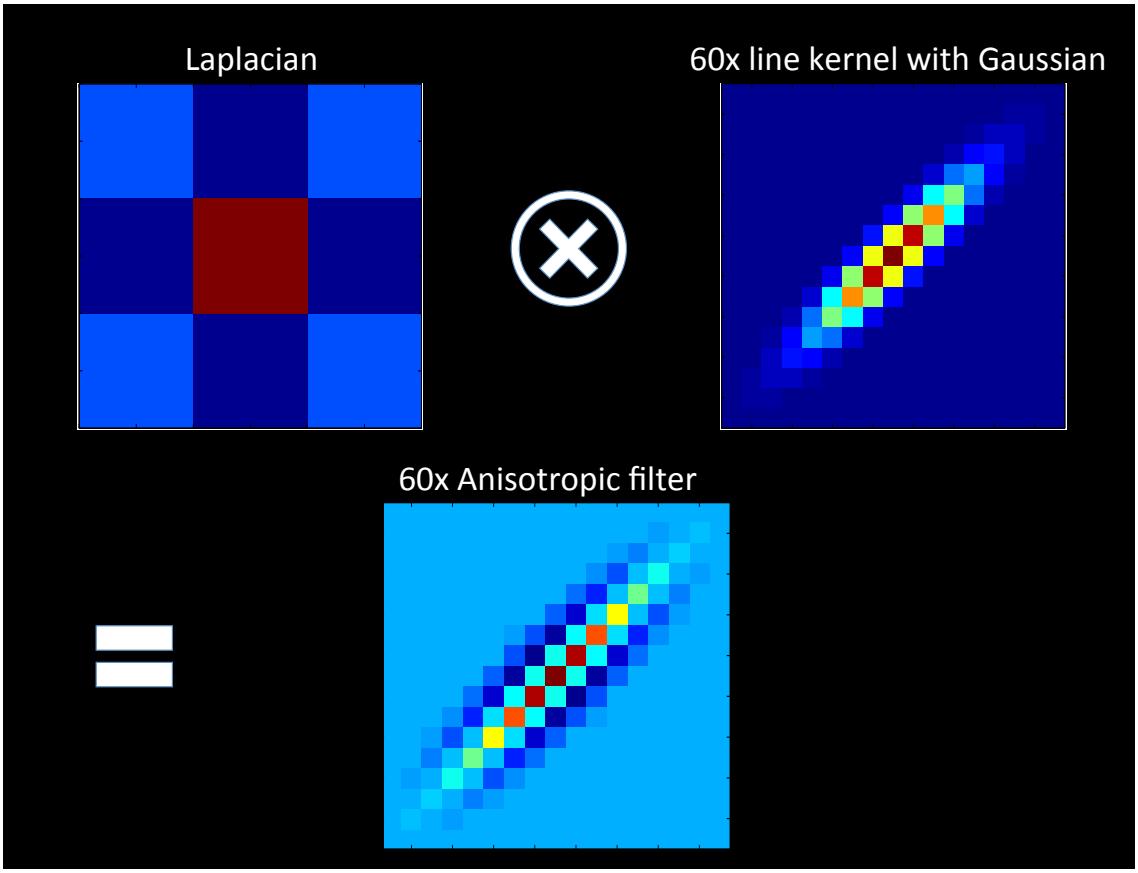

Figure 3.11: Computing rotating Anisotropic filter. A Laplacian kernel (top left) is convolved with 60 Gaussian line kernels (top right) at 60 different angles to get 60 different Anisotropic filters.

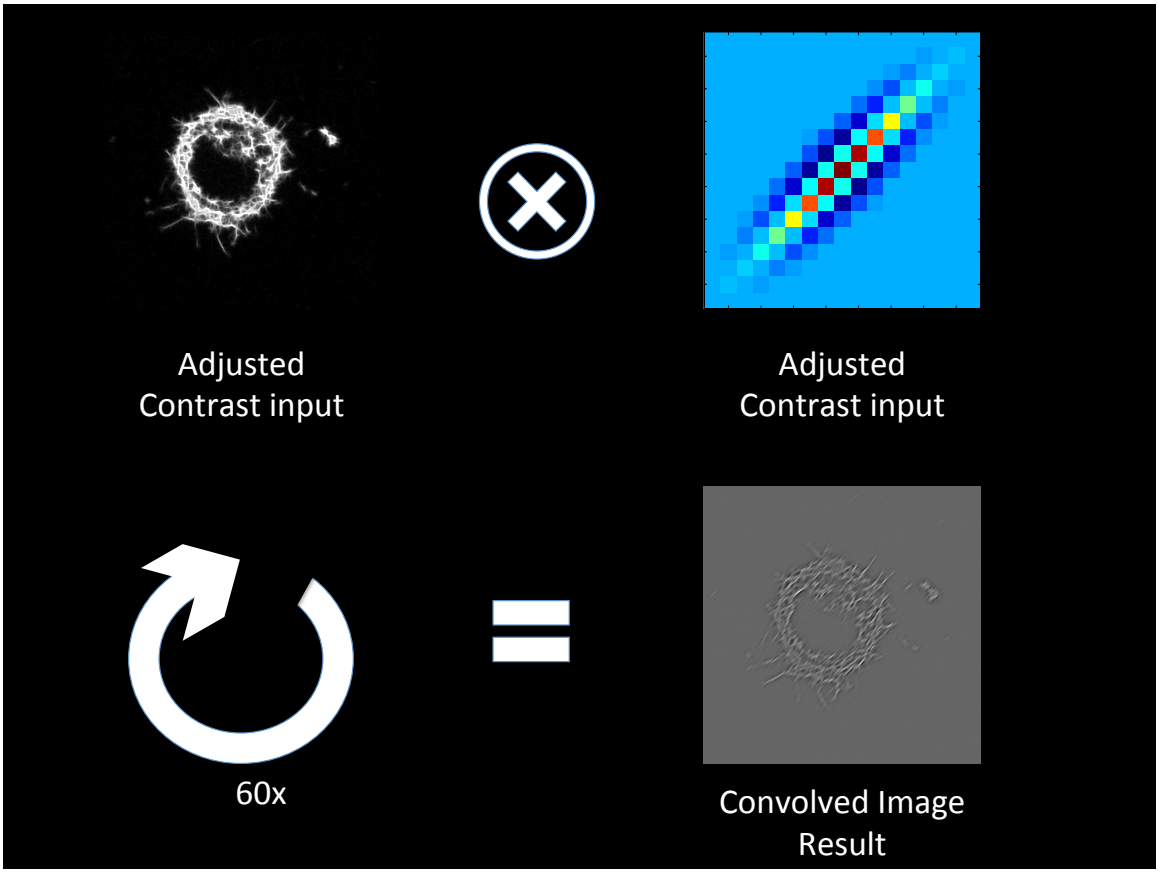

Figure 3.12: Rotating Anisotropic filter. The contrast adjusted image (top left) is convolved with the 60 different anisotropic filters (top right) resulting in 60 filtered results biased at different angles (bottom right).

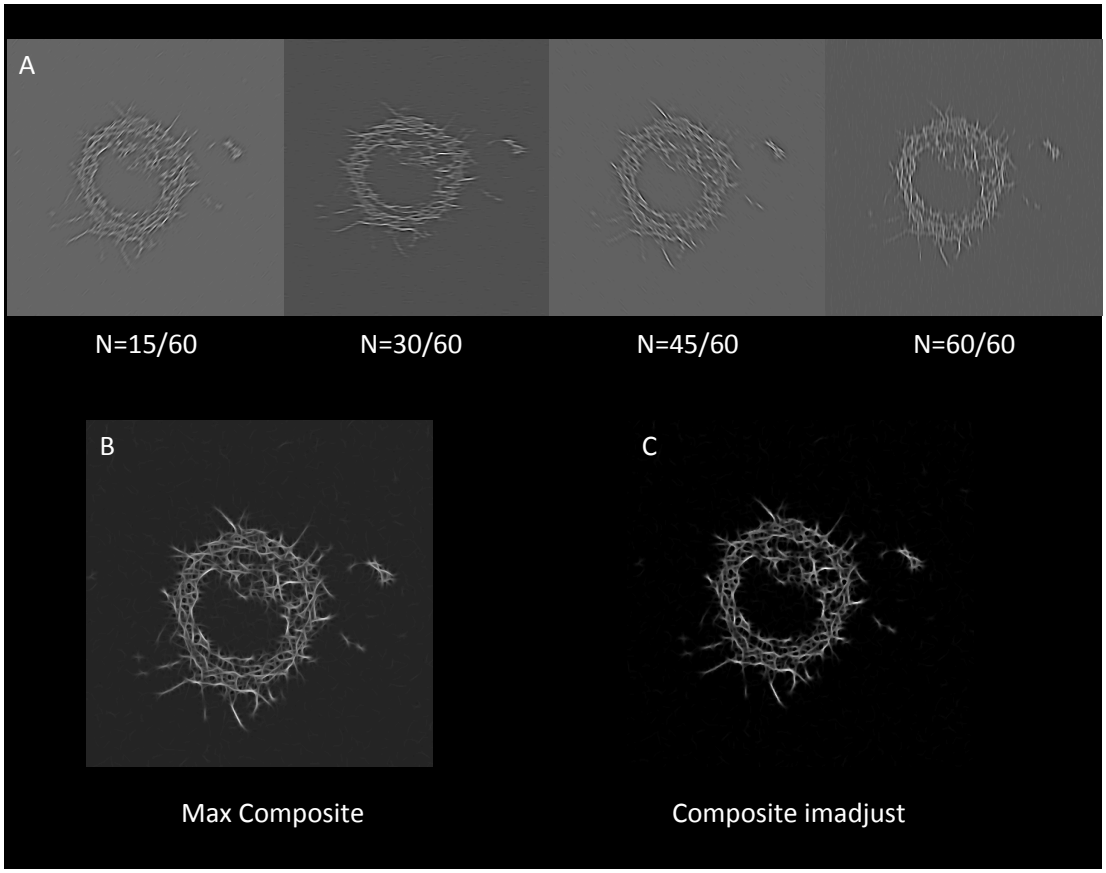

Figure 3.13: Composite rotating Anisotropic filter results. A. Results of Anisotropic at different angles B. Maximum of composite of anisotropic results C. Contrast adjustment results of anisotropic filtering.

3.5.6 *Metrics and Dynamics*

To better understand the dynamics of the cells, the fluctuations of the cumulative tip distance and ratio of full cell perimeter to the cell body perimeter as a function of time, was measured by computing the autocorrelation coefficient in 10 second increment lags 0 to 30 seconds. Autocorrelation code was written in matlab. All dynamic measurements were only conducted on tethered cells.

3.5.7 *Statistics*

All statistical analysis was implemented in MATLAB. Determination of normal distribution was calculated by measuring skewness and kurtosis where any distribution of normal with a skewness of ± 2 or kurtosis 0-6 was considered close enough to normal to apply standard statistical analysis. To measure p-values between two conditions (ie free-floating vs tethered), the built in MATLAB ttest2 was used; for comparing across multiple conditions, ANOVA analyses were implemented. In the event of a non-normal distribution, an additional Kolmogorov-Smirnov (ks-test) was conducted to compare 2 conditions.

Chapter 4: Summary and Future directions

4.1 Summary and Discussion of Results

Prior to the work outlined in my thesis, the only existing techniques for measuring McTNs consisted of making use of double-blinded studies where the evaluator scored samples for the absence or presence of McTNs. Additionally, no McTN studies had quantified the microtubule protrusions in attached cells under actomyosin cortex perturbations. Lastly, no studies had measured morphological fluctuations of McTNs under tubulin drug perturbations.

4.1.1 *EB1 Results*

In chapter 2, I showed that manipulating the actin cortex changes the growth dynamics of microtubules in attached cells. I demonstrated that particle tracking algorithms could successfully be adapted to biological EB1 tips. Results support the hypothesis that the actomyosin cortex acts as a barrier. When the actomyosin barrier is removed by latrunculin or severed via Y-27632, EB1 tips are allowed to move further beyond the cell body boundary compared to control as measured both by average distance from the cell body boundary and percent of EB1 tips outside the cell body boundary. EB1 trajectories move slower outside the cell body

boundary compared to inside the cell body boundary across control and all drug treatments suggesting that the membrane is the larger inhibitor of speed. Speed of EB1 trajectories in Blebbistatin treated cells move the slowest across all regions. Due to the fact that in attached cells there is a protrusive force outward as the result of actin polymerization [116], this may outweigh the inward contractile force of actin for attached cells. Lastly, EB1 tips in cells treated with Blebbistatin move the least straight followed by those treated with Latrunculin. EB1 tips in cells treated with Blebbistatin and Latrunculin also move more slowly.

As demonstrated by the speed of the EB1 tips beyond the cell body boundary, membrane tension most likely places a significant force on microtubule growth. It would be interesting to repeat the above experiments and decrease the membrane tension using sucrose. Decreasing the membrane tension should theoretically increase the ability of EB1 tips to move beyond the cell body boundary for control and Blebbistatin treated cells. Additionally, a reduction of membrane tension should increase the overall speed and straightness of EB1 trajectories in Latrunculin-A. Similar experiments have been conducted to study the effect of membrane tension on clathrin polymerization, where decreasing the tension either by micropipette aspiration or sucrose solution increased clathrin polymerization [140]. Another study shows that decreasing membrane tension in migrating cells results in loss of polarity and more spread out cells; additionally increasing membrane tension caused a decrease in actin polymerization [141].

Finally, some additional considerations should be discussed regarding the limitations of the drug treatments. First, imaging the GFP tagged EB1 tips required

exposure to blue light and research has shown that blue light exposure can inactivate Blebbistatin in *in vitro* cells [142]. Thus, the efficacy of Blebbistatin treatments may have had a limited effect on the cells. On the other hand, because these studies were conducted on a confocal microscope, blue light exposure was confined to a small area of the cell at a time and for a maximum total exposure of only 2 minutes, so diffusion may have maintained continued drug exposure. Also, Y-27632 has some off-target effects like inhibiting PRK2, a kinase involved in cell to cell adhesion [143]. It is unclear how PRK2 inhibition would impact the above results.

4.1.2 *Suspended Cells*

In chapter 3, I show that manipulating tubulin stability manipulates McTNs geometry and dynamics. Successful analysis techniques were developed for analyzing the full outline of cells including McTNs. Results show that tethering cells does not significantly alter McTN length; however, tethering allows visualization of more McTNs than the free-floating method. It is worth noting, however, that the complete absence of attachment in free-floating cells may increase the contractility of the actomyosin cortex which could also conceivably repress McTNs [82,83]. Stabilizing tubulin by using Taxol treatment significantly increases the distance of McTNs tips from the cell body, and destabilizing tubulin using Colchicine treatment significantly decreases distance of McTNs tips from cell body. In order to measure overall McTN morphology, I proposed using 2 composite McTN metrics: cumulative tip distance of McTN tip from cell body boundary and the ratio of the full cell outline

to the cell body outline. Both metrics measure an increase in McTN phenotype for Taxol treated cells compared to control and a decrease in McTN phenotype for Colchicine treated cells when compared to control. All results are consistent with the model where an increase in tubulin stabilization enhances the ability for microtubule protrusions to move beyond the cell body boundary and the converse results for microtubule destabilization. Based on EB1 study above, the average distance of microtubule tip from the cell body boundary in attached cells is 1.6158 μm$\pm$.08 compared to 2.2907 μm$\pm$.13 in tethered cells. This is consistent with the hypothesis where a lack of traction force in suspended cells decreases the ability of actin polymerization to push the plasma membrane outward; thus, allowing the plasma membrane to deform more easily around the microtubule protrusion.

In my experiments looking at suspended cells, I also measure morphological dynamics and find that both drug treatments Taxol and Colchicine cause less morphological fluctuation compared to untreated cells. These results may have implications for how CTCs reattach; previous research studies show that Taxol increases reattachment in impedance assays [40]. However, CTCs *in vivo* have the additional hurdle of getting through an endothelial layer of cells. It is plausible that McTNs might require a requisite amount of flexibility and motion in order to push McTN protrusions between endothelial cells.

A conceivable next step, might be to conduct the same dynamics measurements on tethered cells with the same actomyosin targeting drugs discussed in the EB1 experiments. I would propose that for all drug types (Latrunculin-A, Blebbistatin, and Y-27632), there would most likely be an increase in the length of

McTNs, and that Latrunculin-A with its complete lack of actomyosin cortex may additionally increase the total number of McTNs. Results may have interesting implications if the morphological fluctuations in drug treated cells increase or are comparable to control conditions. I expect that while stabilization of microtubules may decrease morphological fluctuations, destabilizing the actomyosin cortex would preserve fluctuations if not increase them.

4.2 Future Directions

4.2.1 *Effects of Cancer Relevant Mutations*

Work from my thesis demonstrates changes in microtubule dynamics as a result of drug treatment. A natural next step would be to make the same measurements but expand from drugs to genetic modifications. Here, I propose using 4 different genetic modifications spanning a spectrum of different cytoskeletal states and metastatic capabilities. The parental line used as control for these experiments is MCF10A; MCF10A is a non-tumorgenic mammary epithelial cell line well-established in the literature as a model for normal breast cell behavior [144]. The genetic modifications would include MCF10A with a patient mutation in the phosphatidylinositol-4,5-bisphosphate 3-kinase, catalytic subunit alpha or PI3CA; MCF10A with tumor suppressor gene pten homogenously knocked out (PTEN-/-); and MCF10A with the transcription factor twist overexpressed. These choices of cell lines will serve as an *in vitro* cell line model that separates, non-tumorgenic

(control), invasiveness (PIK3CA-H1047R), McTN formation (pten -/-), and cancer stemness (twist).

In terms of McTNs, MCF10As form few McTNs. It has been shown that MCF10A pten(-/-) exhibits McTNs, while MCF10A PIK3CA produce very few McTNs [41]. MCF10As overexpressing twist have not been tested for McTN presence, but McTNs are expected. Previous research demonstrates that ectopic expression of twist in MCF10As induces cancer stemness [145]; also, overexpression of twist in another non-tumorgenic breast cancer cell line HMLE induces McTNs [37].

Within the mechanical framework of McTNs, stronger more stabilized microtubules contribute positively to McTNs, while weaker tubulin contributes negatively. Glu-tubulin has a long persistence time, slow turnover rate, and is potentially an important indicator of McTN formation [51, 59, 146]. Of the 4 cell lines, MCF10A, pten(-/-), and PIK3CA-H1047R are known not to have high levels of glu-tubulin; however, MCF10A cells transfected with twist are expected to have higher levels of glu-tubulin based on experiments that use other cell lines transfected with twist [37]. Expression of vimentin is another potential indicator of microtubule strength and is known to colocalize and align with glu-tubulin [42] which may help stabilize the McTNs. Furthermore, in the clinical scope vimentin has been identified as a marker for breast cancer cells more likely to metastasize [42]. Based on previous research in the Martin lab, only the cell line MCF10A with PIK3CA-H1047R of the 4 cell line models is known to express significant levels of vimentin; we hypothesize that MCF10A with overexpression of twist will also express significant levels of vimentin based on research of other cell lines overexpressing twist [37]. The vimentin contri-

bution to McTNs formation is not completely clear, however. From rheological *in vitro* studies, a direct interaction between actin and vimentin has demonstrated a stiffer actin network [147]; this would contribute negatively to McTN formation and may explain why there are less McTNs in the case of PIK3CA mutation.

The second half of the mechanical framework of McTNs, is the actomyosin cortex where a more contractile actomyosin cortex contributes negatively to McTNs and a weak actomyosin cortex contributes positively to McTNs. There are 4 main ways to weaken the actomyosin network: either by cutting actin filaments, depolymerizing actin, weakening actin crosslinking, or weakening myosin-based contractions. As demonstrated in my EB1 research, removing the actomyosin cortex network as opposed to weakening it has distinctly different growth dynamics. Cofilin, for example is an actin severing protein that would be expected to weaken the actomyosin cortex [148]; The only cell line known to contain high levels of activated cofilin is MCF10A pten(-/-) cells (See Figure 4.1). Another important consideration of the actomyosin cortex is the myosin light chain; the myosin head binds to the actin filaments and allows the actomyosin cortex to contract. Currently, we don′t have direct information about the myosin light chain′s activation state, but based on the presence or absence of McTNs described above, we have formed hypotheses of the myosin light chain′s activation state. Myosin light chain is predicted to contribute to a tighter more contractile actin cortex in MCF10A cells with PIK3CA mutation and twist. For MCF10A control cell line, myosin light chain is predicted to be contractile but significantly less contractile than cells with PIK3CA mutation and twist. Lastly, myosin light chain is expected to cause a loose and non-contractile

actin network in MCF10A pten(-/-) (See Figure 4.1).

Based on all the above information, we hypothesize a positive or negative contribution of the actin cortex state and microtubules towards McTN formation (See Figure 4.1). Using this qualitative model, we hypothesize whether McTN formation is driven more by stable tubulin or weaker actin. For MCF10A, the actin cortical tension and microtubules counteract each other, so very few McTNs form. For MCF10A pten(-/-), the microtubule behavior is normal, but the absence of strong actin cortical tension results in McTNs. For MCF10A PIK3CA-H1047R cells, the vimentin aligns with the microtubules potentially making things stiffer, but vimentin interactions with actin can also make for a stiffer network; thus, actin and microtubule interactions still cancel each other out. For MCF10A with twist overexpression, the glu-tubulin in the microtubules drives the cell to form McTNs.

It is expected that since pten (-/-) cells have a looser actin network compared to MCF10A cells, EB1 tips will move slower on average than MCF10A cells in a manner similar to Latrunculin-A treated cells. EB1 trajectories in Pten (-/-) cells might move slower near the cell body periphery due to the cell membrane acting as a barrier. Different from pten(-/-), PIK3CA-H1047R mutation has an increased expression of vimentin, but is also thought to have a stronger actomyosin cortex. It is expected that EB1 trajectories in PIK3CA-H1047R activated cells move at a slower speed and move less straight due to the actomyosin cortex acting as a barrier. However, because of the potentially vimentin-stabilized microtubules, overall length of trajectories may be longer. As twist-transfected cells are hypothesized to have a weaker actin cortex but stronger tubulin growth due to the increase in glu-tubulin,

EB1 trajectories are expected to move faster in both the bulk and cell-body periphery of the cell compared to control cells. Cells transfected with twist are expected to have slower moving EB1 tips in the cell body periphery, due to a more active actin cortex. EB1 tips in twist-transfected cells are also expected to move well beyond the cell body boundary.

I have conducted preliminary experiments for MCF10As, pten (-/-), and PIK3CA-H1047R. Preliminary results demonstrate successful EB1 transfection and clearly defined EB1 tips. By doing a time average of the videos, we were additionally able to see the 3 phenotypes qualitatively for EB1 trajectories (See Figure 4.2). Overall, results look promising for EB1 tracking.

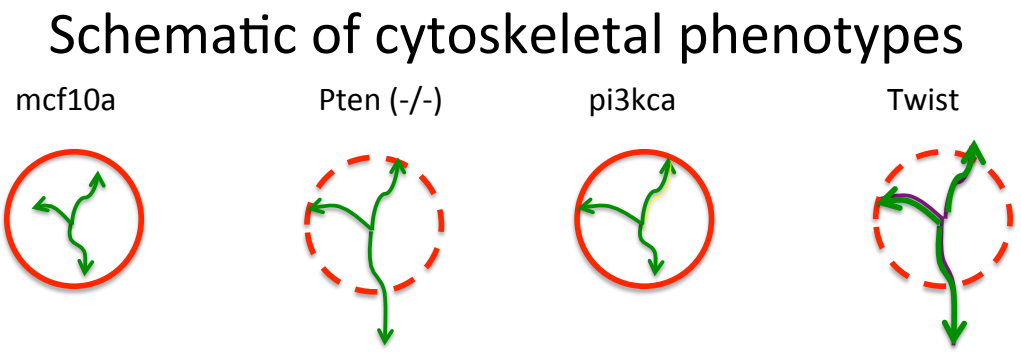

		mf10a	Pten (-/-)	Pi3KCA	Twist
Biomolecular	Glu	-	-	-	+++
	Vimentin	-	-	++	+++
	cofilin	-	+++	-	?
	mLC	+*	-*	++*	++*
Mechanical	Actin	+	-	++	++*
	MT	+	+	++	+++
Overall	mcTn	-	++	-	+++

* Hypothesized cytoskeletal state

Figure 4.1: Different balances of forces between microtubules and actin cortex for 4 different cyotoskeletal phenotypes where thicker lines indicate stronger force and dashed lines indicate weaker force; red is actin, green is tubulin. Chart indicates state of each cytoskeletal component based and overall mechanical contribution, where a '-' indicates not present; '+', present; '+++' strongly present.

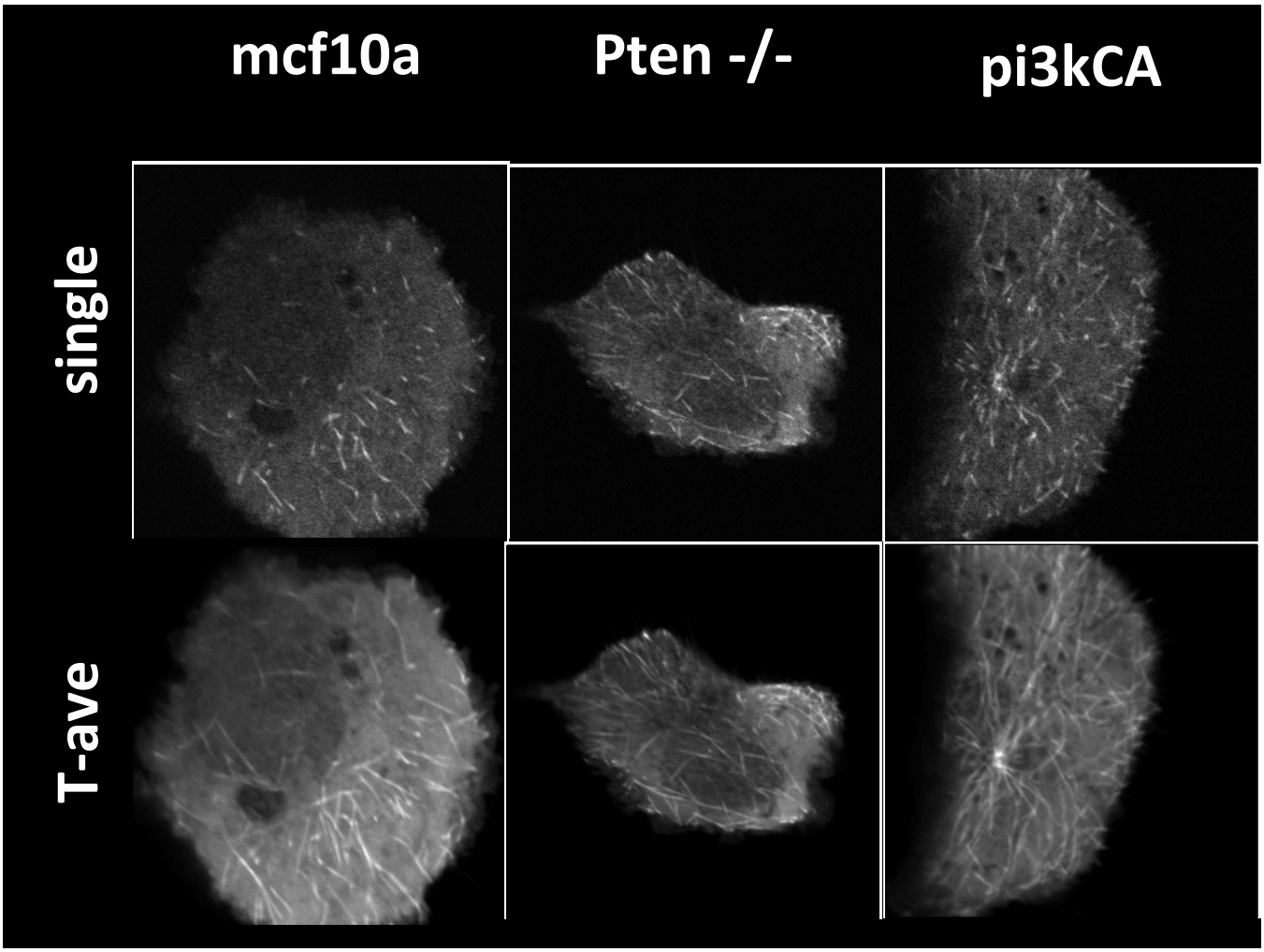

Figure 4.2: Live-cell confocal microscopy of EB1-GFP. (Top) Single image frame of EB1-GFP transfected cells for all 3 conditions: mcf10a, pten (-/-), and PIK3CA-H1047R. (Bottom) Mean image across all 50 frames at time steps 2 seconds apart.

4.2.2 *Direct Mechanical Measurements and Preliminary Optical Stretcher Results*

While the results presented in my thesis show changes in the ability of microtubules to move beyond the cell body boundary both by manipulating either the actomyosin cortex or the tubulin stability, it does not measure direct material properties nor integrity of the actomyosin cortex.

One way to measure actomyosin integrity more directly is to use an optical stretcher to measure properties such as stiffness, deformability, and viscoelasticity. The stretcher consists of two lasers with divergent optics facing each other; due to the higher index of refraction on the inside of the cell, light loses momentum when it exits the cell. The result is a uniaxial tensile force on the order of a few hundred pN exerted on the cell [149]. Using rapidly acquired videos of the 'stretch' in combination with very robust edge-detection image analysis techniques, one can deduce material properties of the cell. In 2012, I was able to collect preliminary results from Josef Kas′s lab in Leipzig Germany.

Preliminary results used Human Mammary Epithelial Cells (HMEC): one GFP-expressing control (HMEC-GFP) and one which over-expresses twist (HMEC-twist). Overexpression of twist has been shown to induce epithelial-to-mesenchymal-transition (EMT) morphology and McTN formation [37]. Measurements consisted of extracting outlines from 182 HMEC-GFP cells and 155 HMEC twist cells. Using

code written by members Josef Kas's lab in Leipzig Germany, the outline of the edge of the cells at 152 time points over the course of 5 seconds were extracted. From the outlines, the long axis along of the cell, or direction of stretch controlled for rotation was computed. To compare across cell types and drug treatments, the rotationally adjusted long axis was normalized or divided by the initial, relaxed state and set to zero (by subtracting normalized relaxed state); the result is the relative, rotation adjusted long axis measurement plotted as a function of time (Figure 4.3). Preliminary results show that twist is more contractile than the control. This suggests that McTNs are driven more by the stability of the MTs than the weakness of actin cortex. One of the disadvantages of the optical stretcher is cell heating; thus, the preliminary results shown above could also indicate that twist cells respond more quickly to cytoplasmic heating.

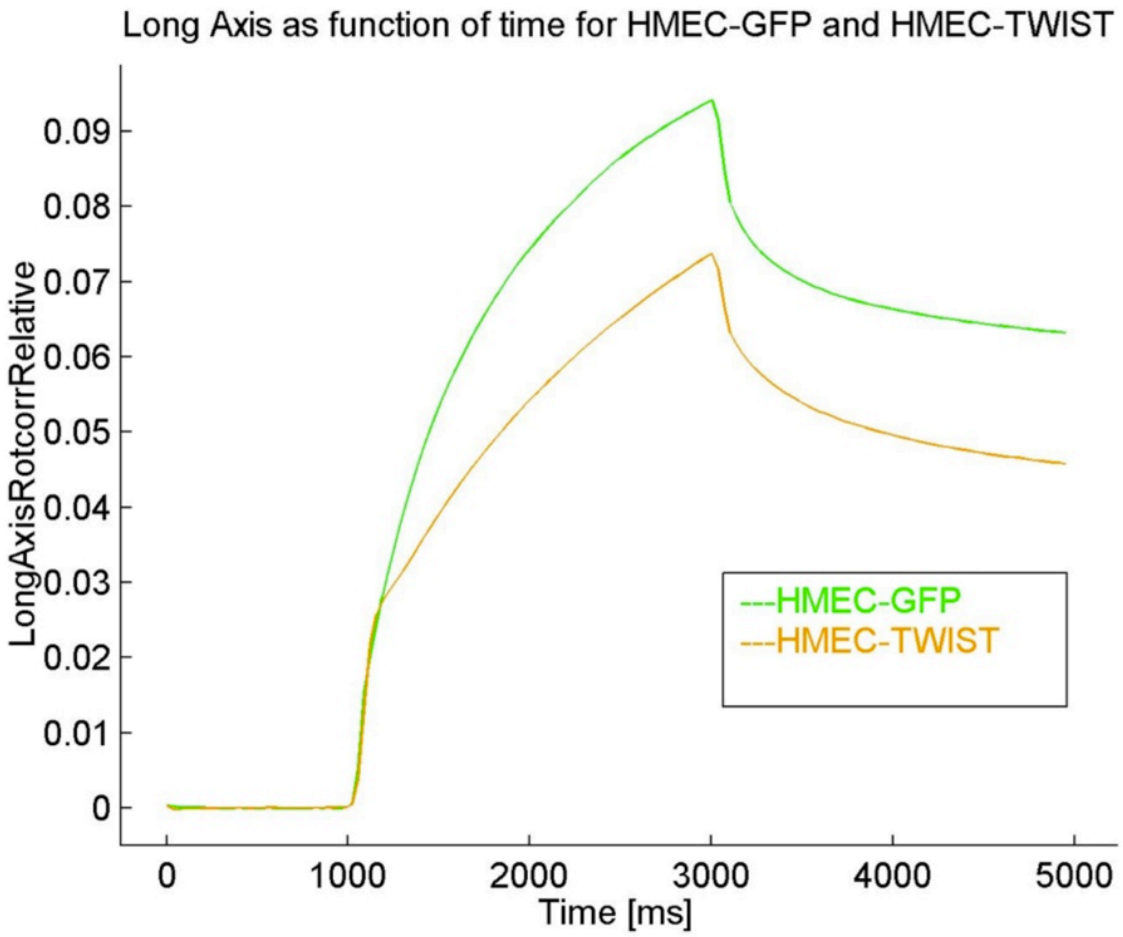

Figure 4.3: Optical Stretcher Results GFP vehicle vs Twist show the normalized, rotation adjusted, relative long-axis results as a function of time. Twist appears to be stiffer or have a more contractile actomyosin cortex.

4.3 Outlook and Final Thoughts

The work outlined in my thesis is just the beginning of understanding the cytoskeletal behavior that gives rise to McTNs. With several emerging technologies on the horizon, comes the promising possibility of further measuring and understanding many of these mechanical questions. For example, there is now new microfluidics stretcher that is even higher-throughput than the optical stretcher without several of the technical challenges like heating the cells up [150]. Nanofabrication of PDMS fabricated ridges may help better understand how CTCs sense the environment once they attach [125]. Considering that currently many cancer drug therapies target the cytoskeleton, better understanding of these mechanisms is of critical importance to clinical therapies.

One interesting area of future work involves better relating cytoskeletal interactions between attached and suspended cells mechanically. One valuable technique that holds promise for assaying both suspended and attached cells is the aspirator micropipette assays where a portion of the membrane is deformed under negative pressure. Already micropipette assays have shown that that bone marrow-derived mesenchymal stem cells (hMSCs) become stiffer on stiffer substrates where E_0 on stiffer substrate was 155±76 Pa and on softer substrates was 35±6 [151]. Another study assayed suspended hMSCs and found viscoelastic solid behavior with a Young′s moduli for E_0 and E∞ to be 886 ± 289 Pa and 372 ± 125 Pa [152]. The

trend of increased Young′s moduli values for attached cells compared to suspended cells is consistent with AFM and optical stretcher results [82, 83].

The study of McTNs is a new area of cancer research and still has many interesting questions remaining. Preliminary unpublished work in the Martin Lab has found McTNs in fresh patient cells, but currently no other *in vivo* discoveries of McTNS in other human systems have been observed. Previously, I discussed the potential role of leukocytes in mediating CTC reattachment, it is currently unknown whether immune cells have any interactions with McTNs, but it may be worth exploring. Likewise, no studies have looked for receptors on the surface of McTNs that may help mediate reattachment. Also, interesting unanswered questions that may help us better answer the cytoskeletal interactions between microtubules and the actomyosin cortex is the amount of force exerted by McTNs as well as McTN stiffness.

Research on McTNs is at the forefront for improving understanding the role of the cytoskeleton on reattachment in metastasis. Already, it is widely accepted that changes in cytoskeleton play a critical role in cancer invasiveness. The vast majority of the cancer invasiveness body of literature is limited to the migration of attached cells though and not the reattachment of CTCs. Clinically, many of the most common chemotherapies already target the cytoskeleton such as Vinblastine, Paclitaxel, and Demecolcine. Given the potential for cytoskeleton alterations to influence CTC reattachment, the implications of improving our understanding in this underappreciated and poorly understood area of research is critical. The work outlined in my thesis lays the foundation of building better analytical techniques

to studying the balance of forces between microtubules and the actomyosin cortex especially in suspended cells. Additionally, I present an organizing framework in order to better understand cytoskeletal interactions and show preliminary results supporting this model.

Bibliography

[1] Patrick Mehlen and Alain Puisieux. Metastasis: a question of life or death. *Nature reviews: Cancer*, 6:449–458, June 2006.

[2] Yibin Kang. New tricks against an old foe: molecular dissection of metastasis tissue tropism in breast cancer. *Breast Disease*, 26:129–38, 2007.

[3] Gaorav P Gupta and Joan Massague. Cancer metastasis: Building a framework. *Cell*, 127:679–695, November 17 2006.

[4] Steven I Hajdu. A note from history: Landmarks in history of cancer, part 1. *Cancer*, 117(5):1097–1102, March 1 2011.

[5] Rosalie David and Michael R. Zimmerman. Cancer: an old disease, a new disease or something in between? *Science and Society*, 10(10), October 2010.

[6] Steven I Hajdu and M Vadmal. A note from history: Landmarks in history of cancer, part 6. *Cancer*, 119(23):14058–82, September 16 2013.

[7] Stephen F Keevil. Physics and medicine: a historical perspective. *The Lancet*, 379(9825), April 21 2012.

[8] Karl Pearson. *The Grammar of Science*, volume 17. Walter Scott, London, UK, 1892.

[9] Wei Wang. Radiotherapy in the management of early breast cancer. *Journal of Medical Radiation Sciences*, 60(1):40–46, March 2013.

[10] Steven I Hajdu. A note from history: Landmarks in history of cancer, part 4. *Cancer*, 118(20):4914–28, October 15 2012.

[11] John S. Laughlin. History of medical physics. *Physics Today*, 36(7), July 1983.

[12] Sridhar Ramaswamy, Ken N Ross, Eric S Lander, and Todd Golub. A molecular signature of metastasis in primary solid tumors. *Nature Genetics*, 33:49–54, December 9 2002.

[13] Andy J Minn, Gaorav P Gupta, Peter M Siegel, Paula D Bos, Weiping Shu, Dilip D Giri, Agnes Viale, Adam B Olshen, William L Gerald, and Joan Massague. Genes that mediate breast cancer metastasis to lung. *Nature*, 436:518–524, July 28 2005.

[14] Victoria Seewaldt. Ecm stiffness paves the way for tumor cells. *Nature Medicine*, 20:332–333, April 2014.

[15] Sanjay Kumar and Valerie M. Weaver. Mechanics, malignancy, and metastasis: the force journey of a tumor cell. *Cancer Metastasis Review*, 28(1-2):113–27, January 21 2009.

[16] Vinay Swaminathan, Karthikeyan Mythreye, E Tim O'brien, Andrew Berchuck, Gerard C Blobe, and Richard Superfine. Mechanical stiffness grades metastatic potential in patient tumor cells and in cancer cell lines. *Cancer Research*, 71(15), 2011.

[17] Ali Rafiq. A glimpse into the historical journey of how we came to understand cancer. *Journal of Pioneering Medical Sciences Blogs*, December 12 2014.

[18] Jiaquan Xu, Sherry L. Murphy, Kenneth D. Kochanek, and Brigham A. Bastian. Deaths: Final data for 2013. *National Vital Statistics Reports*, 64(2), February 16 2016.

[19] Debra L. Blackwell, Jacqueline W Lucas, and Tainya C Clarke. Summary health statistics for u.s. adults: National health interview survey. *Vital Health Statistics*, 10(260), 2014.

[20] Jonathon Sleeman and Patricia S Steeg. Stopping cancer in its tracks: Cancer metastasis as a therapeutic target. *European Journal of Cancer*, 46(7):1177–1180, 2010.

[21] Andrzej B Poplawski, Michal Jankowski, Stephen W Erickson, Teresita Dõaz de Stahl, E Christopher Partridge, Chiquito Crasto, Jingyu Guo, John Gibson, Uwe Menzel, Carl EG Bruder, Aneta Kaczmarczyk, Magdalena Benetkiewicz, Robin Andersson, Johanna Sandgren, Barbara Zegarska, Dariusz Bala, Ewa Srutek, David B Allison, Arkadiusz Piotrowski, Wojciech Zegarski, and Jan P Dumanski. Frequent genetic differences between matched primary and metastatic breast cancer provide an approach to identification of biomarkers for disease progression. *European Journal of Human Genetics*, 18:560–568, 2010.

[22] Mika Suzuki and David Tarin. Gene expression profiling of human lymph node metastases and matched primary breast carcinomas: Clinical implications. *Molecular Oncology*, 1:172–180, April 7 2007.

[23] Myriam Labelle and Richard O Hynes. The initial hours of metastasis: the importance of cooperative host-tumor cell interactions during hematogenous dissemination. *Cancer Discovery*, 2(12):1091–1099, December 2012.

[24] Patricia S Steeg. Tumor metastasis: mechanistic insights and clinical challenges. *Nature Medicine*, 12(8):895–904, August 2006.

[25] David Owen Morgan. *The Cell Cycle: Principles of Control*. New Science Press, Sunderland, Massachusetts, 2007.

[26] Peter Gassman and Joerg Haier. The tumor cell-host organ interface in the early onset of metastatic organ colonisation. *Clinical Experimental Metastasis*, 25:171–181, December 5 2008.

[27] Neta Erez and Lisa M. Coussens. Leukocytes as paracrine regulators of metastasis and determinants of organ-specific colonization. *International Journal of Cancer*, 128(11):2536–2544, June 1 2011.

[28] Carina Strell and Frank Entschladen. Extravasation of leukocytes in comparison to tumor cells. *Cell Communication and Signaling*, 6(10), December 4 2008.

[29] Simone Bersini, Jessie S. Jeon, Matteo Moretti, and Roger D. Kamm. In vitro models of the metastatic cascade: from local invasion to extravasation. *Drug Discovery Today*, 19(6):735Ð742, June 2014.

[30] Carina Strell, Kerstin Lang, Bernd Niggemann, Kurt Zaenker, and Frank Entschladen. Surface molecules regulating rolling and adhesion to endothelium of neutrophil granulocytes and mda-mb-468 breast carcinoma cells and their interaction. *Cellular and Molecular Life Sciences*, December 2007.

[31] Ja Hye Myung, Khyati A. Gajjar, Ryan M. Pearson, Cari A. Launiere, David T. Eddington, and Seungpyo Hong. Direct measurements on cd24-mediated rolling of human breast cancer mcf-7 cells on e-selectin. *Analytical Chemistry*, 83(3):1078–83, February 1 2011.

[32] Joseph S. Palumbo, Kathryn E. Talmage, Jessica V. Massari, Christine M. La Jeunesse, Matthew J. Flick, Keith W. Kombrinck, Markeńta Jirouskova, and Jay L. Degen. Platelets and fibrin(ogen) increase metastatic potential by impeding natural killer cellÐmediated elimination of tumor cells. *Blood*, 104(1):178–185, 2005.

[33] Nicolas Reymond, Barbara Borda d'Agua, and Anne J.ÊRidley. Crossing the endothelial barrier during metastasis. *Nature Reviews Cancer*, 13:858–870, December 2013.

[34] Jonathan GarcŠa-RomĞn and Alejandro Zentella-Dehesa. Vascular permeability changes involved in tumor metastasis. *Cancer Letters*, 335(2):259–269, July 28 2013.

[35] Jorg Haier and Garth L. Nicolson. Tumor cell adhesion under hydrodynamic conditions of fluid flow. *Acta Pathologica, Microbiologica et Immunologica Scandinavica*, 109(4):241–262, April 2001.

[36] Matthew Barnes, Jones T Nauseef, and Michael D Henry. Resistance to fluid shear stress is a conserved biophysical property of malignant cells. *PloS ONE*, December 2012.

[37] Rebecca A Whipple, Michael A Matrone, Edward H Cho, Eric M Balzer, Michele I Vitolo, Jennifer R Yoon, Olga B Ioffe, Kimberly C Tuttle, Jing Yang, and Stuart S Martin. Epithelial-to-mesenchymal transition promotes tubulin detyrosinatiion and microtentacles that enhance endothelial engagement. *Cancer Research*, 70:8127–8137, 2010.

[38] Michael A Matrone, Rebecca A Whipple, Eric M Balzer, and Stuart S Martin. Microtentacles tip the balance of cytoskeletal forces in circulating tumor cells. *Cancer Research*, 70, October 2010.

[39] Lekhana Bhandary, Rebecca A. Whipple, Michele I. Vitolo, Monica S. Charpentier, Amanda E. Boggs, Kristi R. Chakrabarti, Keyata N. Thompson, and Stuart S. Martin. Rock inhibition promotes microtentacles that enhance reattachment of breast cancer cells. *Oncotarget*, 6(8):6251–66, January 31 2015.

[40] Rebecca A Whipple, Michele I Vitolo, Amanda E Boggs, Monica S Charpentier, Keyata Thompson, and Stuart S Martin. Parthenolide and costunolide reduce microtentacles and tumor cell attachment by selectively targeting detyrosinated tubulin independent from nf-κb inhibition. *Breast Cancer Research*, 15(5), 2013.

[41] Michele I. Vitolo, Amanda E. Boggs, Rebecca A. Whipple, Jennifer R. Yoon, Keyata Thompson, Michael A. Matrone, Edward H. Cho, Eric M. Balzer, and Stuart S. Martin. Loss of pten induces microtentacles through pi3k-independent activation of cofilin. *Oncogene*, June 11 2013.

[42] Rebecca A Whipple, Eric M Balzer, Edward H Cho, Michael A Matrone, Jennifer R Yoon, and Stuart S Martin. Vimentin filaments support extension of tubulin-based microtentacles in detached breast tumor cells. *Cancer Research*, 2008.

[43] Kristi R. Chakrabarti, Rebecca A. Whipple, Amanda E. Boggs, Lindsay K. Hessler, Lekhana Bhandary, Michele I. Vitolo, Keyata Thompson, and Stuart S. Martin1. Pharmacologic regulation of ampk in breast cancer affects cytoskeletal properties involved with microtentacle formation and re-attachment. *Oncotarget*, 6(34):36292–307, November 3 2015.

[44] Jennifer R. Yoon, Rebecca A. Whipple, Eric M. Balzer, Edward H. Cho, Michael A. Matrone, Michelle Peckham, and Stuart S. Martin. Local anesthetics inhibit kinesin motility and microtentacle protrusions in human epithelial and breast tumor cells. *Breast Cancer Research and Treatment*, 129(3):691–701, 2011.

[45] Preeti Shah, Yael Gau, and Gauri Sabnis. Histone deacetylase inhibitor entinostat reverses epithelial to mesenchymal transition of breast cancer cells by reversing the repression of e-cadherin. *Breast Cancer Research and Treatment*, 143(1):99–111, 2014.

[46] Nicole A. Perry, Michele I. Vitolo, Stuart S. Martin, and Aikaterini Kontrogianni Konstantopoulos. Loss of the obscurin-rhogef downregulates rhoa signaling and increases microtentacle formation and attachment of breast epithelial cells. *Oncotarget*, 5(18):8558–8568, August 10 2014.

[47] Eric M. Balzer, Rebecca A. Whipple, Keyata Thompson, Amanda E. Boggs, Jana Slovic, Edward H. Cho, Michael A. Matrone, Toshiyuki Yoneda, Susette C. Mueller, and Stuart S. Martin. c-src differentially regulates the functions of microtentacles and invadopodia. *Oncogene*, 29(48):6402–6408, 2010.

[48] RA Whipple, AM Cheung, and SS Martin. Detyrosinated microtubule protrusions in suspended mammary epithelial cells promote reattachment. *Experimental Cell Research*, 313(7):1326–1336, April 2007.

[49] Alison NKillilea, Roseann Csencsits, Sam Kenny, Ke Xu, and Kenneth H. Downing. Structure of microtubule-based microtentacles. *Microscopy and Microanalysis*, 21:235–236, August 2015.

[50] A Mialhe, L Lafanechere, I Treilleux, N Peloux, C Dumontet, A Bremond, MH Panh, R Payan, J Wehland, RL Margolis, and D Job. Tubulin detyrosination is a frequent occurrence in breast cancers of poor prognosis. *Cancer Research*, 61:5024–5027, 2001.

[51] Sadiqa Khawaja, Gregg Gundersen, and Jeannette Bulinski. Enhanced stability of microtubules enriched in detyrosnated tubulin is not a direct function of detyrosination level. *Journal of Cell Biology*, 106:141–149, 1988.

[52] Eric M. Balzer, Ziqiu Tong, Colin D. Paul, Wei-Chien Hung, Kimberly M. Stroka, Amanda E. Boggs, Stuart S. Martin, and Konstantinos Konstantopoulos. Physical confinement alters tumor cell adhesion and migration phenotypes. *Federation of American Societies for Experimental Biology*, 26, June 15 2012.

[53] Monica S. Charpentier, Rebecca A. Whipple, Michele I. Vitolo, Amanda E. Boggs, Jana Slovic, Keyata N. Thompson, Lekhana Bhandary, and Stuart S. Martin. Curcumin targets breast cancer stemÐlike cells with microtentacles that persist in mammospheres and promote reattachment. *Cancer Research*, 74(4):1250–1260, February 15 2014.

[54] Sendurai A. Mani, Wenjun Guo, Mai-Jing Liao, Elinor Ng. Eaton, Ayyakkannu Ayyanan, Alicia Y. Zhou, Mary Brooks, Ferenc Reinhard, Cheng Cheng Zhang, Michail Shipitsin, Lauren L. Campbell, Kornelia Polyak, Cathrin Brisken, Jing Yang, and Robert A. Weinberg. The epithelial-mesenchymal

transition generates cells with properties of stem cells. *Cell*, 133(4):704 –715, May 16 2008.

[55] Lao H. Saal, Karolina Holm, Matthew Maurer, Lorenzo Memeo, Xiaomei Wang Tao Su, Jennifer S. Yu, Per-Olof Malmstrom, Mahesh Mansukhani, Jens Enoksson, Hanina Hibshoosh, Ake Borg, and Ramon Parson. Pik3ca mutations correlate with hormone receptors, node metastasis, and erbb2, and are mutually exclusive with pten loss in human breast carcinoma. *Cancer Research*, 65(7), April 1 2005.

[56] Jing Li, Clifford Yen, Danny Liaw, Katrina Podsypanina, Shikha Bose, Steven I. Wang, Janusz Puc, Christa Miliaresis, Linda Rodgers, Richard McCombie, Sandra H. Bigner, Beppino C. Giovanella, Michael Ittmann, Ben Tycko, Hanina Hibshoosh, Michael H. Wigler, and Ramon Parsons. Pten, a putative protein tyrosine phosphatase gene mutated in human brain, breast, and prostate cancer. *Science*, 275(5308):1943–1947, 1997.

[57] Shunyou Wang, Jing Gao, Qunying Lei, Nora Rozengurt, Colin Pritchard, Jing Jiao, George V. Thomas, Gang Li, Pradip Roy-Burman, Peter S. Nelson, Xin Liu, and Hong Wu. Prostate-specific deletion of the murine pten tumor suppressor gene leads to metastatic prostate cancer. *Cancer Cell*, 4(3):209–221, September 2003.

[58] Kanika A. Bowen, Hung Q. Doan, Binhua P. Zhou, Qingding Wang, Yuning Zhou, Piotr G. Rychahou, and B. Mark Evers. Pten loss induces epithelial-mesenchymal transition in human colon cancer cells. *Anticancer Research*, 29(11):4439–4449, 2009.

[59] MA Matrone, RA Whipple, K Thompson, EH Cho, MI Vitolo, JR Yoon EM Balzer, OB Ioffe, KC Tuttle, M Tan, and SS Martin. Metastatic breast tumors express increased tau, which promotes microtentacle formation and the reattachment of detached breast tumor cells. *Oncogene*, 29:3217–3227, June 2010.

[60] Donald E. Ingber. Tensegrity i. cell structure and hierarchical systems biology. *Journal of Cell Science*, 116:1157–1173, April 1 2003.

[61] Donald E Ingber, Ning Wang, and Dimitrije Stamenovi? Tensegrity, cellular biophysics, and the mechanics of living systems. *Reports on Progress in Physics*, 77(4), April 2 2014.

[62] Mechanobiology Institute, National University of Singapore. https://www.mechanobio.info/what-is-mechanobiology/, 2016. [Online; accessed 19-July-2016].

[63] N Kumar and M Flavin. Modulation of some parameters of assembly of microtubules in vitro by tyrosination of tubulin. *European Journal of Biochemistry*, 127:215–222, 1982.

[64] Leticia Peris, Michael Wagenbach, Laurence LafanechŔre, Jacques Brocard, Ayana T. Moore, Frank Kozielski, Didier Job, Linda Wordeman, and Annie Andrieux. Motor-dependent microtubule disassembly driven by tubulin tyrosination. *Journal of Cell Biology*, 185(7):1159–1166, 2009.

[65] Daniel Webster, Juergen Wehland, Klaus Weber, and Gary Borisy. Detyrosination of alpha tubulin does not stabilize microtubules in vivo. *Journal of Cell Biology*, 111, July 1990.

[66] Daniel Webster, Gregg Gundersen, Jeannette Bulinski, and Gary Borisy. Assembly and turnover of detyrosinated tubulin in vivo. *Journal of Cell Biology*, 105:265–276, 1987.

[67] Geri Gurland and Gregg G. Gundersen. Stable, detyrosinated microtubules function to localize vimentin intermediate filaments in fibroblasts. *Journal of Cell Biology*, 131(5):1275–1290, 1995.

[68] Geri Kreitzer, Liao Guojuan, and Gregg Gundersen. Detyrosination of tubulin regulates the interaction of intermediate filaments with microtubules in vivo via a kinesin-dependent mechanism. *Molecular Biology of the Cell*, 10, January 28 1999.

[69] P. Wagner, B. Wang, E. Clark, H. Lee, R. Rouzier, and L. Pusztai. Microtubule associated protein (map)-tau: a novel mediator of paclitaxel sensitivity in vitro and in vivo. *Cell Cycle*, 4(9):1149Đ1152, July 19 2005.

[70] Roman Rouzier, Radhika Rajan, Peter Wagner, Kenneth R. Hess, David L. Gold, James Stec, Mark Ayers, Jeffrey S. Ross, Peter Zhang andThomas A. Buchholz, Henry Kuerer, Marjorie Green, Banu Arun, Gabriel N. Hortobagyi, W. Fraser Symmans, and Lajos Pusztaia. Microtubule-associated protein tau: a marker of paclitaxel sensitivity in breast cancer. *Proceedings of the National Academy of Sciences of the United States of America*, 102(23):8315–20, June 7 2005.

[71] Mohammad Soheilypour, Mohaddeseh Peyro, Stephen J. Peter, and Mohammad R. K. Mofrad. Buckling behavior of individual and bundled microtubules. *Biophysical Journal*, 106:1718Đ1726, April 2015.

[72] Guillaume Salbreux, Guillaume Charras, and Ewa Paluchemail. Actin cortex mechanics and cellular morphogenesis. *Trends in Cell Biology*, 22(10), 2012.

[73] Andrew G. Clark, Ortrud Wartlick, Guillaume Salbreux, and Ewa K. Paluch. Stresses at the cell surface during animal cell morphogenesis. *Current Biology*, 24(10):484–494, May 19 2014.

[74] Guillaume T. Charras andChi Kuo Hu, Margaret Coughlin, and Timothy J. Mitchison. Reassembly of contractile actin cortex in cell blebs. *Journal of Cell Biology*, 175(3):477–490, November 6 2006.

[75] Hydrostatic pressure and the actomyosin cortex drive mitotic cell rounding. *Nature Letter*, 469:226Ð230, January 2 2011.

[76] Dimitrije Stamenovic and Donald E. Ingber. Tensegrity-guided self assembly: from molecules to living cells. *Soft Matter*, 5(6):1093, March 21 2009.

[77] Andrei I. Ivanov, Ann M. Hopkins, G. Thomas Brown, Kirsten Gerner-Smidt, Brian A. Babbin, Charles A. Parkos, and Asma Nusrat. Myosin ii regulates the shape of three-dimensional intestinal epithelial cysts. *Journal of Cell Science*, 121(11):1803–1814, 2008.

[78] Meng-Horng Lee, Pei-Hsun Wu, Daniele Gilkes Ivie Aifuwa, and Denis Wirtz. Normal mammary epithelial cells promote carcinoma basement membrane invasion by inducing microtubule-rich protrusions. *Oncotarget*, 6(32):32634–45, August 3 2015.

[79] Carsten Schwan, Barbel Stecher, Tina Tzivelekidis, Marco van Ham, Manfred Rohde, Wolf-Dietrich Hardt, Jurgen Wehland, and Klaus Aktories. Clostridium difficile toxin cdt induces formation of microtubule-based protrusions and increases adherence of bacteria. *PLOS Pathogens*, 5(10), October 16 2009.

[80] Ewa Paluch, Matthieu Piel, Jacques Prost, Michel Bornens, and Cecile Sykes. Cortical actomyosin breakage triggers shape oscillations in cells and cell fragments. *Biophysical Journal*, 89(1):724–733, July 2005.

[81] Ning Wang and Donald E. Ingber. Control of cytoskeletal mechanics by extracellular matrix, cell shape, and mechanical tension. *Biophysical Journal*, 66(6):2181–2189, June 1994.

[82] Seyed Mohammad Ali Haghparast, Takanori Kihara, and Jun Miyake. Distinct mechanical behavior of hek293 cells in adherent and suspended states. *PeerJ*, 3(e1131), July 30 2015.

[83] John M. Maloney, Dessy Nikova, Franziska Lautenschlager, Emer Clarke, Robert Langer, Jochen Guck, and Krystyn J. Van Vliet. Mesenchymal stem cell mechanics from the attached to the suspended state. *Biophysical Journal*, 99(8):2479–2487, October 10 2010.

[84] Nir S. Gov and Ajay Gopinathany. Dynamics of membranes driven by actin polymerization. *Biophysical Journal*, 90(2):454–469, January 15 2006.

[85] Jay D. Humphrey, Eric R. Dufresne, and Martin A. Schwartz. Mechanotransduction and extracellular matrix homeostasis. *Nature Reviews Molecular Cell Biology*, 15(12):802–812, December 2014.

[86] John D.Hood and David A. Cheresh. Role of integrins in cell invasion and migration. *Nature Reviews Cancer*, 2:91–100, February 2002.

[87] Anna Huttenlocher and Alan Rick Horwitz. Integrins in cell migration. *Cold Spring Harbor Perspectives in Biology*, 3(9), September 2011.

[88] Thomas W. Marshall, Isaac E. Lloyda, Jean Marie Delalandea, Inke NŁthkeb, and Jody Rosenblatt. The tumor suppressor adenomatous polyposis coli controls the direction in which a cell extrudes from an epithelium. *Molecular Biology of the Cell*, 22(21):3962–70, September 7 2011.

[89] Carmen Birchmeier, Walter Birchmeier, and Beate Brand-Saberi. Epithelial-mesenchymal transitions in cancer progression. *Acta Anatomica*, 1996.

[90] Sharona Even-Ram, Andrew D. Doyle, Mary Anne Conti, Kazue Matsumoto, Robert S. Adelstein, and Kenneth M. Yamada. Myosin iia regulates cell motility and actomyosinÐmicrotubule crosstalk. *Nature Cell Biology*, 9(3):299–309, February 18 2007.

[91] Ying Wen, Christina H. Eng, Jan Schmoranzer, Noemi Cabrera-Poch, Edward J. S. Morris, Michael Chen, Bradley J. Wallar andArthur S. Alberts, and Gregg G. Gundersen. Eb1 and apc bind to mdia to stabilize microtubules downstream of rho and promote cell migration. *Nature Cell Biology*, 6(9):820–30, 2004.

[92] James B. Moseley, Francesca Bartolini, Kyoko Okada, Ying Wen, Gregg G. Gundersen, and Bruce L. Goode. Regulated binding of adenomatous polyposis coli protein to actin. *Journal of Biological Chemistry*, 282(17):12661–8, 2007.

[93] Clifford P. Brangwynne, Frederick C. MacKintosh, Sanjay Kumar, Nicholas A. Geisse, Jennifer Talbot, L. Mahadevan, Kevin K. Parker, Donald E. Ingber, and David A. Weitz. Microtubules can bear enhanced compressive loads in living cells because of lateral reinforcement. *Journal of Cell Biology*, 173, 2006.

[94] Donald E. Ingber. Cancer as a disease of epithelial-mesenchymal interactions and extracellular matrix regulation. *Differentiation*, 70(9-10):547–60, 2002.

[95] Hideki Yamaguchia and John Condeelis. Regulation of the actin cytoskeleton in cancer cell migration and invasion. *Biochimica et Biophysica Acta (BBA) - Molecular Cell Research*, 1773(5):642–52, 2007.

[96] Eric M Balzer, Rebecca A Whipple, Edward H Cho, Michael A Matrone, and Stuart S Martin. Antimitotic chemotherapeutics promote adhesive responses in detached and circulating tumor cells. *Breast Cancer Research Treatment*, 121:65–78, 2010.

[97] Jian Yu Rao and Ning Li. Microfilament actin remodeling as a potential target for cancer drug development. *Current Cancer Drug Targets*, 4(4):345–54, 2004.

[98] Gerhard Fritz and Bernd Kaina. Rho gtpases promising cellular targets for novel anticancer drugs. *Current Cancer Drug Targets*, 6(1):1–14, 2006.

[99] Kazuyuki Itoh, Kiyoko Yoshioka, Hitoshi Akedo, Masayoshi Uehata, Toshimasa Ishizaki, and Shuh Narumiya. An essential part for rho-associated kinase in the transcellular invasion of tumor cells. *Nature Medicine*, 5(2):221–225, 1999.

[100] Dominico Vigil, Tai Young Kim, Ana Plachco andAndrew J. Garton, Linda Castaldo, Jonathan A. Pachter, Hanqing Dong, Brianna Tokar Xin Chen, Sharon L. Campbell, and Channing J. Der. Rock1 and rock2 are required for non-small cell lung cancer anchorage-independent growth and invasion. *Cancer Research*, 72(20):5338–47, 2012.

[101] Lili Wang, Lexun Xue, Hongxia Yan, Jie Li, and Yucheng Lu. Effects of rock inhibitor, y-27632, on adhesion and mobility in esophageal squamous cell cancer cells. *Molecular Biology Reports*, 37(4):1971–7, 2010.

[102] Francis J. Alenghat, Surya M. Naulib, Robert Kolbb, Jing Zhoub, and Donald E. Ingber. Global cytoskeletal control of mechanotransduction in kidney epithelial cells. *Experimental Cell Research*, 301(1):23–30, November 15 2004.

[103] Hirokazu Ohata, Tatsuya Ishiguro, Yuki Aihara, Ai Sato, Hiroaki Sakai, Shigeki Sekine, Hirokazu Taniguchi, Takayuki Akasu, Shin Fujita, Hitoshi Nakagama, and Koji Okamoto. Induction of the stem-like cell regulator cd44 by rho kinase inhibition contributes to the maintenance of colon cancer-initiating cells. *Cancer Research*, 72(19):5101–10, October 2 2012.

[104] Xuefeng Liu, Virginie Ory, Sandra Chapman, Hang Yuan, Chris Albanese, Bhaskar Kallakury, Olga A. Timofeeva, Caitlin Nealon, Aleksandra Dakic, Vera Simic, Bassem R. Haddad, Johng S. Rhim, Anatoly Dritschilo, Anna Riegel, Alison McBride, and Richard Schlegel. Rock inhibitor and feeder cells induce the conditional reprogramming of epithelial cells. *American Journal of Pathology*, 180(2):599–607, February 2012.

[105] Frank A. Suprynowicza, Geeta Upadhyaya, Ewa Krawczyka, Sarah C. Kramera, Jess D. Heberta, Xuefeng Liua, Hang Yuana, Chaitra Cheluvarajub, Phillip W. Clappb, Richard C. Boucher, Christopher M. Kamonjoha, Scott H. Randellb, and Richard Schlegela. Conditionally reprogrammed cells represent a stem-like state of adult epithelial cells. *Proceedings of the National Academy of Sciences of the United States*, December 4 2012.

[106] Mihaly Kovacs, Judit Toth, Csaba Hetenyi, Andras Malnasi-Csizmadia, and James R. Sellers. Mechanism of blebbistatin inhibition of myosin ii. *Journal of Biological Chemistry*, 279(34):35557–63, June 16 2004.

[107] Michelle Piehl and Lynne Cassimeris. Organization and dynamics of growing microtubule plus ends during early mitosis. *Molecular Biology of the Cell*, 14(3):916–25, December 7 2003.

[108] Michelle Piehl, U. Serdar Tulu, Pat Wadsworth, and Lynne Cassimeris. Centrosome maturation: measurement of microtubule nucleation throughout the cell cycle by using gfp-tagged eb1. *Proceedings of the National Academy of Sciences of the United States*, 101, September 4 2004.

[109] Guillermo Velasco, Chris Armstrong, Nick Morrice, Sheelagh Frame, and Philip Cohen. Phosphorylation of the regulatory subunit of smooth muscle protein phosphatase 1m at thr850 induces its dissociation from myosin. *Federation of European Biochemical Societies Letters*, 527(1-3):101–4, September 11 2002.

[110] Takahiro Tsuji, Toshimasa Ishizaki, Muneo Okamoto, Chiharu Higashida, Kazuhiro Kimura, Tomoyuki Furuyashiki, Yoshiki Arakawa, Raymond B. Birge, Tetsuya Nakamoto, Hisamaru Hirai, and Shuh Narumiya. Rock and mdia1 antagonize in rho-dependent rac activation in swiss 3t3 fibroblasts. *Journal of Cell Biology*, May 20 2002.

[111] Ilan Spector, Nava R. Shochet, Dina Blasberger, and Yoel Kashman. Latrunculins–novel marine macrolides that disrupt microfilament organization and affect cell growth: I. comparison with cytochalasin d. *Cell Motility and the Cytoskeleton*, 13(3):127–44, 1989.

[112] Walter M. Morton, Kathryn R. Ayscough, and Paul J. McLaughlin. Latrunculin alters the actin-monomer subunit interface to prevent polymerization. *Nature Cell Biology*, 2(6):376–8, June 1 2000.

[113] Adam G. Hendricks, Jacob E. Lazarus, Eran Perlson, Melissa K. Gardner, David J. Odde, Yale E. Goldman, and Erika L.F. Holzbaur. Dynein tethers and stabilizes dynamic microtubule plus ends. *Current Biology*, 22(7):632–7, April 10 2012.

[114] Aaron Christian Ponti, Matthias Machacek, Stephanie L. Gupton, Clare M Waterman-Storer, and Gaudenz Danuser. Two distinct actin networks drive the protrusion of migrating cells. *Science*, 305(5691):1782–1786, September 17 2004.

[115] Pieta K. Mattila and Pekka Lappalainen. Filopodia: molecular architecture and cellular functions. *Nature Reviews Molecular Cell Biology*, 9(6):446–454, June 2008.

[116] Wasim A. Sayyad, Ladan Amin, Paolo Fabris, Erika Ercolini, and Vincent Torre. The role of myosin-ii in force generation of drg filopodia and lamellipodia. *Scientific Reports*, 5(7842), January 19 2015.

[117] Margaret L. Gardel, Benedikt Sabass, Lin Ji, Gaudenz Danuser, Ulrich S. Schwarz, and Clare M. Waterman. Traction stress in focal adhesions correlates biphasically with actin retrograde flow speed. *Journal of Cell Biology*, 183(6):999–1005, December 15 2008.

[118] Clifford P. Brangwynne, F. C. MacKintosh, and David A. Weitz. Force fluctuations and polymerization dynamics of intracellular microtubules. *Proceedings of the National Academy of Sciences of the United States*, October 9 2007.

[119] Dominique Seetapun and David J. Odde. Cell-length-dependent microtubule accumulation during polarization. *Current Biology*, 20(11):979–88, June 8 2010.

[120] Gianluca De Santis, Alex B. Lennon, Federica Boschetti, Benedict Verhegghe, Pascal Verdonck, and Patrick J. Prendergast. How can cells sense the elasticity of a substrate? an analysis using a cell tensegrity model. *Eur Cell Mater*, 22:202–13, October 11 2011.

[121] Piyush B. Gupta, Tamer T. Onder, Guozhi Jiang, Kai Tao, Charlotte Kuperwasser, Robert A. Weinberg, and Eric S. Lander. Identification of selective inhibitors of cancer stem cells by high-throughput screening. *Cell*, 138(4):645–59, August 21 2009.

[122] Birthe Willipinski-Stapelfeldt, Sabine Riethdorf, Volker Assmann, Ute Woelfle, Thomas Rau, Guido Sauter, Jochen Heukeshoven, and Klaus Pantel. Changes in cytoskeletal protein composition indicative of an epithelial-mesenchymal transition in human micrometastatic and primary breast carcinoma cells. *Clinical Cancer Research*, 11(22):8006–14, November 15 2005.

[123] Linda A. Gordon, Kellie T. Mulligan, Helen Maxwell-Jones, Matthew Adams, Rosemary A. Walker, and J. Louise Jones. Breast cell invasive potential relates to the myoepithelial phenotype. *International Journal of Cancer*, 106(1):8–16, April 16 2003.

[124] John Crocker and David Grier. Methods of digital video microscopy for colloidal studies. *Journal of Colloid and Interface Science*, 179(1):298–310, April 15 1996.

[125] Meghan K Driscoll, Xiaoyu Sun, Can Guven, John T Fourkas, and Wolfgang Losert. Cellular contact guidance through dynamic sensing of nanotopography. *The Journal of Physical Chemistry Nano*, 8(4):3546–3555, 2014.

[126] Meghaan M. Ferreira, Vishnu C. Ramani, and Stefanie S. Jeffrey. Circulating tumor cell technologies. *Molecular Oncology*, 10(3), March 2016.

[127] Emilian Racila, David Euhus, Arthur J. Weiss, Chandra Rao, John McConnell, Leon W. M. M. Terstappen, and Jonathan W. Uhr. Detection and characterization of carcinoma cells in the blood. *Proceedings of the National Academy of Sciences of the United States of America*, 95(8):4589–4594, April 14 1998.

[128] Priya Gogoi, Saedeh Sepehri, Yi Zhou, Michael A. Gorin, Carmela Paolillo, Ettore Capoluongo, Kyle Gleason, Austin Payne, Brian Boniface, Massimo Cristofanilli, Todd M. Morgan, Paolo Fortina, Kenneth J. Pienta, Kalyan

Handique, and Yixin Wang. Development of an automated and sensitive microfluidic device for capturing and characterizing circulating tumor cells (ctcs) from clinical blood samples. *Plos One*, 11(1), January 25 2016.

[129] James Che, Victor Yu, Manjima Dhar, Corinne Renier, Melissa Matsumoto, Kyra Heirich, Edward B. Garon, Jonathan Goldman, Jianyu Rao, George W. Sledge, Mark D. Pegram, Shruti Sheth, Stefanie S. Jeffrey, Rajan P. Kulkarni, Elodie Sollier, and Dino Di Carlo. Classification of large circulating tumor cells isolated with ultrahigh throughput microfluidic vortex technology. *Oncotarget*, 7(11):12748–12760, February 6 2016.

[130] Daniel L. Adams, R. Katherine Alpaugh, Stuart S. Martin, Monica Charpentier, Saranya Chumsri, Massimo Cristofanilli, Diane K. Adams, Olga V. Makarova, Peixuan Zhu, Shuhong Li, Cha-Mei Tangh, and Steingrimur Stefanssoni. Precision microfilters as an all in one system for multiplex analysis of circulating tumor cells. *Royal Society of Chemistry*, 6:6405–6414, January 11 2016.

[131] Joan Massague and Anna C. Obenauf. Metastatic colonization by circulating tumour cells. *Nature*, 529(7586):298–306, january 21 2016.

[132] Amanda E. Boggs, Michele I. Vitolo, Rebecca A. Whipple, Monica S. Charpentier, Olga G. Goloubeva, Olga B. Ioffe, Kimberly C. Tuttle, Jana Slovic, Yiling Lu, Gordon B. Mills, and Stuart S. Martin. ?-tubulin acetylation elevated in metastatic and basal-like breast cancer cells promotes microtentacle formation, adhesion and invasive migration. *Cancer Research*, 75(1):203–215, January 1 2015.

[133] Kristi R. Chakrabarti, James I. Andorko, Rebecca A. Whipple, Peipei Zhang, Elisabeth L. Sooklal, Stuart S. Martin, and Christopher M. Jewell. Lipid tethering of breast tumor cells enables real-time imaging of free-floating cell dynamics and drug response. *Oncotarget*, 7(9):10486–10497, February 8 2016.

[134] Meghan K Driscoll, John T Fourkas, and Wolfgang Losert1. Local and global measures of shape dynamics. *Physical Biology*, August 10 2011.

[135] Assaf Zemel, Florian Rehfeldt, Andre E X Brown, Dennis E. Discher, and Samuel A. Safran. Optimal matrix rigidity for stress-fibre polarization in stem cells. *Nature Physics*, 6:468–473, March 21 2010.

[136] Maria Romina Girotti, Gabriela Gremel, Rebecca Lee, Elena Galvani, Dominic Rothwell, Amaya Viros, Amit Kumar Mandal, Kok Haw Jonathan Lim, Grazia Saturno, Simon J. Furney, Franziska Baenke, Malin Pedersen, Jane Rogan, Jacqueline Swan, Matthew Smith, Alberto Fusi, Deemesh Oudit, Nathalie Dhomen, Ged Brady, Paul Lorigan, Caroline Dive, and Richard Marais. Application of sequencing, liquid biopsies, and patient-derived xenografts for personalized medicine in melanoma. *Cancer Discovery*, 6(3):286–99, December 29 2015.

[137] Despina Siolas and Gregory J. Hannon. Patient derived tumor xenografts: transforming clinical samples into mouse models. *Cancer Research*, 73(17):5315–5319, September 1 2013.

[138] Hyeong-Gon Moon, Keunhee Oh, Jiwoo Lee, Minju Lee, Ju-Yeon Kim, Tae-Kyung Yoo, Myung Won Seo, Ae Kyung Park, Han Suk Ryu, Eun-Jung Jung, Namshin Kim, Seongmun Jeong, Wonshik Han, Dong-Sup Lee, and Dong-Young Noh. Prognostic and functional importance of the engraftment-associated genes in the patient-derived xenograft models of triple-negative breast cancers. *Breast Cancer Research and Treatment*, 154(1), 2015.

[139] Thitiporn Chanwimaluang and Guoliang Fan. An efficient blood vessel detection algorithm for retinal images using local entropy thresholding. *Circuits and Systems*, 5, May 25-28 2003.

[140] Mohammed Saleem, Sandrine Morlot andAnnika Hohendahl, John Manzi, Martin Lenz, and Aurelien Roux. A balance between membrane elasticity and polymerization energy sets the shape of spherical clathrin coats. *Nature Communications*, 6(6249), February 2015 2015.

[141] Kazuya Tsujita, Tadaomi Takenawa, and Toshiki Itoh. Feedback regulation between plasma membrane tension and membrane-bending proteins organizes cell polarity during leading edge formation. *Nature Cell Biology*, 17:749–758, May 4 2015.

[142] Takeshi Sakamoto, John Limouze, Christian A. Combs, Aaron F. Straight, and James R. Sellers. Blebbistatin, a myosin ii inhibitor, is photoinactivated by blue light. *Biochemistry*, 44(2):584–588, December 15 2005.

[143] Stephen P. Davies, Helen Reddy, Matilde Caivano, and Philip Cohen. Specificity and mechanism of action of some commonly used protein kinase inhibitors. *Biochemical Journal*, 351(1):95–105, October 1 2001.

[144] Physical Sciences le Oncology Centers Network. A physical sciences network characterization of non-tumorgenic and metastatic cells. *Scientific Report*, 2013.

[145] Farhad Vesuna, Ala Lisok, Brian Kimble, and Venu Raman. Twist modulates breast cancer stem cells by transcriptional regulation of cd24 expression. *Neoplasia*, 11(12):1318–1328, December 2009.

[146] Daniel R Webster, Gregg G Gundersenand Jeannette C Bulinski, and Gary G Borisy. Differential turnover of tyrosinated and detyrosinated microtubules. *Proceedings of the National Academy of Sciences*, 84(24):9040–9044, December 1987.

[147] Osigwe Esue, Ashley A Carson, Yiider Tseng, and Denis Wirtz. A direct interaction between actin and vimentin filaments mediated by the tail domain of vimentin. *Journal of Biological Chemistry*, 281(41):30393–30399, 2006.

[148] Dmitry Pavlov, Andras Muhlrad, John Cooper, Martin Wear, and Emil Reisler. Actin filament severing by cofilin. *Journal of Molecular Biology*, 365(5):1350–1358, February 2007.

[149] J Guck, R Ananthakrishnan, T. J. Moon, C Cunningham, and J Kas. Optical deformability of soft biological dielectrics. *PRL*, 84:5451–5454, 2000.

[150] Alexander Mietke, Oliver Otto, Salvatore Girardo, Philipp Rosendahl, Anna Taubenberger, Stefan Golfier, Elke Ulbricht, Sebastian Aland, Guck, and Elisabeth Fischer-Friedrich. Extracting cell stiffness from real-time deformability cytometry: Theory and experiment. *Biophysical Journal*, 109:2023–2036, November 15 2015.

[151] Qinwei Xu, Cheng Li, Yuejun Kang, and Yilei Zhang. Long term effects of substrate stiffness on the development of hmsc mechanical properties. *Royal Society of Chemistry*, 5:105651–105660, December 8 2015.

[152] Samuel CW Tan, Wen X Pan, Gang Ma, Ning Cai, Kam W Leong, and Kin Liao. Viscoelastic behaviour of human mesenchymal stem cells. *BMC Cell Biology*, 9(1):1–7, 2008.